ACOUSTIC WAVE SCATTERING FROM ROUGH SEA SURFACE AND SEABED
– A new look on an old problem

by

CHEN-FEN HUANG
B.S. in Marine Environment, National Sun Yat-sen University
(1995)
M.S. in Marine Environment, National Sun Yat-sen University
(1997)

Submitted to the Institute of
Undersea Technology
in Partial Fulfillment of the
Requirements of the Degree of

SCIENTIAE MASTER

at the
NATIONAL SUN YAT-SEN UNIVERSITY
1998

©CHEN-FEN HUANG, 1998; All rights reserved.
The author hereby grants to NSYSU permission to reproduce and
to distribute copies of this thesis document in whole or in part.

Signature of Author _____

Institute of Undersea Technology, 1998

Certified by _____

Dr. Jin-Yuan Liu, Associate Professor, Thesis Supervisor

Abstract

The main theme of this thesis is to study plane wave scattering from perfectly reflecting rough surfaces attempting to simulate the scenarios of wave scattering from rough sea surface and seabed. From the practical point of view, the ocean surface separating the air and water may be considered as a perfectly reflecting pressure-release surface because of the strong impedance contrast between these two media. As for the seabed, it is assumed to be a rigid rough surface. This assumption may not be completely acceptable because in reality the seafloor, particularly the upper part of the sediment layer, is a medium with finite bulk and shear modulus so that the interface allows energy to be penetrated into bottom through both compressional and shear waves. However, in this study, we shall approximate the seafloor as a rigid bottom, and consider the effect of roughness on the acoustic scattering from such interface. A complete model which considers wave scattering from a rough interface overlying on a penetrable medium with gradual variation of acoustic properties is included and discussed in the thesis. Further investigation will soon be undertaken.

The rough surfaces under consideration are described by various statistical quantities, including height probability function, correlation function, power spectrum, and realization. To suit for the types of rough surfaces of our interests, we place our emphases on three kinds of power spectrum: the Pierson-Moskowitz spectrum, the Gaussian spectrum, and the Goff-Jordan spectrum. A realization process for the power spectrum is developed. The scattered pressure fields, the scattering coefficient, and the correlation function are generated and analyzed for a wide range of controlling parameters.

Despite the fact that the scattering from a single rough interface is an old subject which has been studied extensively, most studies have been concerned with the solution of spectral distribution of the scattered field. Little has been done in applying modern data processing software such as MATLAB in solving these problems in time domain. The dynamic simulation of the scattered fields and other acoustic phenomena provide a vivid presentation of the acoustic fields, which not only eases the way of communication with others but also provides a perfect tool for classroom demonstration. Therefore, it is highly desirable that a complete toolbox in acoustic wave propagation in an oceanic environment is available, and, in this regard, the present study serves as an initiation of the development along this line.

Acknowledgments

I am gratefully indebted to Professor Jin-Yuan Liu for suggesting this thesis problem and for guiding it to its completion. His guiding hand is evident throughout this thesis. As faculty advisor, he encouraged individual expression by granting complete freedom in developing the analysis, yet was *always* available for judicial advice. I had *never* left his office without gaining more understanding of the investigated problem throughout this study. His dedication and commitment to guidance of his students have almost completely changed my view for being a mentor, and I hope, some of his approaches are now also my own. My indebtedness to him extends far more beyond my capability of exercising this language.

I would also like to express my gratitude to the members of my thesis review committee for their time and suggestions. The thesis committee members include Professor C. C. Wang in our Institute, Professor G. P. Too in the Department of Naval Architecture and Marine Engineering at National Cheng Kung University, Professor S. S. Leu in the Department of Naval Architecture Department at National Kaohsiung Institute of Marine Sciences and Technology, and Professor. B. F. Chen in the Department of Marine Environment and Engineering at this University. My special thanks go to Professor C. C. Wang; In particular, I have greatly benefited from his advice on editorial and MATLAB comments.

Special thanks are also due to my officemate, Mr. Nan, from him I have gotten a lot of help during the preparation of this thesis work. Also, I would like to thank all of my classmates for their encouragement.

The work was supported in part by National Science Council through contract NSC87-2611-E-110-001; to them I would like to express my profound thanks for their financial support.

Finally, I wish to express my most grateful thanks to my parents for their spiritual and financial support throughout the years at NSYSU. Without their understanding and support I would not have been able to give full attention to this work and to complete it successfully.

另一份感受...

這是我第二個碩士學位，因為我選擇了一條與別人比較不一樣的路子，所以有一些些感想或許可做為學習過程中的一點註腳。

對於水中聲學的認識乃緣由大四時修了劉老師的一門「水中聲學與應用」的課。在這門課中，由於修課的學生很少，因此有很多機會與老師討論問題。當然，學生少並不一定足以構成相互討論問題的動機，其中最主要的原因乃在於老師很強調對問題基本原理的探討，因此引發我對問題追根究底的學習態度，每每一有問題就提出發問，而且都能獲致滿意的答覆。之後，在幾次偶然的機會中，側聽到老師與學長在 Independent Studies 的課程上討論論文問題時，都能針對學長所提的問題給予適當的指引，並在獲致結果後對數字後面所代表的意義，做深入的探討與分析。這種追求 Why 的因素在我大學時期就一直在我心裡發酵。

接著，在我進入研究所之後又選修了另一門較深入的課程「海洋震聲學」，在這門課中探討有關水中聲學的核心理論，這時我理解到理論對於物理現象詮釋的完美性，更知曉在不同領域當中有很多相通的物理原理，甚至於有很多的理論都可應用在前一論文有關結構分析的探討上，這也正是劉老師常強調的物理原理的貫穿性(unification)。因此，引發我對水中聲學進一步學習的動機。在前一碩士學位即將完成的一次午餐中，諮詢劉老師有關學習的途徑時，老師鼓勵我出國進修，然而礙於我對此學門認知僅止於課程的層面上，且英語語言能力亦有待加強，因此，在思索之後決定跟隨劉老師做一篇有關水中聲學的論文，且以英文撰寫以便增強語文能力。

疏爾間，在海下技術研究所近一年時間已經過去，完成這篇論文也算達成初衷。然而，更令我驚訝的是感受到學海的浩瀚以及追求完美所需擁有的內涵與秉持的意志力。在海下所的一年當中，付出了相當的心力從老師那裡學習到做事的嚴謹性、完美性，也深深的感受到老師的「總體能量(general capacity)」以及對學理的洞悉力更是我望塵莫及，有時思及至此，不免心生悵然與挫折，然而老師卻在這節骨眼上笑稱「你終於進步了，因為這是 "Still water runs deep" 的道理」，我希望眞的是如此。

前不久中研院院長李遠哲先生在大學博覽會上說了一句令我觸目心驚的話，他說「學位是最沒有用的東西」。這樣的說法我不竟然同意，可是，如果稍加修改成「假如在追求學位的過程當中，僅追求學位的頭銜而未追求到學位的內涵，則學位是最沒有用的東西」，則我百分之百的同意，因為果眞如此，學位是拿來嚇唬人的名器，這也是我們社會的問題。以我現在的理解，學位的內涵至少包括學習過程當中對於基本學理的追求、做事能力的增進、意志力的養成、獨立思考能力的培養、眼光的放大等，這怎能說是沒有用的東西呢？怕的只是做不到而已。

學海無涯，我想我只是匍匐到學門的邊緣而已，不過，在這條道路上我應該已經有了一個起步。在過去一年當中，我感謝所有幫過我忙的人，特別是我的指導教授以及王兆璋老師，他們眞的有很多值得學習的地方，且都全然不吝的教導我，讓我在海下所豐富的過了一年。

對於學弟妹我有一點點「交代」。有道是「師父引進門，學道在個人」。因此，好的師父雖然不是學道的充分條件，卻是絕對的必要條件。老師所指定的論文題目，不僅要是「創新而適當」的問題而且要是「思考過」的問題，這也許是考驗老師的地方。如此，當你百般思索不解的問題或是論文墜入一個不著邊際的深坑時，老師方能犀利的指點而將問題迎刃而解，那種 "realization" 感覺眞好。選擇一個好的指導老師，可以學得自在、學得豁然，而這也是我近一年來在海下所的另一份感受。

1998.7.27
於西子灣

TO
MY PARENTS
FOR THEIR
UPBRINGING
AND
ENCOURAGEMENT
THROUGHOUT THE YEARS AT
NSYSU

Contents

1 Introduction **1**

1.1 Background and Motivation 1

1.2 A Concise Survey of Literature 3

1.3 Objectives 5

1.4 Scopes of the Thesis 6

2 Random Rough Surfaces **7**

2.1 Stationarity and Ergodicity 7

2.2 Height Probability Density Function 10

2.2.1 Gaussian Height Distribution 11

2.2.2 Joint Probability Density Function 12

2.3 Surface Correlation Function 13

2.4 Power Spectrum 14

2.4.1 Gaussian Power Spectrum 15

2.4.2 Goff-Jordan Power Spectrum 15

2.4.3 Gaussian Versus Goff-Jordan Power Spectrum 18

2.4.4 Pierson-Moskowitz Power Spectrum 18

2.5 Artificial Generation of Random Surfaces 20

2.5.1 Realizations of Gaussian Power Spectrum 24

2.5.2 Realizations of Goff-Jordan Power Spectrum 24

2.5.3 Realizations of Pierson-Moskowitz Power Spectrum 24

2.6 Summary 27

3 Scattering From Perfectly Reflecting Surfaces **33**

3.1 Prelude: Rayleigh Reflection Problem 33

3.2 Spectral Regions 39

3.3 Dynamic Simulation for Rayleigh Reflection Problem 41

3.4 Scattering From Perfectly Reflecting Rough Surfaces 42

3.4.1 Formulation of the Scattered Field 43

3.4.2 Validity of the Perturbation Approximation 46

3.5 Scattering From One-Dimensional Periodic Surface 47

3.6 Scattering From Random Rough Surfaces 48

3.6.1 Random Surface With Gaussian Spectrum 48

3.6.2 Random Surfaces With Goff-Jordan Spectrum 49

3.6.3 Random Surfaces With Pierson-Moskowitz Spectrum 50

3.7 Summary 50

4 Intensity and Correlation of the Scattered Field **51**

4.1 Average Intensity 51

4.2 Scattering Coefficients 52

4.3 Correlation Function of the Scattered Field 57

4.4 Summary 62

5 Scattering From an Interface over a Penetrable Layered Medium **63**

5.1 A Realistic Model 64

5.2 General Perturbation Theory for Wave Scattering From Rough Surfaces Over a Stratified Medium 65

5.2.1 Wave Equation for Nonhomogeneous Media 65

5.2.2 Solutions of Wave Equation for Homogeneous Media 66

5.3 Solution for Rough Boundaries 68

5.4 Numerical Examples 70

6 Conclusions **73**

A Derivation of Correlation For Amplitude Spectrum **74**

B Scattering From an Interface Over a Medium With Continuous Varying Sound Speed and Density **76**

B.1 Introduction 76

B.2 Solutions for Unperturbed Problem 76

B.2.1 Density Stratification 77

B.2.2 Sound Speed Stratification 78

B.2.3 Solutions of the Wave Equation 78

B.3 Linear Systems 80

B.3.1 Wavenumber Integrals 80

B.3.2 Unperturbed Problem 81

B.3.3 Perturbed Problem 82

B.4 Summary 83

Bibliography **84**

Color Plates follow page **87**

List of Figures

1.1 Schematic diagram of rough surface scattering. 2

2.1 Sample surfaces of a rough sea. 8

2.2 A zero-mean Gaussian distribution with standard deviation σ. 12

2.3 Gaussian surfaces of the same RMS height (5 m) but different correlation lengths. (a) $\lambda_0 = 17$ m, (b) $\lambda_0 = 10$ m, (c) $\lambda_0 = 30$ m. 14

2.4 Definition of correlation length based upon Gaussian correlation function. 14

2.5 Goff-Jordan correlation function and its power spectrum for $H = 5$ m, $k_s = 0.86$ m^{-1}, $k_n = 2.14$ m^{-1}, $\zeta_s = 109.3°$, and $\nu = 0.5$. 17

2.6 Roughness power spectra. 18

2.7 Pierson-Moskowitz frequency spectrum as function of wind speed (in m/s). . . . 20

2.8 Pierson-Moskowitz wavenumber spectrum with $U = 10$ m/s. 21

2.9 Pierson-Moskowitz wavenumber spectrum with $U = 14$ m/s. 22

2.10 Three realizations for Gaussian power spectrum with RMS 5 m and correlation length 17 m. 23

2.11 Isotropic Gaussian power spectrum with $\lambda_1 = \lambda_2 = 15$ m and $\sigma = 5$ m. 25

2.12 Non-isotropic Gaussian power spectrum with $\lambda_1 = 10$ m, $\lambda_2 = 60$ m and $\sigma = 5$ m. 26

2.13 Goff-Jordan spectrum and its realization for $k_0 = 0.15\,\mathrm{m}^{-1}$, $H = 5$ m and $\nu = 1.0$. 28

2.14 Goff-Jordan spectrum and its realization for $k_s = 0.03\,\mathrm{m}^{-1}$, $k_n = 0.1\,\mathrm{m}^{-1}$, $\zeta_s = 30°$, $H = 5$ m, and $\nu = 1.0$. 29

2.15 The realization of Goff-Jordan spectrum for $k_s = 0.03\,\mathrm{m}^{-1}$, $k_n = 0.1\,\mathrm{m}^{-1}$, $\zeta_s = 30°$, $H = 5$ m, and $\nu = 1.0$. 30

2.16 Pierson-Moskowitz wavenumber spectrum with $U = 12$ m/s. 31

2.17 Pierson-Moskowitz wavenumber spectrum with $U = 20$ m/s. 32

3.1 Plane wave reflection from and transmission across a plane interface between two fluid media. 34

3.2 Reflection coefficient as a function of grazing angle for a hard-bottom half-space. Solid curve is for the modulus and the dashed curve is for phase. 36

3.3 Transmission coefficient as a function of grazing angle for a hard-bottom half-space. Solid curve is for the magnitude and the dashed curve is phase. 36

3.4 Reflection coefficient as a function of grazing angle for a soft-bottom half-space. Solid curve for magnitude and dashed curve for phase. 38

3.5 Transmission coefficient as a function of grazing angle for a soft-bottom half-space. Solid curve for magnitude and dashed curve for phase. 38

3.6 Spectral domains for a hard bottom, $k_2 < k_1$. 39

3.7 Spectral regions for a soft bottom, $k_1 < k_2$. 40

3.8 Coordinate system of a rough surface. 43

3.9 Sample periodic rough surfaces. 48

4.1 Intensity as function of grazing angles and wind speeds. 53

4.2 Coordinate system for the scattered field. 54

4.3 Scattering coefficients for rigid isotropic Gaussian spectrum with RMS height of 5 m, and four correlation lengths: 5, 15, 25, and 50 m. 55

4.4 Scattering coefficients for pressure-release isotropic Gaussian spectrum with RMS height of 5 m, and four correlation lengths: 5, 15, 25, and 50 m. 56

4.5 Horizontal correlation function for Pierson-Moskowitz power spectrum with wind speed 12 m/s. The plane incident upon the surface normally. 58

4.6 Horizontal correlation function for Pierson-Moskowitz power spectrum with wind speed 12 m/s. The plane incident upon the surface with 45° incident grazing angle and along the direction of the wind field. 59

4.7 Horizontal correlation function for Pierson-Moskowitz power spectrum with wind speed 12 m/s. The plane incident upon the surface with 45° incident grazing angle and normal to the direction of the wind field. 60

4.8 Correlation function for Pierson-Moskowitz power spectrum with wind speed 20 m/s. The plane incident upon the surface normally. 61

5.1 A realistic model. 64

5.2 A model for discretized horizontally-stratified medium. 65

5.3 Coordinate system of a rough surface 69
5.4 Scattering spectrum for correlation length 1 m. 71
5.5 Scattering spectrum for correlation length 5 m. 72
5.6 Scattering spectrum for correlation length 10 m. 72

All graphs and figures in this thesis are originally produced by the author.

Nomenclature

A	amplitude spectrum of the roughness
B	boundary operator defined by Equation (5.20)
B_s	spatial correlation function
c	sound speed
C	correlation function
C_{hh}	autocovariance function defined by Equation (2.18)
D	*fractal dimension* defined in Equation (2.22)
f	frequency in Hz
F	function of random variable
g	acceleration due to gravity
h	root-mean-square height of the roughness defined in Equation (3.40)
H	root-mean-square height of the roughness defined in Equation (2.18)
I	intensity
k_n	characteristic wavenumber in the Goff-Jordan roughness spectrum defined in Equation (2.24)
k_s	characteristic wavenumber in the Goff-Jordan roughness spectrum defined in Equation (2.24)
k_0	characteristic wavenumber defined in Equation (2.25)
$\mathbf{k}$	medium wavevector
$\mathbf{k_r}$	horizontal wavevector
l	correlation length defined in Equation (3.40)
L	linear dimension of the area
m	mass ration
m_s	*scattering coefficient*
n	index of refraction
p	probability density function, or acoustic pressure
P	probability distribution function, or power spectrum, or *Rayleigh parameter*

$\mathbf{p}$	roughness wavevector
$\mathbf{q}$	scattered horizontal wavevector
Q	matrix defined by Equation (2.20)
R	reflection coefficient, or
	distance from the observation point to the scatterer
$\mathbf{R}$	separation between the two points chosen to be correlated
$\mathbf{r}$	coordinate in range
$\bar{\mathbf{r}}$	horizontal separation
s	scattered field
S	area of the mean surface defined in Equation (2.14), or
	Pierson-Moskowitz frequency spectrum
T	transmission coefficient
t	time
u, U	displacement in x-coordinate, or
	U is the wind speed in Equations (2.26) and (2.27)
$\mathbf{v}$	vector of the particle velocity
v, V	displacement in y-coordinate
w, W	vertical displacement
z	depth coordinate
z_s	source depth

Greek Symbols

α	vertical component of the compressional wavevector,
	$\alpha = \sqrt{k^2 - K^2}$
β	vertical component of the shear wavevector
δ	Dirac delta function
η	vertical separation
γ	roughness elevation
κ	bulk modulus
λ_0	correlation length defined in Equation (2.14)
λ_1, λ_2	surface correlation lengths in the x and y directions, respectively
μ	mean value of the rough surface defined in Equation (2.9)
ν	parameter in Goff-Jordan roughness power spectrum defined in Equation (2.18)
ω	angular frequency
ϕ	azimuth angle
ρ	density
σ	root-mean-square height of the rough surface
ζ	parameter in Goff-Jordan roughness power spectrum defined in Equation (2.24)

Superscripts

$\star$	complex conjugate
$+$	upgoing wave
$-$	downgoing wave
T	transpose of a vector/matrix
θ	tangential direction

Subscript

i	i^{th} layer
s	spatial average
ω	quantities at frequency ω

Special Symbols

$\tilde{}$	Fourier coefficients of the related quantities
$\langle\,\rangle$	ensemble average

... I have only knocked on
the door of *Acoustic Wave Scattering* [Chemistry], and I see
how much remains to be said.

— with poetic license from *The Six-Cornered Snowflake*,
Johannes Kepler, 1611.

Chapter 1

Introduction

1.1 Background and Motivation

The problems of rough surface scattering have long been an interest in underwater acoustics. The reasons are simple: both the sea surface and the seabed are rough. Any practice exercising long-range wave propagation in an oceanic environment, particularly in shallow water, must consider the effect of these two surfaces, simply because of the fact that both two surfaces are strong scatterers. As a result of interactions with these two boundaries, the acoustic field not only becomes random but also attenuates rapidly as the range of propagation increases, rendering applications of underwater acoustics a very challenging problem.

However, the effects are not all bad, as evidenced by many recent studies, in which it was demonstrated that the scattered field carries many useful information, allowing the inversion of the environmental parameters as well as the source geometry. In order to achieve these purposes, the first step is to model the acoustic field accurately. The main theme of this study is to analyze the rough surface scattering from an interface closely resembling the two major rough surfaces in the oceanic environment, i.e., the ocean surface and the seabed.

Practically speaking, the ocean surface separating the air and water may be considered as a perfectly reflecting surface, owing to the fact that the impedance of water is nearly 3500 times larger than that of air. Therefore, if a plane wave impinges upon the sea surface which is assumed to be completely flat, then the incident plane wave is coherently reflected into the specular direction with a phase shift of 180° relative to the incoming wave.

If the sea surface is rough, as it should be treated in reality, the situation becomes more complicated. Figure 1.1 schematically demonstrates the effect of roughness. The figure shows that for a flat surface [Case (a)], the wave is reflected into the specular direction without disturbance, and for slightly rough surface [Case (b)], the wave is scattered into certain range of angles with major energy still propagating in the specular direction. As the surface becomes even rougher [Case (c)], the scattered waves spread over a wider angle, and eventually, when the

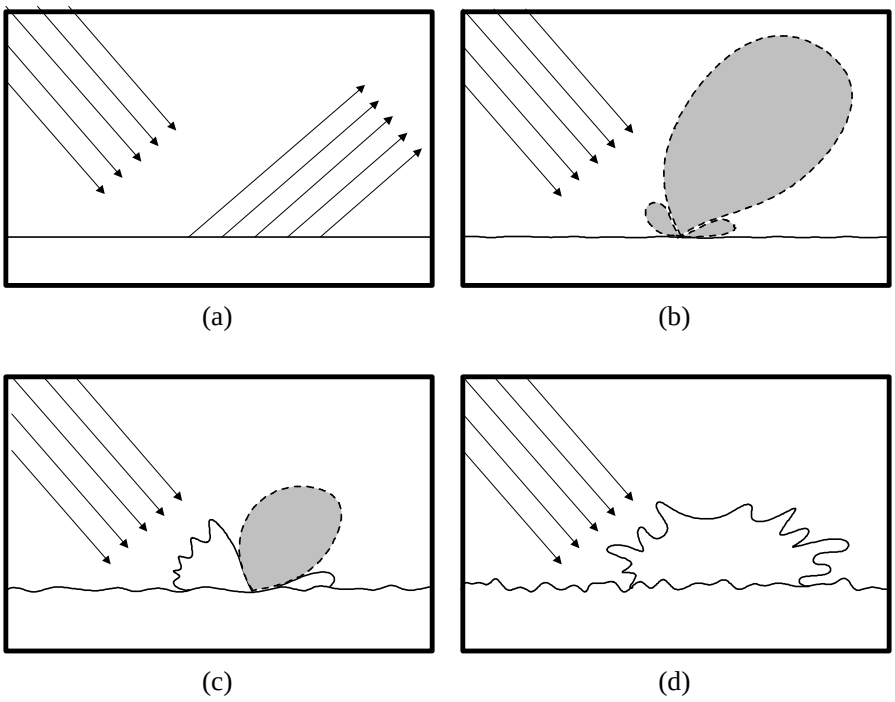

Figure 1.1: Schematic diagram of rough surface scattering.

surface becomes very rough [Case (d)], the scattered wave field shows no preferred angle, with the energy randomly spreading all over space, and the specular reflection ceases to exist.

A plane wave impinges upon the seafloor will also demonstrate a similar scenario, except that in this case the seafloor is relatively hard with respect to water. In real situation, the seafloor should be considered as an elastic medium, allowing energy to be penetrated into bottom through both compressional and shear waves. However, in this study, we shall approximate the seabed as a rigid rough surface, and consider the effect of roughness on acoustic scattering in this case.

Despite the fact that the scattering from a single rough interface is an old subject, most studies have been concerned with the solution of spectral distribution of the scattered field. Little has been done to examine the problem systematically in all aspects. Even though, there are ample results which are available in literature, many of them are found to be quite theoretical, and more often than not, the formulation is lengthy and esoteric, making the whole theory difficult for comprehension and application.

Modern programming language and data processing software such as MATLAB have advanced to the point that many tedious computations and data manipulations may be accomplished by the kernels built in the language with much faster pace than the traditional methods, so that the task can be resolved more efficiently and effectively. For example, dynamic simulation of the scattered fields and other acoustic phenomena may be obtained with moderate computational effort and the results presented by its graphical capacity offer a vivid presentation of the acoustic fields, which not only ease the way of communication with others but also provide

a perfect tool for demonstrations. It is therefore highly desirable that a complete toolbox in acoustic wave propagation in an oceanic environment is available, and the present study serves as an initiation of the development following this line.

1.2 A Concise Survey of Literature

As mentioned previously, the topic of wave scattering from randomly rough surfaces has been a subject of interest for many decades. This becomes the case because the subject covers a wide range of areas involving wave interaction with surfaces. These fields of study include sonar detection, radar imaging, medical ultrasonics, solid-state physics, optics, and ultrasonic non-destructive testing, to name a few. To some extent, all real surfaces are rough with respect to the wavelength, especially for high frequency waves, and therefore, the problems of wave scattering from rough surface naturally arise in the study of the above-mentioned areas.

The most frequently cited book on wave scattering from rough surfaces is that of Beckmann and Spizzichino [3]. The book considers Kirchhoff solutions of electromagnetic wave scattering from periodic and random surfaces; most results of the book are equally well be applied to acoustic waves. The later part of the book discusses experimental study of the effects of surface roughness on the reflection of terrestrial bodies such as Moon, Sun, and Earth. More recently, Bass and Fuks [1] wrote a book on the subject in which both perturbation and Kirchhoff theory are considered. Moreover, this book includes some complicating effects such as surface self-shadowing and multiple scales of roughness. The effect of multiple scattering is also considered through integral equation method.

In the last decade, two new volumes on the wave scattering from rough surfaces were added into literature: one by Ogilvy [34] and the other by Voronovich [49]. The book by Ogilvy is a general book on the subject which serves as a review of the theories developed up to the date of its publication. Discussion on the nature of rough surfaces is first provided, followed by a development of methods by the perturbation and Kirchhoff theories. Both scalar and vector waves are included. The book concluded with a summary of numerical simulation techniques. On the other hand, the book by Voronovich is theoretical in nature, which represents the most recent publication on the subject. The book covers broad range of issues including traditional topics such as perturbation method and Kirchhoff approximation, and non-traditional topics such as small slope approximation, phase perturbation technique, phase operator method for Dirchlet problems, and others. The scattering of rough boundary in a waveguide environment is also discussed in the book.

In addition to the above-mentioned books, which obviously represent only a small fraction of relevant books in the literature, there are *numerous* articles published in various journals in the related fields, notably the Journal of Acoustical Society of America (JASA). Here, it is emphasized that we make no attempt to conduct a complete survey on the whole subject, except

concentrating on the articles which are closely related to the presents analysis.

An earlier survey of literature on acoustic wave scattering from the sea surface was performed by Eckart [9] and another by Fortuin [10] in 1960's, in which the authors discussed the scattering from both random and periodic surfaces, and the results predicted from theories were compared with the experimental data. During 1970's, the advent of modern computing facility had greatly enhanced the ability of the investigation on subject. To list a few, these include Lynch [28], Fortuin and Boer [11], Caruthers and Novarini [7], Novarini and Caruthers [33], Galybin [13], Kuperman [21], and many more. These work has been largely emphasized on the development of numerical models which are capable of solving scattering problems from various kinds of rough surfaces.

The 1980's has entered a booming period of research in underwater acoustics. Theories for wave scattering in an oceanic waveguide were developed. Kuperman and Ingenito [24] formulated a model for the calculation of the spatial properties of the noise field produced in a stratified ocean by the action of wind at the surface, and the results show that the sound-speed profile and the presence of the bottom can be important in determining the spatial properties of the noise field. Later, Kuperman and Schmidt [22] extended a previously developed boundary perturbation method [21] to treat scattering at a randomly rough interface which separates viscoelastic media. Before the end of the decade, the same authors developed a unified, self-consistent perturbation approach to rough surface scattering in stratified ocean, in which a boundary-condition operator formulation was developed. The new approach makes the formulation of scattering compatible with existing propagation models for stratified media citeberman, allowing simulation of scattering loss of the coherent component of the field due to the generation of a scattered field in the stratified fluid-solid media with an arbitrary number of rough interfaces [23]. Liu *el al.* [26, 27] combined the theories due to Kuperman [24] and Schmidt [23] to study the scattering from rough interfaces due to noise sources near the surface of the ocean waveguide.

Dashen *et al.* [8] developed a formalism that describes the scattering of a wave off a finite object. The scattering cross section is evaluated numerically and it was concluded that the observed cross section for scattering near the ocean surface cannot be explained by ocean surface scattering alone. Goalwin [14] applied the method of stationary phase approach to the calculate the correlation of the acoustic field scattered from a two-dimensional random sea surface, however, the results were limited to some particular separations in space. Thorsos and Jackson [48] and Thorsos [47] examined the validity of the methods which are frequently employed in the study of rough surface scattering, and later applied the theory to examine the validity of acoustic scattering from a Pierson-Moskowitz sea surface.

Even though the relevant literature on rough surface scattering is abundant, as evidenced by the above short review, it is still not readily available in the literature in which a systematic development on various aspects of scattering from sea surface and seabed is made. For example, it is still yet to be seen that a systematic presentation of scattering characteristics of sea surface

in terms of a complete two-dimensional correlation function and of its spatial realization. The present analysis attempts to deal with this old subject with a new look, within which the complicated formalisms in terms of mathematics are deliberately suppressed in favor of graphical and dynamical presentations. In this way, the author wish that the present study may illuminate many obscure phenomena frequently undermined by the unfriendly formulation employed on the subject. At minimum level, this thesis launches a planned project in our research group, and is intended to serve as a source of reference for many years to come.

1.3 Objectives

The objectives of this thesis project are:

1. To study the characteristics of rough surfaces which are relevant to oceanic environment, in particular, the rough sea surface and seabed;
2. To study the plane wave scattering from rough sea surface and seabed, which are modeled as a pressure-release or rigid surface, respectively.
3. To develop a software using MATLAB which is capable of demonstrating the acoustic propagation and scattering; and
4. To propose a model which closely resembles the seabed interface.

Both the sea surface and the sea floor are characterized by its own special roughness spectrum. The scattering for a plane wave impinging upon these surfaces provide many useful information both for the scattered field and for the rough surface themselves. Our interests include understanding of the energy spectrum and correlation of the scattered fields in relation with the various roughness spectra employed in the simulation.

The later part of the thesis concerns with a problem which addresses the rough interface scattering from a semi-infinite space with continuous varying sound speed and density; this problem attempts to simulate the realistic seabed conditions. A wave-theoretical model which describes the problem will be developed, and current existing software package OASES will be invoked to analyze the problem.

Our laboratory has launched an effort[1] to develop a MATLAB-based toolbox which deals with acoustic propagation problems in marine environment. The present analysis serves as a primal study, and is expected to extend to become a comprehensive code so that the capacity is enhanced to solve for many ocean acoustic problems of our interests.

[1] The endeavor is temporarily named **Project Poseidon**, Poseidon being the god of sea according to Greek mythology.

1.4 Scopes of the Thesis

Chapter 2 of this thesis is to study the random rough surfaces encountered in oceanic environment. The basic concepts and assumptions for a random process are reviewed. Various ways for the presentation of a rough surface are studied and analyzed. The chapter serves as a basis for interpretations of many results obtained in later chapters.

The first part of Chapter 3 is to demonstrate the Rayleigh reflection problem in a dynamic manner. This problem allows us to gain appreciation of reflection and transmission which are not achievable in line graphs. The second part of this chapter is to study the scattered field in spatial domain. The random scattered fields are directly generated using the exact integral formulas for the scattered fields.

Chapter 4 deals with the statistics of the scattered fields, including the average intensity, scattering coefficients and spatial correlation of the scattered fields.

Chapter 5 concerned the rough surface scattering from a semi-infinite space with continuous sound speed and density variation. A model is proposed and derived. Preliminary results will be generated by modern acoustic software OASES. The last chapter summarizes what have been done in this thesis, followed by two appendices within which a formulation for a particular problem is derived.

Chapter 2

Random Rough Surfaces

Many surfaces in nature are characterized by their unpredictability, which means that any part of the surface is not derivable from the knowledge of its adjacent parts in a deterministic manner. This type of surface is referred to as random surface. In this chapter, we shall discuss the characteristics of random rough surfaces, in particular, the sea surface and the seabed. Even though this is not a new topic, many reports on the subject are fragmental and limited. Therefore, a consistent presentation deserves a special attention.

There are four aspects to be emphasized in relation to the description of a random rough surface in this chapter: *probability density function*, *correlation function*, *power spectrum*, and *realization*. Each one of them demonstrates a particular feature of a rough surface, and in view of its non-deterministic nature, many discussions in this chapter have lent themselves to the theories of probability and statistics. As such, we shall have a brief discussion on these subjects.

We shall begin with a review of some important concepts about a random process, followed by a discussion of the description of a random surface in terms of its probability distribution and correlation functions. We then analyze and compare various models which are used to describe the power spectra of the sea surface and seafloor. Artificial random rough surfaces corresponding to the various power spectra are generated and discussed. The chapter is concluded with a few comments with respect to the applications of these statistical models on the seafloor topography in combination with acoustic image obtained by a sounding system.

2.1 Stationarity and Ergodicity

In this section we shall briefly review some important concepts about a random process, and also place the basic assumptions which are invoked throughout this study. To facilitate our discussion, we shall consider a surface which is intrinsically random in nature, the one with which we are really concerned, that is, the surface of the random sea.

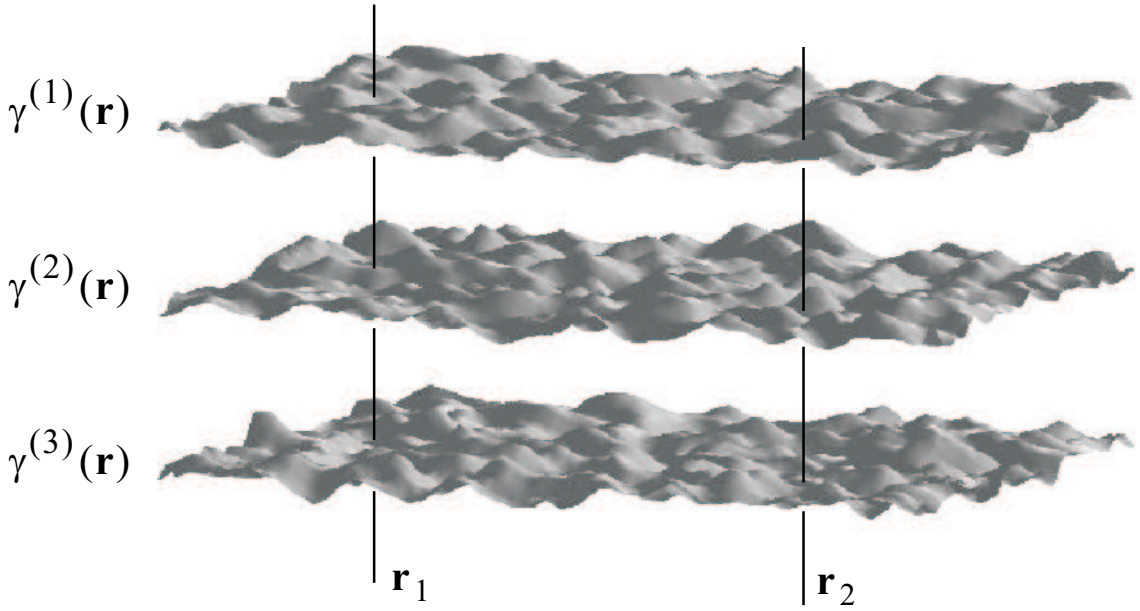

Figure 2.1: Sample surfaces of a rough sea.

Suppose at a particular moment, a snap shot of the sea surface is taken, it is conceivable that the surface elevation demonstrates a random distribution. If later on, other snap shots are taken under the *same* conditions, then the compilation of these snap shots forms a set of random surfaces as shown in Figure 2.1. This collection of surfaces taken at the same conditions is referred to as *ensemble* of the random sea surface; each of which in the ensemble may be a representative of the rough sea surface, and is referred to as a *sample*.

In theory, the number of the samples in the ensemble should be denumerably infinite, and each sample should be infinite in length. Clearly, this is only conceivable but not realizable, and therefore, an ensemble is only a conceptual object.

Owing to its stochastic nature, the description of a random surface requires the use of the probability and statistics theories. We therefore review a few essential concepts in these subjects in relation to the description of random processes.

Let the ensemble be denoted by $\left\{\gamma^{(k)}(\mathbf{r})\right\}$, where $\gamma^{(k)}(\mathbf{r})$ represents the kth sample of the random processes as a function of range $\mathbf{r}$. The variable γ is a random variable representing the deviation of the surface from a reference level. It is obvious that the random variable γ depends upon the position $\mathbf{r}$. Now, select a particular position $\mathbf{r}_1$, and consider the set $\left\{\gamma^{(k)}(\mathbf{r}_1)\right\}$. The set of values may be used with any function, say, F, to give a function of random variable, $F\left(\gamma^{(k)}(\mathbf{r}_1)\right)$. Clearly, the value of the function F is also a random number, which can be anything within reason and each will lead to a statistic. Here we are concerned with the function F, which is the γ value itself.

The mean value of the random variable $\gamma(\mathbf{r}_1)$ is defined as

$$\langle \gamma(\mathbf{r}_1) \rangle \equiv \lim_{N\to\infty} \frac{\sum_{k=1}^{N} \gamma^{(k)}(\mathbf{r}_1)}{N} \tag{2.1}$$

This is called ensemble average, or statistical average, or mean value. If we now choose another location, $\mathbf{r}_2$, and compute the ensemble average, then, we expect that for the most general case they are not equal, i.e.,

$$\langle \gamma(\mathbf{r}_1) \rangle \neq \langle \gamma(\mathbf{r}_2) \rangle \tag{2.2}$$

It should be stressed here that, for a general random process, the ensemble average is completely different from the spatial average, which is defined for each sample as follows:

$$\left\langle \gamma^{(k)} \right\rangle_s \equiv \lim_{R\to\infty} \frac{1}{2R} \int_{-R}^{R} \gamma^{(k)}(\mathbf{r})\, d\mathbf{r} \tag{2.3}$$

Here the subscript s stands for "spatial average". However, there are cases in which the spatial average may be taken as ensemble average; those will be discussed later.

The mean value is only the simplest statistics, or the first order statistics, of a random process. The most important aspects of a random process are embedded in the correlation among any specified number of points. A correlation function, defined as an ensemble average of the product between the random variables, is a measure which gauges the coherence or degree of consistency in a statistical sense, among the points under consideration. Therefore, a good correlation would mean higher degree of coherence or less random, and vice versa. If the variables being correlated are the same, it is referred to as auto-correlation function, and if different, it is referred to as cross-correlation. For example, $\langle \gamma(\mathbf{r}_1)\gamma(\mathbf{r}_2) \rangle$ is the two-point auto-correlation (second-order statistics) or simply correlation, which in a sense relates what the process is doing in the location $\mathbf{r}_1$ to what is doing in the location $\mathbf{r}_2$. Likewise, there are three-point correlation (third-order statistics) $\langle \gamma(\mathbf{r}_1)\gamma(\mathbf{r}_2)\gamma(\mathbf{r}_3) \rangle$, and so on. Processes such as those described above are of the most general kind. The governing probability functions as well as the statistics appropriate to each instant may be different. Such very general random processes are quite common in nature, and these are referred to *nonstationary random processes*; their properties can only be calculated from the ensembles.

In practice, however, it is impossible to have a full collection of the samples, and assumptions will have to be made to relieve the difficulties. Suppose we have a random process whose statistics are invariant with respect to its argument. That is to say that, for *all* $\Delta\mathbf{r}$,

$$\langle \gamma(\mathbf{r}_1) \rangle = \langle \gamma(\mathbf{r}_2) \rangle = \langle \gamma(\mathbf{r} + \Delta\mathbf{r}) \rangle \tag{2.4}$$

and

$$\langle \gamma(\mathbf{r}_1)\gamma(\mathbf{r}_2) \rangle = \langle \gamma(\mathbf{r}_1 + \Delta\mathbf{r})\gamma(\mathbf{r}_2 + \Delta\mathbf{r}) \rangle \tag{2.5}$$

and similarly for high-order statistics, then this type of random processes are called *stationary*. This imposes a very strong restriction on the properties of the random process, and is therefore

unlikely to exist in practice. However, if the statistics is invariant only for the first and second-order, then it is referred to as *weakly stationary*, which is more likely to exist in reality.

Even under the assumption of weakly stationarity, one still faces the difficulty to obtain the statistics from the ensembles, simply because that very often the only data available are the one-time measurement along the process coordinate (e.g., time or spatial). Under these circumstances, one is forced to relegate even further, and pursue the statistics based upon one-time data. We therefore assume that the coordinate average may be used to substitute for the ensemble average, i.e.,

$$\left\langle \gamma^{(k)} \right\rangle_s = \langle \gamma(\mathbf{r}) \rangle \tag{2.6}$$

This places an even stronger assumption, in that it implies that the entire statistics of the random process are completely characterized by a one-time measurement. A random process possessing such characteristics is called an *ergodic process*. It is noted that if a random process is ergodic it must be stationary, as ergodicity demands that samples from a different parts of a random process all lead to the same statistical descriptions. However, the converse is not true, that is, stationarity does not guarantee ergodicity.

While in theory the measurement of the ocean surface roughness may be taken for a number of times to enable calculation of the ensemble average, an attempt to repeatedly measuring seafloor roughness to establish ensemble should not even be entertained, as evidenced by the high cost of survey, especially in the deep water environment. As such, we shall be content ourselves to make any assumptions whenever needed, no matter how strict it is, and very often we find ourselves in a compulsory situation in that the very assumption we have to make is the most stringent one, namely, the assumption of ergodicity.

2.2 Height Probability Density Function

There are essentially two aspects to the nature of a random rough surface: the spread of heights about the reference surface and the variation of these heights along the surface. The former may be described by the surface *height probability density function*, abbreviated as height p.d.f., and the later by the *surface correlation function*. In this section we shall discuss the common models which are used to describe the height probability density function.

The likelihood for an event to occur for a random variable, say x, may be specified by the probability density function $p(x)$, which is so defined that $p(x)dx$ is the probability that the random variable x lies between x and $x + dx$. In the same token, the deviation of a surface from the smooth reference surface is represented here by the random function $\gamma(\mathbf{r})$, where γ is the height of the surface from the reference surface and $\mathbf{r}$ is the position vector of points. The surface is assumed to be a continuous random process. Thus, the distribution of surface heights may be described by the height p.d.f., $p(\gamma)$.

It should be noted a probability density function has the following properties:

1. $p(\gamma) \geq 0$;
2. $\int_{-\infty}^{\infty} p(\gamma) d\gamma = 1$;
3. $p(\gamma)d\gamma = \text{Probability}\,(\gamma \leq \gamma(\mathbf{r}) \leq \gamma + d\gamma)$;
4. The function: $P(\gamma) = \int_{-\infty}^{\gamma} p(\gamma)d\gamma$ is referred to as *probability distribution function*, which represents the accumulative probability for γ from $-\infty$ to present value γ, so that it relates to p.d.f. as $\frac{dP}{d\gamma} = p(\gamma)$.

There are many other useful properties and theorems which are very helpful in our study; those can be found from many standard textbooks, e.g., [36][41], therefore, we are not to reiterate here.

In general, the mean value of a random process is extracted to result in a zero-mean random process, so that

$$\langle \gamma \rangle = \int_{-\infty}^{\infty} \gamma\, p(\gamma) d\gamma = 0 \tag{2.7}$$

where $\langle \cdot \rangle$ denotes the spatial average. We shall be following the common practice to assume that the spatial average is the same as ensemble average, and therefore, we are implicitly to assume that the random process is ergodic. The root mean square (RMS) height of the surface is then equal to the standard deviation and is given by

$$\sigma = \sqrt{\langle \gamma^2 \rangle_s} \tag{2.8}$$

and variance is equal to σ^2.

2.2.1 Gaussian Height Distribution

Much of the literature on rough surfaces assumes that the probability density function of the height distribution are Gaussian, which means that the likelihood of the surface height to appear a given value γ is dictated by the following function:

$$p(\gamma) = \frac{1}{\sigma\sqrt{2\pi}} \exp\left[-\frac{(\gamma - \mu)^2}{2\sigma^2}\right] \tag{2.9}$$

where μ is the mean value, which will be chosen to be zero in this study. This function has a famous "bell-shaped" variation as shown in Figure 2.2. A random surface obeying Gaussian height distribution is referred to as Gaussian random surface. It can be shown that a random variable obeying the Gaussian distribution has 96% of its distribution within two standard deviations of the mean. This implies that most events are occurred near the mean value of the random variable.

Although many surfaces arising from engineering methods do not obey Gaussian distribution, those surfaces with a profile that is everywhere a cumulative effect of a large number

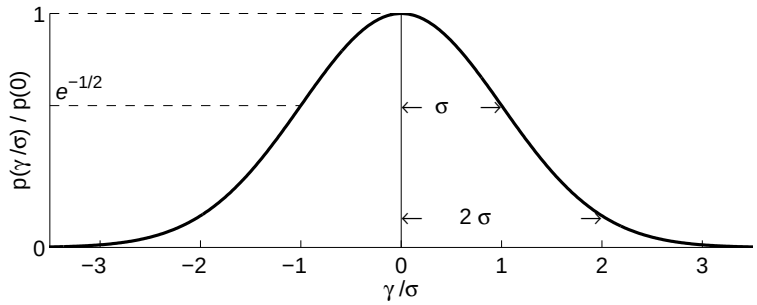

Figure 2.2: A zero-mean Gaussian distribution with standard deviation σ.

of local events are likely to be Gaussian. Therefore, surfaces produced by engineering methods such as turning are less likely to obey Gaussian height statistics than those arising from natural processes such as geographical terrain. In addition, the Gaussian function has many operational properties which are convenient for mathematical manipulation.

There are many other probability distribution functions such as Binomial distribution, Poisson distribution, Student's t-distribution, Chi-square distribution. However, since they are rarely encountered in an oceanic environment, they are not to be discussed here.

2.2.2 Joint Probability Density Function

In the previous section, we discuss the height p.d.f. at each individual point. Although a single-point height p.d.f. is most often used in describing the random surface, this function alone does not completely characterize the height distribution of a random surface. There are other structures of the randomnesses which are embedded in the higher-order surface properties, such as two-point height p.d.f., and three-point height p.d.f., etc. These are referred to as higher order surface statistics. The higher-order surface statistics are often of interest in the theory of wave scattering from such surfaces, or for the classification of measured surface profiles.

Let $p_2(\gamma_1, \gamma_2; \mathbf{r}_1, \mathbf{r}_2)$ denote the two-point height probability density function, where

$$p_2(\gamma_1, \gamma_2; \mathbf{r}_1, \mathbf{r}_2) d\gamma_1 d\gamma_2$$

is the probability that the surface height at $\mathbf{r}_1$ is between γ_1 and $\gamma_1 + d\gamma_1$ and that the surface height at $\mathbf{r}_2$ is between γ_2 and $\gamma_2 + d\gamma_2$. As an example, for a Gaussian surface that is both isotropic (see Section 2.3) and stationary, the two-point probability function takes the form

$$p_2(\gamma_1, \gamma_2, \mathbf{R}) = \frac{1}{2\pi\sigma^2\sqrt{1 - C^2(\mathbf{R})}} \exp\left\{ -\frac{\gamma_1^2 + \gamma_2^2 - 2\gamma_1\gamma_2 C(\mathbf{R})}{2\sigma^2[1 - C^2(\mathbf{R})]} \right\} \tag{2.10}$$

where $C(\mathbf{R})$ is the surface correlation function to be discussed below. Equation (2.10) has the following two limits:

$$p_2(\gamma_1, \gamma_2, \mathbf{R}) \quad \rightarrow \quad p(\gamma_1)p(\gamma_2), \text{ as } |\mathbf{R}| \rightarrow \infty \tag{2.11}$$

$$p_2(\gamma_1, \gamma_2, \mathbf{R}) \quad \rightarrow \quad p(\gamma_1)\delta(\gamma_1 - \gamma_2), \text{ as } |\mathbf{R}| \rightarrow 0 \tag{2.12}$$

It can be shown that if the single-point height p.d.f. is Gaussian, then the two-point height p.d.f. and all higher order derivatives are themselves Gaussian. Also, the higher-order derivatives of any two-point correlation function may be obtained from the surface height correlation (see Section 2.3). That is to say that the single-point height p.d.f. and the surface height correlation completely determine the height statistics and surface correlation to all orders.

The height distribution function discussed above only indicates the probability of height γ of any surface point, but it can't express the relationship among any number of surface points. The property which truly characterizes the randomnesses is embedded in its surface correlation as will be discussed below.

2.3 Surface Correlation Function

The specification of the height distribution alone does not describe the random surface. For example, in Figure 2.3 each surface has a Gaussian height distribution and an RMS height of 5 cm. However, the surface characteristic are very different. Such surfaces may be distinguished by their correlation functions, which is defined as

$$C(\mathbf{R}) = \langle \gamma(\mathbf{r})\, \gamma(\mathbf{r}+\mathbf{R}) \rangle_s = \lim_{S\to\infty} \frac{1}{S} \int_S \gamma(\mathbf{r})\gamma(\mathbf{r}+\mathbf{R}) d\mathbf{r} \tag{2.13}$$

where S is the area of the mean surface, and $\mathbf{R}$ is the separation between the two points chosen to be correlated. It should be noted that for a stationary random process $C(\mathbf{R})$ is a symmetric function and $C(0) = \sigma^2$. As $|\mathbf{R}|$ increases $C(\mathbf{R})$ will usually decay to zero, with the shape of this decay being dependent on the type of surface and the rate of decay dependent on the distance over which points become uncorrelated for truly random surface.

The theory of wave scattering from rough surfaces often assumes that surface correlations are Gaussian which is given by

$$C(\mathbf{R}) = \sigma^2 \exp\left(-\frac{|\mathbf{R}|^2}{\lambda_0^2}\right) \tag{2.14}$$

where λ_0 is called the correlation length, this being the distance over which the correlation function falls by $1/e$. However, this is only a nominal definition, different author may have different definition. If the surface is isotropic, meaning that the correlation function depends upon the separation of the points being correlated, and not the direction, then the Gaussian surface correlation function is as shown in Figure 2.4, in which the definition of the correlation length is as indicated.

The Gaussian correlation is often employed due to its simplicity, however, there are more general formulations which were proposed to include broader features of the rough surface, such as Goff-Jordan[15] correlation function which will be discussed in Section 2.4.2.

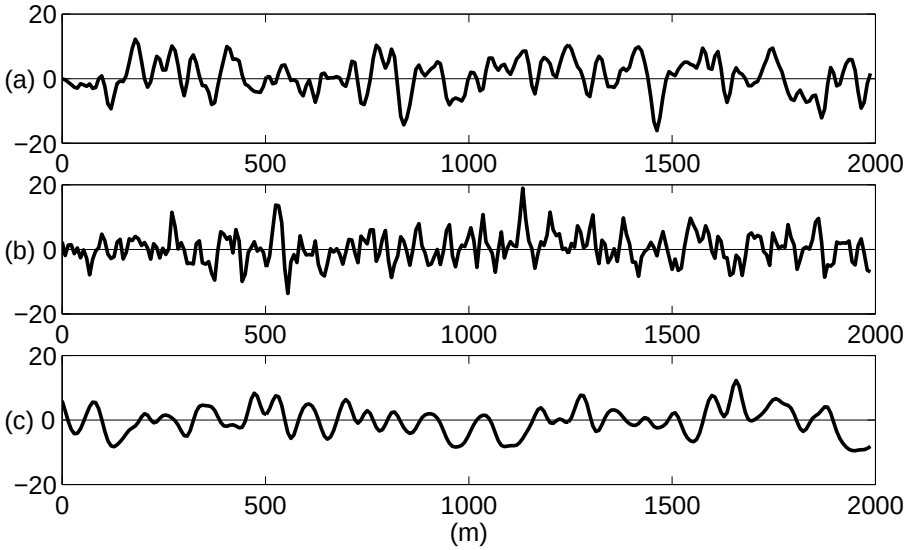

Figure 2.3: Gaussian surfaces of the same RMS height (5 m) but different correlation lengths. (a) $\lambda_0 = 17$ m, (b) $\lambda_0 = 10$ m, (c) $\lambda_0 = 30$ m.

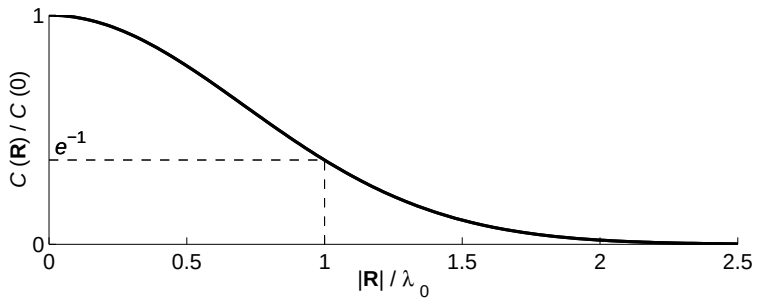

Figure 2.4: Definition of correlation length based upon Gaussian correlation function.

Next, we introduce an alternative description of a randomly rough surface, the power spectrum.

2.4 Power Spectrum

In the problems of acoustic wave scattering from random rough surfaces, many formulations of the concerned quantities are often expressed in terms of the power spectrum of the rough surface. The power spectrum is defined as the Fourier transform of the correlation function

$$P(\mathbf{k}) = \frac{1}{(2\pi)^2} \int_{-\infty}^{\infty} d\mathbf{R}\, C(\mathbf{R}) e^{-i\,\mathbf{k}\cdot\mathbf{R}} \tag{2.15}$$

The power spectrum specifies the characteristics of the rough surfaces in wavenumber

domain as opposed to the correlation function which is the description in the spatial domain. The power spectrum differs from all the previously defined surface functions, as it can describe both aspects of a rough surface represented by the RMS roughness and the correlation length. The total area under the power spectrum gives the variance, or "power", of the surface:

$$\int_{-\infty}^{\infty} P(\mathbf{k}) d\,\mathbf{k} = \sigma^2 \tag{2.16}$$

In more general case, the power spectrum may also contain parameters which are capable of describing the non-isotropy of a random field.

In this section we shall discuss and compare various power spectra and which are commonly employed in the study of ocean surface and bottom roughness.

2.4.1 Gaussian Power Spectrum

As was mentioned in Section 2.3, many studies on random processes frequently assume that the correlation function is Gaussian, and as a result of Fourier transformation, it can shown that the corresponding power spectrum is also a Gaussian. Thus, we shall often use the Gaussian spectrum to model the random field. Also, in many cases, when other models are less illustrative, the Gaussian model is applied and the results can be considered as a benchmark solution.

The Gaussian spectrum for a non-isotropic surface is

$$P(k_x, k_y) = \frac{\sigma^2 \lambda_1 \lambda_2}{4\pi} \exp\left(-\frac{k_x^2 \lambda_1^2}{4}\right) \exp\left(-\frac{k_y^2 \lambda_2^2}{4}\right) \tag{2.17}$$

where λ_1 and λ_2 are the surface correlation lengths in the x and y directions, respectively. If $\lambda_1 = \lambda_2 = \lambda_0$, the spectrum reduces to an isotropic form. The Gaussian spectrum represents an exponential decay as a function of wavenumber, which means that most "energy" of the roughness is contained in the low wavenumer regime. The implication of this energy content will be discussed later.

2.4.2 Goff-Jordan Power Spectrum

For the statistical model of the randomly rough sea floor, most perturbation approaches assume a Gaussian spectrum for simplicity. In spite of its popularity, most experimental data have shown that the spectrum of the sea floor topography tends to be a power-law rather than a Gaussian distribution [2, 12]. Thus, we shall adopt a recently proposed model by Goff and Jordan [15] which behaves as power law at the high frequency components. The model may well represent a non-isotropic sea floor topography having stationarity with respect to an elliptic "window" by five parameters: root-mean-square height H, a roughness parameter ν, two characteristic wavenumbers, k_s and k_n, and an orientation parameter ζ_s. Since we use this model extensively, This model which is based upon Ref. [15] is summarized here.

The above-mentioned five parameters are incorporated in an autocovariance function of the form

$$C_{hh}(\mathbf{x}) = H^2 \frac{G_\nu(r(\mathbf{x}))}{G_\nu(0)}, \tag{2.18}$$

with $G_\nu(r)$ defined as

$$G_\nu(r) = r^\nu K_\nu(r), \qquad 0 \le r < \infty \qquad \nu \in [0,1] \tag{2.19}$$

where K_ν is the modified Bessel function of the order ν. This correlation function describes the azimuthal variation through the dimensionless ellipsoidal norm

$$r(\mathbf{x}) = \left[\mathbf{x}^T Q \mathbf{x}\right]^{1/2} = \sqrt{q_{11}x_1^2 + 2q_{12}x_1x_2 + q_{22}x_2^2} \tag{2.20}$$

where Q is a positive-definite, symmetric matrix whose Cartesian elements q_{ij} have dimension of (length)$^{-2}$. In terms of its eigenvalues $k_n^2 \ge k_s^2$ and its normalized eigenvectors $\hat{\mathbf{e}}_n$ and $\hat{\mathbf{e}}_s$, Q may be expressed as

$$Q = k_n^2 \hat{\mathbf{e}}_n \hat{\mathbf{e}}_n^T + k_s^2 \hat{\mathbf{e}}_s \hat{\mathbf{e}}_s^T. \tag{2.21}$$

The parameters k_n and k_s play the same role as the correlation length in defining the topographic characteristics; thus $2\pi/k_n$ and $2\pi/k_s$ represent, respectively, the characteristic length of the minor and major axis of the ellipsoidal topography. The variable ζ_s is an orientation parameter which is conveniently chosen to be the angle between the major axis and y-axis, measured clockwise from y-axis. This model is capable of describing the non-isotropic feature of the sea floor morphology such as the local strikes formed by the abyssal hills commonly found on the ocean floor.

The roughness parameter ν determines the behavior of the autocovariance function as r approaches to zero lag, which also determines the roll-off rate of the power spectra at the high frequencies. In the physical terms, ν measures the degree of the roughness, with the limiting cases of unity and zero corresponding to a random surface with continuous derivative and one which is "space-filling", respectively. All realizations of this covariance model are bounded self-affine fractal surfaces (appendix of [15]), with the special case $\nu = 1.0$ being a bounded self-similar. It was shown [15] that ν relates to the *Hausdorff-Besicovitch* dimension D (or *fractal* dimension[29]) as

$$D = 3 - \nu. \tag{2.22}$$

The corresponding power spectrum may be obtained by a Fourier transform, and is given by [15]

$$P(\mathbf{k}) = 4\pi\nu H^2 |Q|^{-1/2} [u^2(\mathbf{k}) + 1]^{-(\nu+1)}, \tag{2.23}$$

where

$$\begin{aligned} u(\mathbf{k}) &= [\mathbf{k}^T Q^{-1} \mathbf{k}]^{1/2} \\ &= \sqrt{\left(\frac{k}{k_s}\right)^2 \cos^2(\zeta - \zeta_s) + \left(\frac{k}{k_n}\right)^2 \sin^2(\zeta - \zeta_s)}, \end{aligned} \tag{2.24}$$

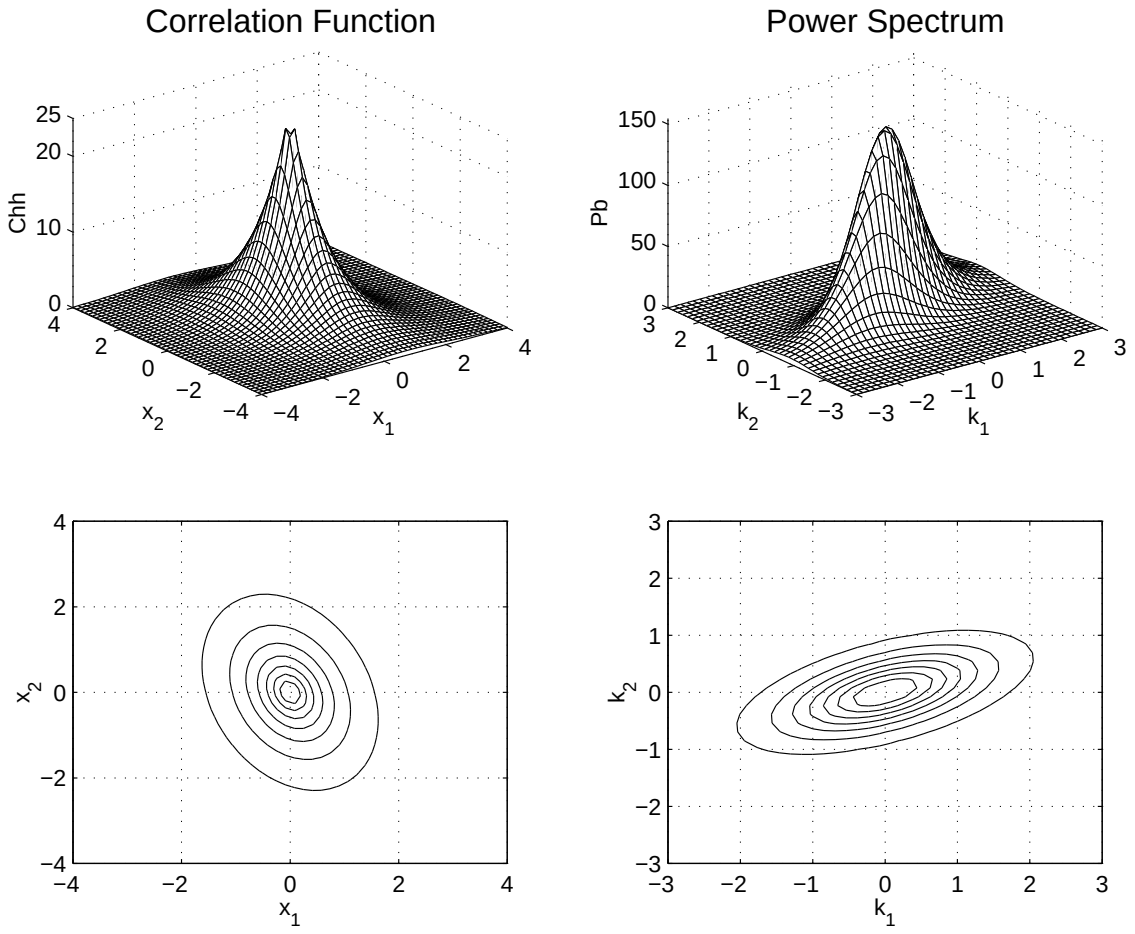

Figure 2.5: Goff-Jordan correlation function and its power spectrum for $H = 5$ m, $k_s = 0.86$ m^{-1}, $k_n = 2.14$ m^{-1}, $\zeta_s = 109.3°$, and $\nu = 0.5$.

The special case of isotropic rough surface corresponds to $k_n = k_s = k_0$, which simplifies the power spectrum, Equation (2.23), to become

$$P(\mathbf{k}) = \frac{4\pi\nu H^2}{k_0^2}\left[\left(\frac{|\mathbf{k}|}{k_0}\right)^2 + 1\right]^{-(\nu+1)}, \tag{2.25}$$

where $2\pi/k_0$ is a characteristic length similar to the correlation length for the Gaussian spectrum. Equation (2.25) shows that the spectrum has a finite value as $|\mathbf{k}| \to 0$, and its decay rate for the high spatial frequencies is $k^{-2(\nu+1)}$.

Figure 2.5 is an example of non-isotropic Goff-Jordan correlation function with its corresponding power spectrum for $H = 5$ m, $k_s = 0.86$ m^{-1}, $k_n = 2.14$ m^{-1}, $\zeta_s = 109.3°$, and $\nu = 0.5$. It is seen that the orientation of the correlation function and the power spectrum is orthogonal, i.e., the direction of the major/minor axes is perpendicular to each other. This is an important property of Fourier transform in that a higher coherence in spatial domain renders a narrower band in wavenumber domain, and vice versa.

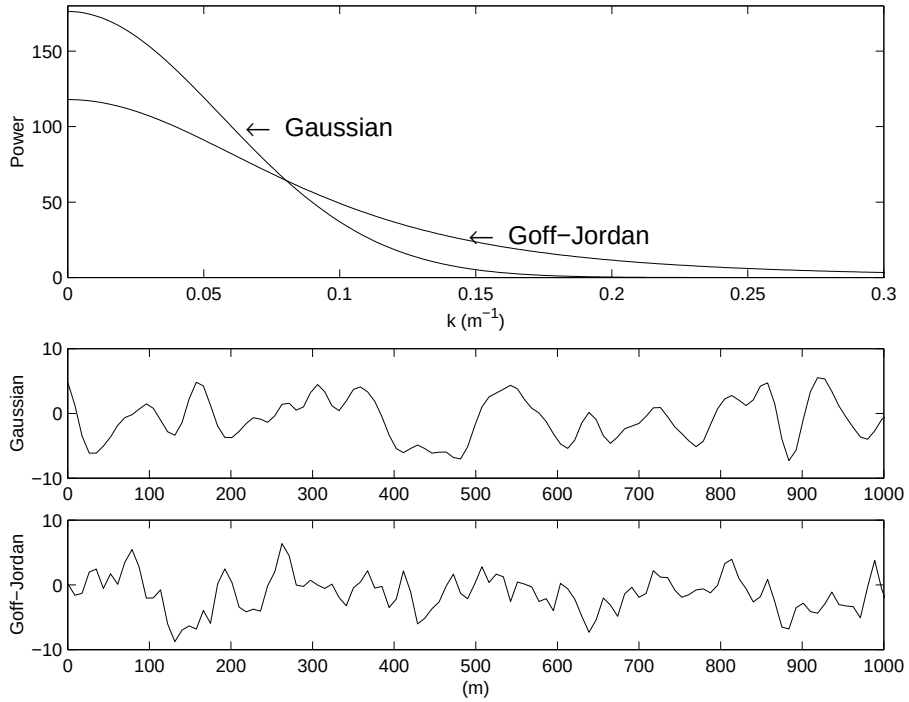

Figure 2.6: Roughness power spectra.

2.4.3 Gaussian Versus Goff-Jordan Power Spectrum

Figure 2.6 presents two representative cases for the isotropic Goff-Jordan spectrum, Equation (2.25), for $k_0 = 0.135$ m^{-1} (equivalent to correlation length about 18 m), $H = 0.5$ m, $\nu = 1.0$, and Gaussian spectrum, Equation (2.17), for $\lambda_0 = 25$ m, $\sigma = 0.5$ m, and their corresponding representative rough surfaces. It should be noted that the correlation length may be computed by $2/k_c$, where k_c the value of the wavenumber which corresponds to e^{-1} percent of the maximum value.

It is seen that the Goff-Jordan spectrum decays much slower than the Gaussian spectrum at the high frequency components, which means that the Goff-Jordan spectrum contains much more higher frequency components than those of Gaussian spectrum. From the representative surfaces (lower parts of the figure), it is easily seen that the surface representing Goff-Jordan model is much rougher than that representing Gaussian model. Thus, a surface with small-scale features is better approximated by the Goff-Jordan model. More about this will be discussed in Section 2.5.

2.4.4 Pierson-Moskowitz Power Spectrum

The sea surface is another important rough surface in the oceanic environment. It is more complicated than the sea floor because the sea surface is rough both dynamically and geographically. The sea surface changes shapes from moment to moment, and therefore, a complete description

of the surface involves Fourier spectrum both in frequency domain and in wavenumber domain.

In the analysis of random sea surface, one is usually concentrated on the frequency components of a wave height measured at a particular location. In this regard, Pierson and Moskowitz analyzed the data for the spectra of fully developed seas obtained by Moskowitz [31], and used the results to test the similarity hypothesis and the idea proposed by Kitaigorodskii [20]. They proposed a spectral form for fully developed sea state with wind speed from 20 to 40 knots (about 10 to 20 m/s) [37]. The Pierson-Moskowitz (PM) spectrum is

$$S(\omega) = \frac{\alpha g^2}{\omega^5} \exp\left[-\beta \left(\frac{g}{\omega U}\right)^4\right], \tag{2.26}$$

where ω is the angular frequency, $\alpha = 8.1 \times 10^{-3}$ and $\beta = 0.74$. The Pierson-Moskowitz power spectrum differs significantly from the Gaussian spectrum in that the former represents a rough surface which contains a wide range of roughness scales, and thus referring to as multiple scale roughness, while the latter describes a single-scale rough surface.

Figure 2.7 shows the Pierson-Moskowitz frequency spectrum for several values of wind speeds. This figure shows that the dominant frequency shifts towards lower frequency as the wind speed becomes larger. Knowing that a lower-frequency wave represents a wave with larger amplitude and longer wave length, it is conceivable that at higher wind speed, more energy is input into the ocean, and as time elapsed the waves are gradually built up and eventually reach a steady peak value.

The Pierson-Moskowitz spectrum has been universally acknowledged as the best description for surface wind waves, thus we use it to simulate random sea surface produced by wind waves. Since we require the power spectrum in wavenumber form to evaluate the spatial correlation of the noise field. We must transform the frequency spectrum into the wavenumber spectrum.

The wavenumber-form Pierson-Moskowitz spectrum may be obtained from the application of the dispersion relation for deep ocean gravity waves and the formula for transformation between frequency domain and wavenumber domain. The results were derived by Liu and Shiao [45, 25] as

$$P(k,\theta) = \begin{cases} \frac{4.05\times10^{-3}\cos^2\theta}{\pi k^4} \exp\left[-0.74\left(\frac{g^2}{U^4k^2}\right)\right] & ,|\theta| \le \pi/2 \\ 0 & ,|\theta| > \pi/2 \end{cases} \tag{2.27}$$

Figures 2.8 and 2.9 show the Pierson-Moskowitz wavenumber spectrum for wind speed 10 m/s and 14 m/s, respectively. As these figures show that they are non-isotropic and have non-zero value only in the region $|\theta| \le \frac{\pi}{2}$. This structure of the Pierson-Moskowitz power spectrum is very different from either Gaussian or Goff-Jordan spectrum, in that it contains no negative wavenumber components. It is conceivable that waves driven by winds can only propagate in the directions within a sector encompassing the forward half plane along the direction of the wind.

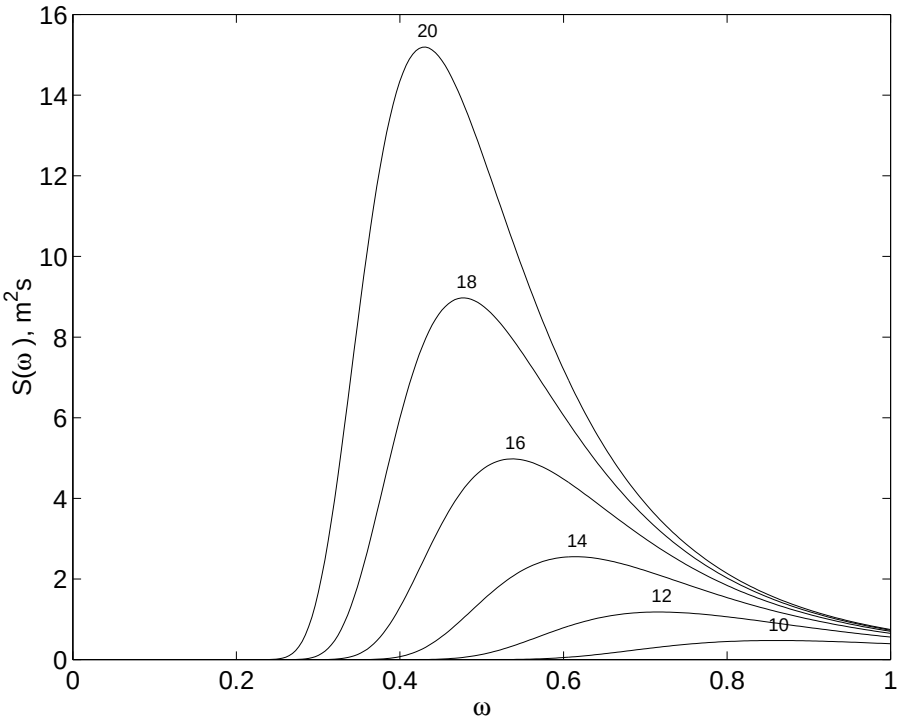

Figure 2.7: Pierson-Moskowitz frequency spectrum as function of wind speed (in m/s).

For the case of $U = 10$ m/s, the maximum power occurs at $\mathbf{k} \simeq 0.06\hat{\mathbf{i}}$, corresponding to wavelength approximately equal to 105 m. It can be found from literature [32] that in this case the average wavelength is 89 m and significant wave height 2.5 m. As the wind speed increases, as for the case $U = 14$ m/s, the spectrum becomes narrower, which implies that the most waves are long waves with maximum occurs at $\mathbf{k} = 0.033\hat{\mathbf{i}}$, corresponding to wavelength roughly equal to 190 m, and significant wave height 4.2 m.

2.5 Artificial Generation of Random Surfaces

The power spectrum is useful in the analysis of energy contents of a random process or a random field. However, it provides little information on the random features of the surface itself perceptible in visualization. It is, therefore, desirable that an artificial random surface be generated based upon a given power spectrum, with which a vivid presentation of the roughness can easily be seen. Each random surface thus generated represents a sample in the ensemble, and is referred to as a *realization*.

The technique of generating the artificial random surfaces based upon power spectrum is as follows. Given a one-dimensional power spectrum $P(k)$,

1. Consider N incremental steps of length Δr. Each step is given a random value h_n based on Gaussian probability distribution. Note that this is a Gaussian white noise sequence

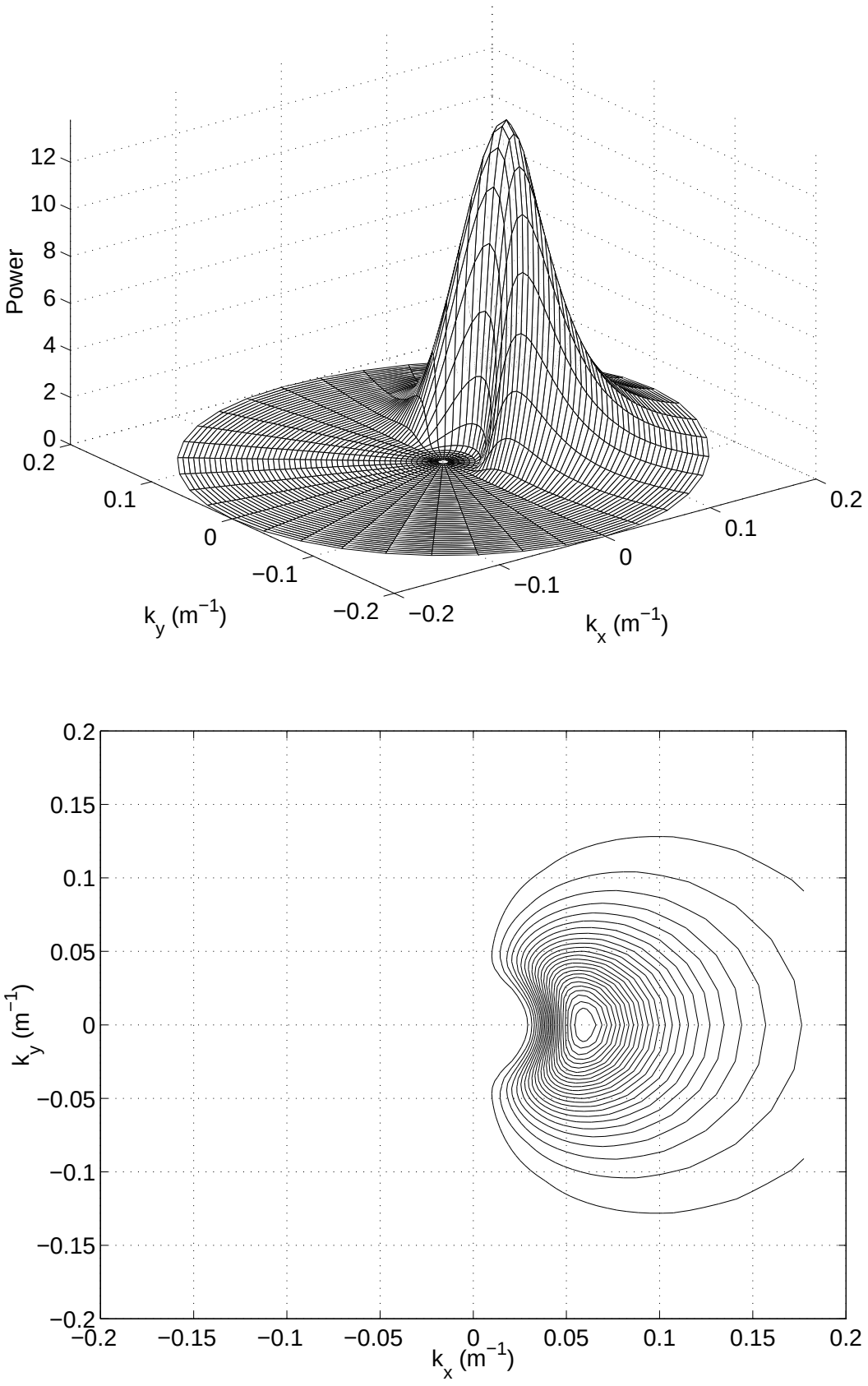

Figure 2.8: Pierson-Moskowitz wavenumber spectrum with $U = 10$ m/s.

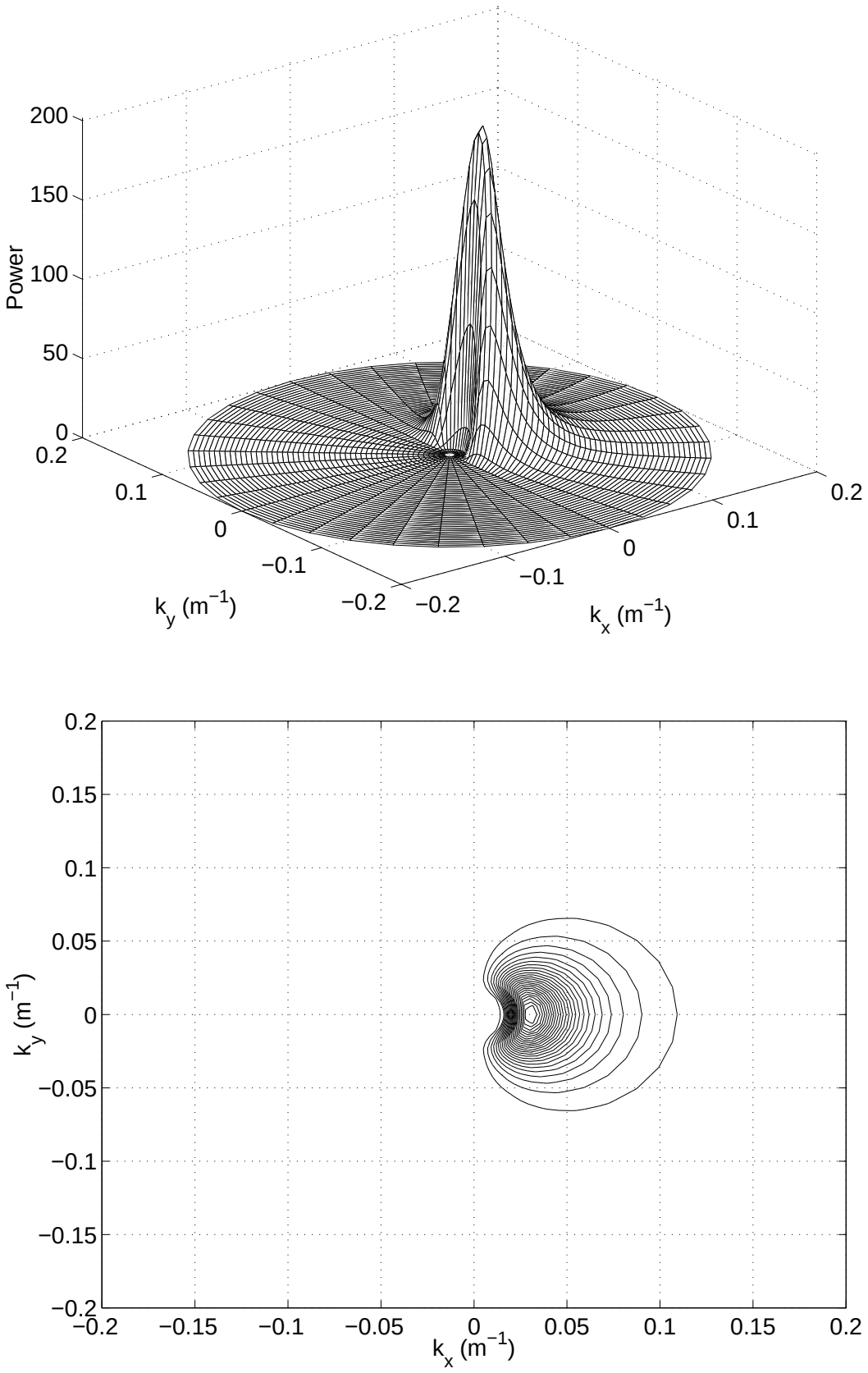

Figure 2.9: Pierson-Moskowitz wavenumber spectrum with $U = 14$ m/s.

and adjacent values are totally uncorrelated.

2. A discrete Fourier transform is taken of the random values. The Fourier coefficients are given by

$$H_k = \Delta r \sum_{n=0}^{N-1} h_n \mathrm{e}^{i2\pi nk/N}.$$

Because the transform is taken of a Gaussian white noise sequence the Fourier spectrum will be flat (the amplitudes of the $|H_k|$ will be equal).

3. The resulting Fourier coefficients H_k are filtered using the relation

$$Y_k = \sqrt{P_k} H_k$$

where P_k represents the discrete form of the power spectrum $P(k)$ with the sampling $\Delta k = \frac{2\pi}{N\Delta r}$. The square-root is taken because the power spectral density is proportional to the amplitude squared.

4. An inverse discrete Fourier transform is taken to result a sequence of number representing the rough surface:

$$y_n = \frac{1}{N\Delta r} \sum_{k=0}^{N-1} Y_k \mathrm{e}^{-i2\pi kn/N}.$$

The sequence generated by the above procedure has the prescribed power spectrum as the spectral coefficients of the random process. This can be shown to have a Gaussian probability distribution in the limit as $N \to \infty$ by the *Central Limit Theorem* [41].

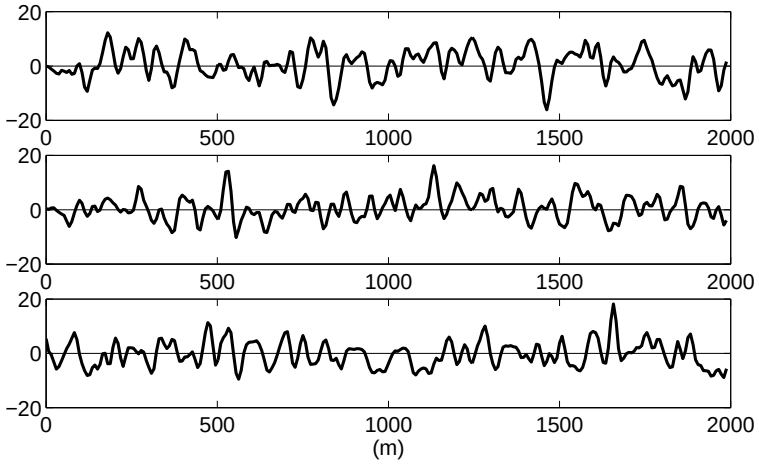

Figure 2.10: Three realizations for Gaussian power spectrum with RMS 5 m and correlation length 17 m.

Figure 2.10 shows three sample realizations for a Gaussian power spectrum with RMS height 5 m and correlation length 17 m. It is seen that each surface has its own unique distribution, but they all look similar in statistical sense.

2.5.1 Realizations of Gaussian Power Spectrum

Figures 2.11 shows the isotropic Gaussian spectrum along with its realization for correlation length $\lambda_0 = 15$ m and RMS height $\sigma = 5$ m. The spectrum clearly demonstrates a bell shape as mentioned before, and the realization shows an evenly distributive roughness over the surface without preference orientation in its distribution.

To demonstrate the non-isotropic case, the correlation lengths are chosen to be $\lambda_1 = 10$ m, and $\lambda_2 = 60$ m. Figure 2.12 shows the spectrum and its corresponding realizations. These figures vividly display the non-isotropic nature of the random field with higher correlation, or less random, in y-direction, and shorter correlation in x-direction.

From the above two artificially-generated rough surfaces, it can be seen that realization offers more lively information as far as the rough surface itself is concerned, and therefore provides a very good way for the description of a random surface.

2.5.2 Realizations of Goff-Jordan Power Spectrum

Figure 2.13 shows a power spectrum and its corresponding realization for an isotropic Goff-Jodan model for $k_0 = 0.15$ m^{-1}, $H = 5$ m, and $\nu = 1.0$. Comparing with Figure 2.11, it is found that that the surface for Goff-Jordan spectrum is much rougher than that for Gaussian spectrum as expected.

Figures 2.14 and 2.15 display a non-isotropic case for the Goff-Jordan model. The parameters are chosen to be $k_s = 0.03$ m^{-1}, $k_n = 0.1$ m^{-1}, $\zeta_s = 30°$, $H = 5$ m and $\nu = 1.0$. It is seen that the characteristic of the roughness is quite different from that as shown in Figure 2.12 for Gaussian spectrum, with the scale of the relief described by the Goff-Jordan being smaller than that for Gaussian model. The pattern of the local strikes are clearly demonstrated in Figure 2.15, in which it shows that the strikes makes an angle of 30° from y-axis.

The above set of figures indicates that the Goff-Jordan model has a high adaptability for the variations of the roughness and orientation, suggesting that it can well fit the topography of the sea floor for the roughness scale within a few hundreds of kilometers, as the original authors proposed.

2.5.3 Realizations of Pierson-Moskowitz Power Spectrum

The peculiar structure of the Pierson-Moskowitz power spectrum presents itself a quite different feature in its realization in comparison with either Gaussian or Goff-Jordan as Figures 2.16 and 2.17 show. These figures indicate that the random surface contains many crests and troughs scattered all over the surface.

Figure 2.16 is the Pierson-Moskowitz power spectrum and its realization for wind speed

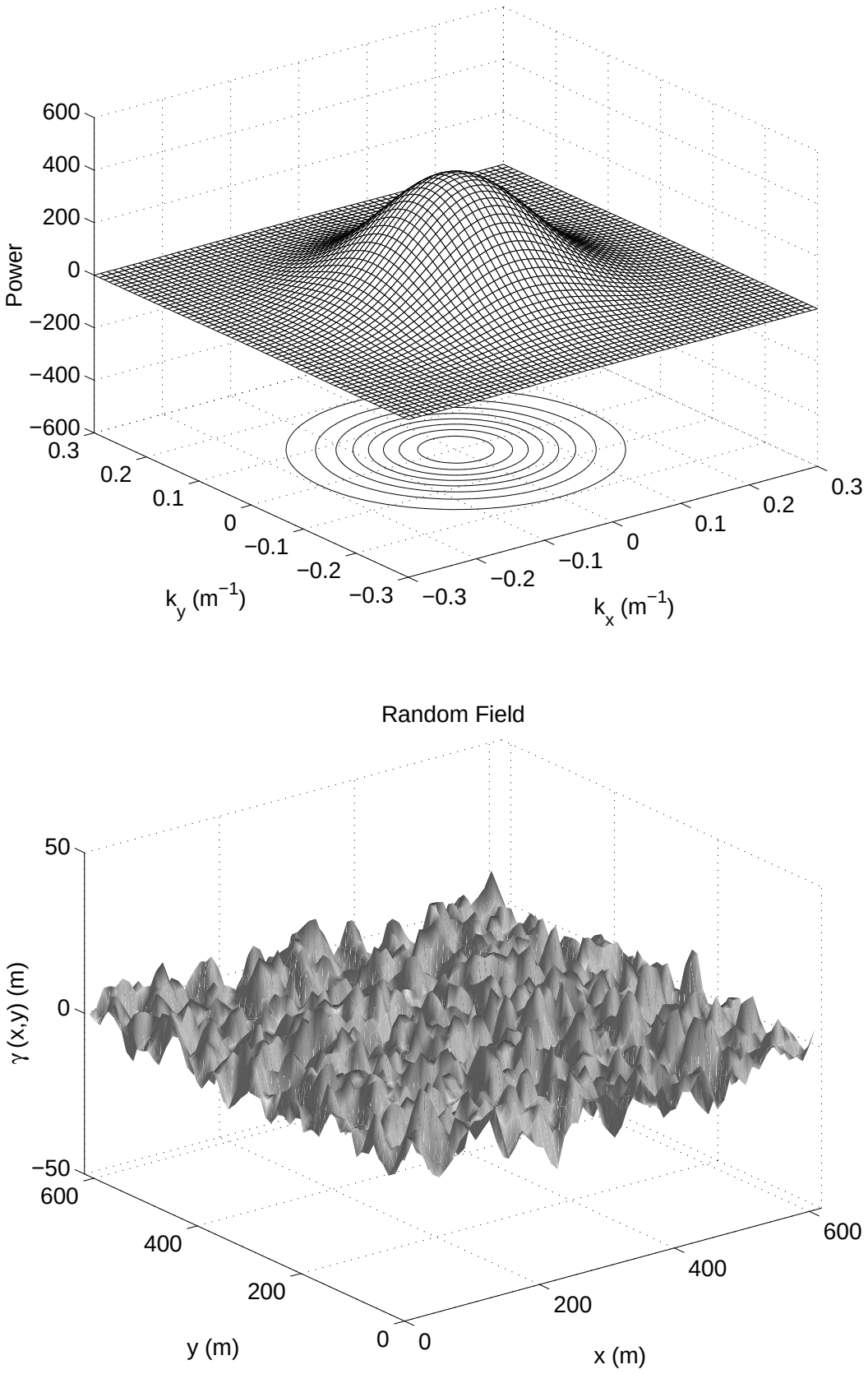

Figure 2.11: Isotropic Gaussian power spectrum with $\lambda_1 = \lambda_2 = 15$ m and $\sigma = 5$ m.

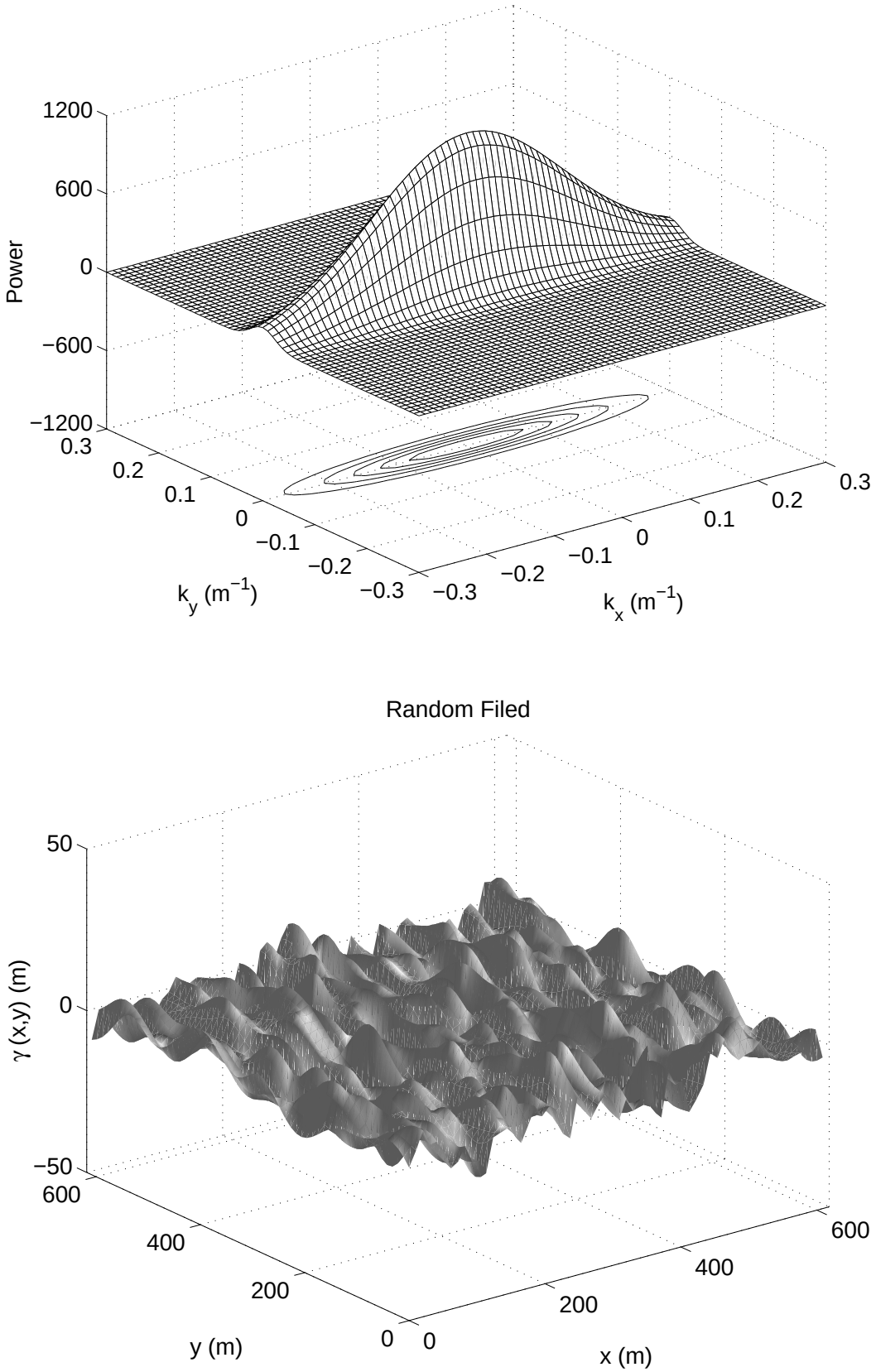

Figure 2.12: Non-isotropic Gaussian power spectrum with $\lambda_1 = 10$ m, $\lambda_2 = 60$ m and $\sigma = 5$ m.

12 m/s. For this case, the sea surface is characterized by many random surface waves. However, as the wind speed increases to 20 m/s, the sea surface is populated with a train of long waves. These results are in consistence with the images as one can often observe on a surface of rough sea.

2.6 Summary

This chapter has been devoted to the study of the random rough surfaces. Some most important concepts relevant to the description of a random process are first reviewed, followed by the discussion of the height probability density function, in particular, the Gaussian distribution.

The bulk of the chapter is to analyze the various models for the power spectrum which are appropriate for the description of sea surface or seabed. These include Gaussian spectrum, Goff-Jordan spectrum, and Pierson-Moskowitz. The characteristic of each model is illustrated and analyzed.

A few words about treating the sea floor as a random field are in order. In reality, the sea floor is a well-defined, deterministic surface which changes shape only in a very slowly manner. Thus, to treat seabed topography as a stochastic field often raises a certain level of metaphysical anxiety among many marine geologists. However, for marine acousticians, the study of acoustic wave scattering from seabed such as the one we are undertaking will involve geological features with scales comparable with the acoustic wavelengths, which in general are much smaller than the major features of the sea floor. In this case, the number and variability of small-scale features are so large that it becomes necessary for the morphological characteristics be averaged over families or ensemble, which naturally leads to a statistical representation.

In the following chapters, we shall employ the roughness power spectra discussed in this chapter to study the acoustic scattering problem.

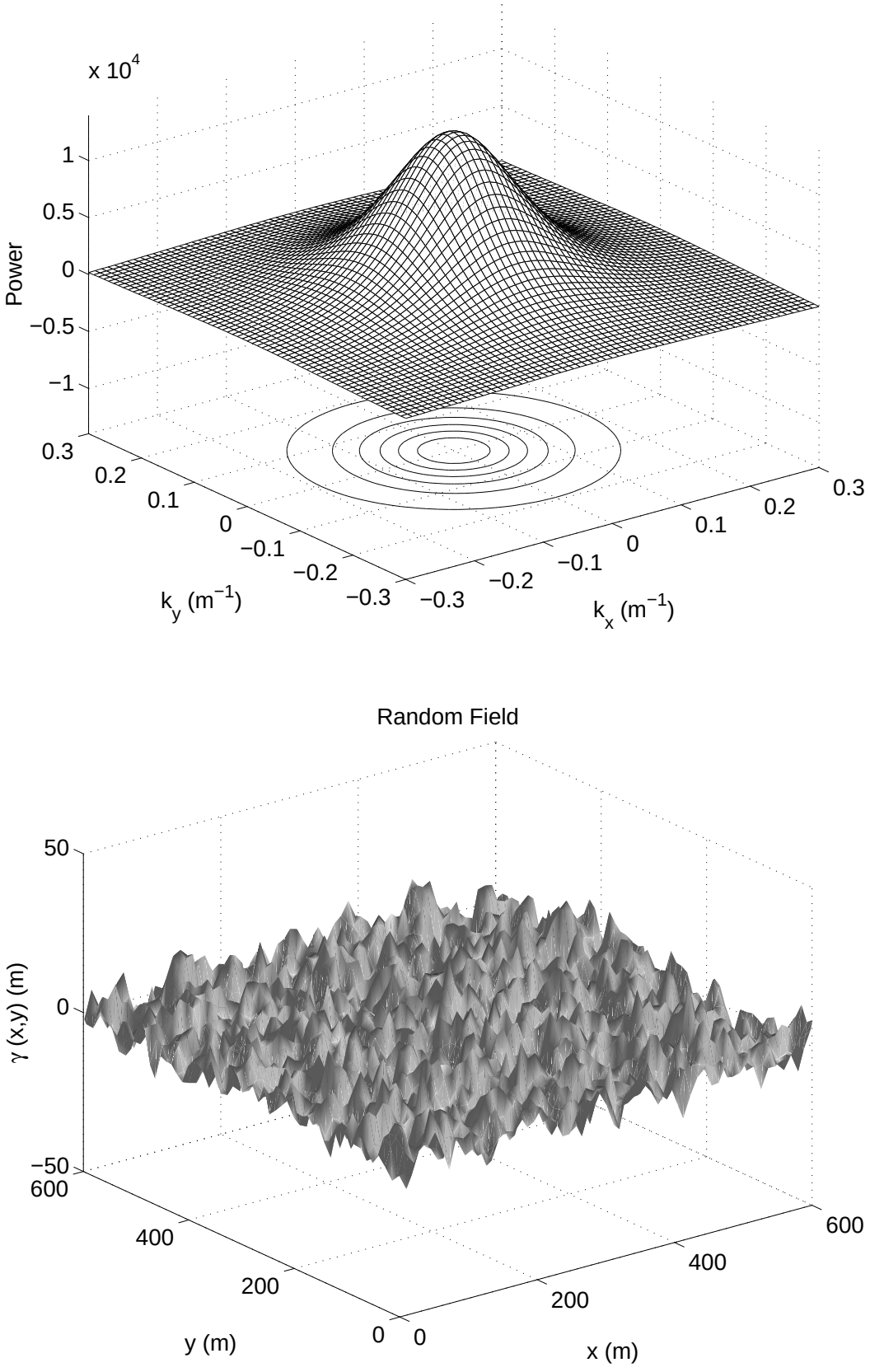

Figure 2.13: Goff-Jordan spectrum and its realization for $k_0 = 0.15\,\mathrm{m}^{-1}$, $H = 5$ m and $\nu = 1.0$.

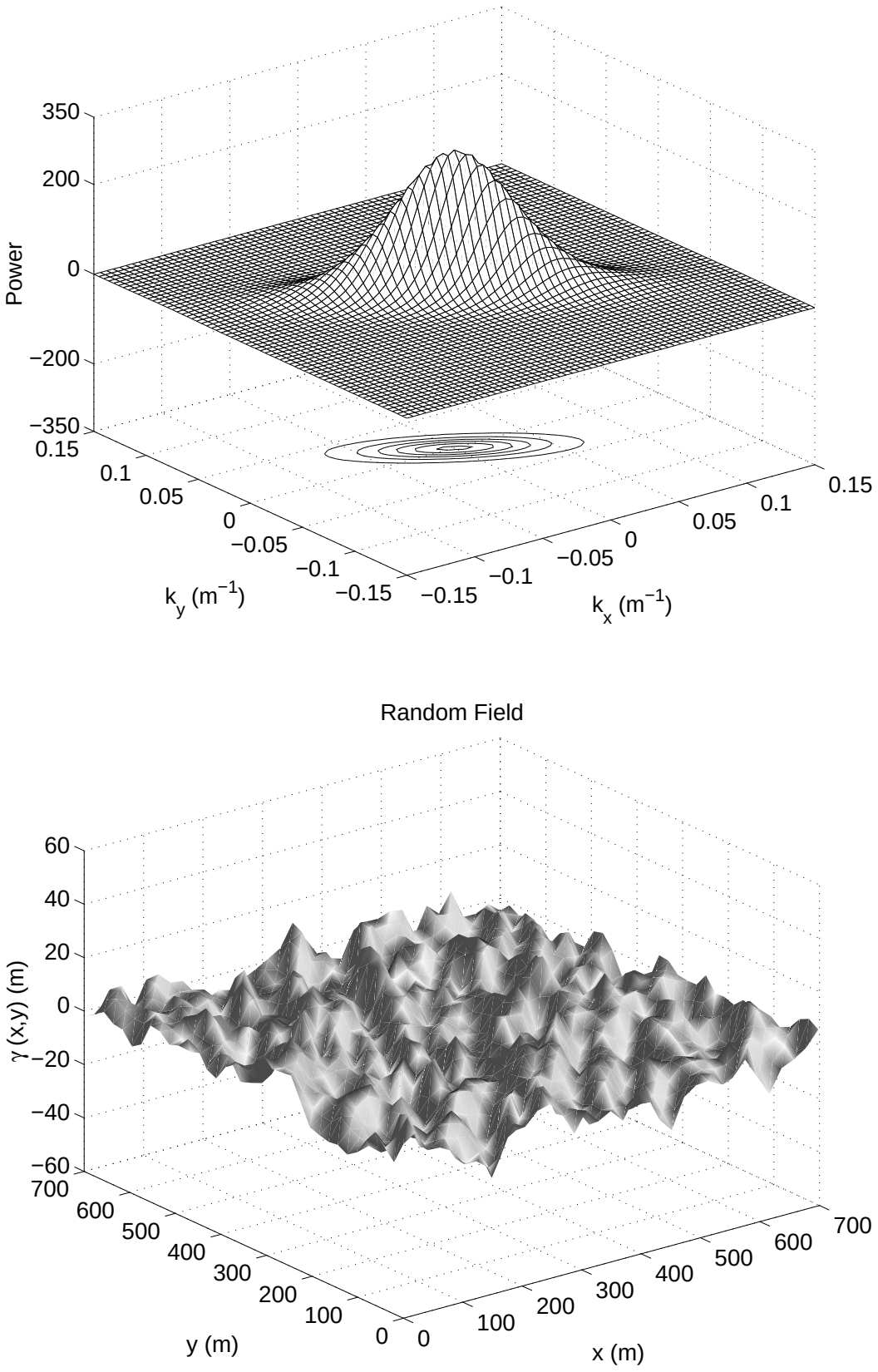

Figure 2.14: Goff-Jordan spectrum and its realization for $k_s = 0.03\,\mathrm{m}^{-1}$, $k_n = 0.1\,\mathrm{m}^{-1}$, $\zeta_s = 30°$, $H = 5$ m, and $\nu = 1.0$.

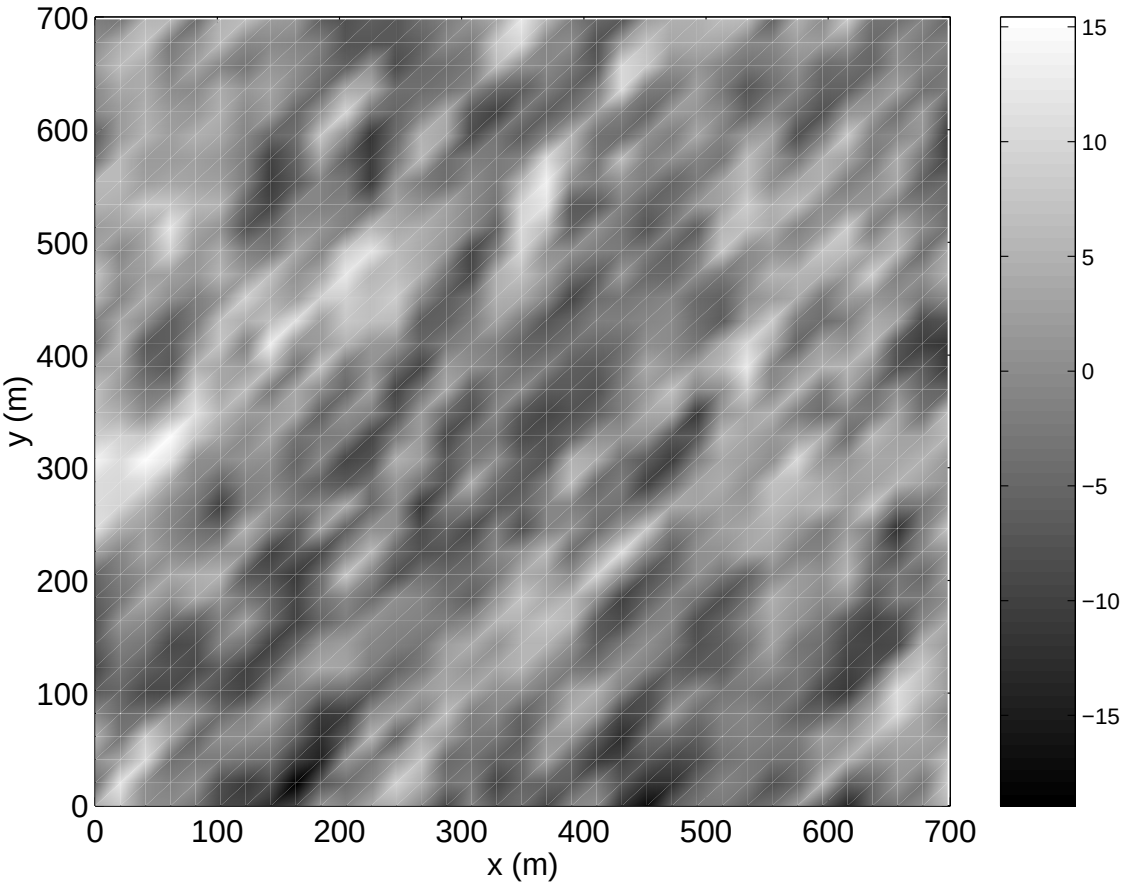

Figure 2.15: The realization of Goff-Jordan spectrum for $k_s = 0.03\,\mathrm{m}^{-1}$, $k_n = 0.1\,\mathrm{m}^{-1}$, $\zeta_s = 30°$, $H = 5$ m, and $\nu = 1.0$.

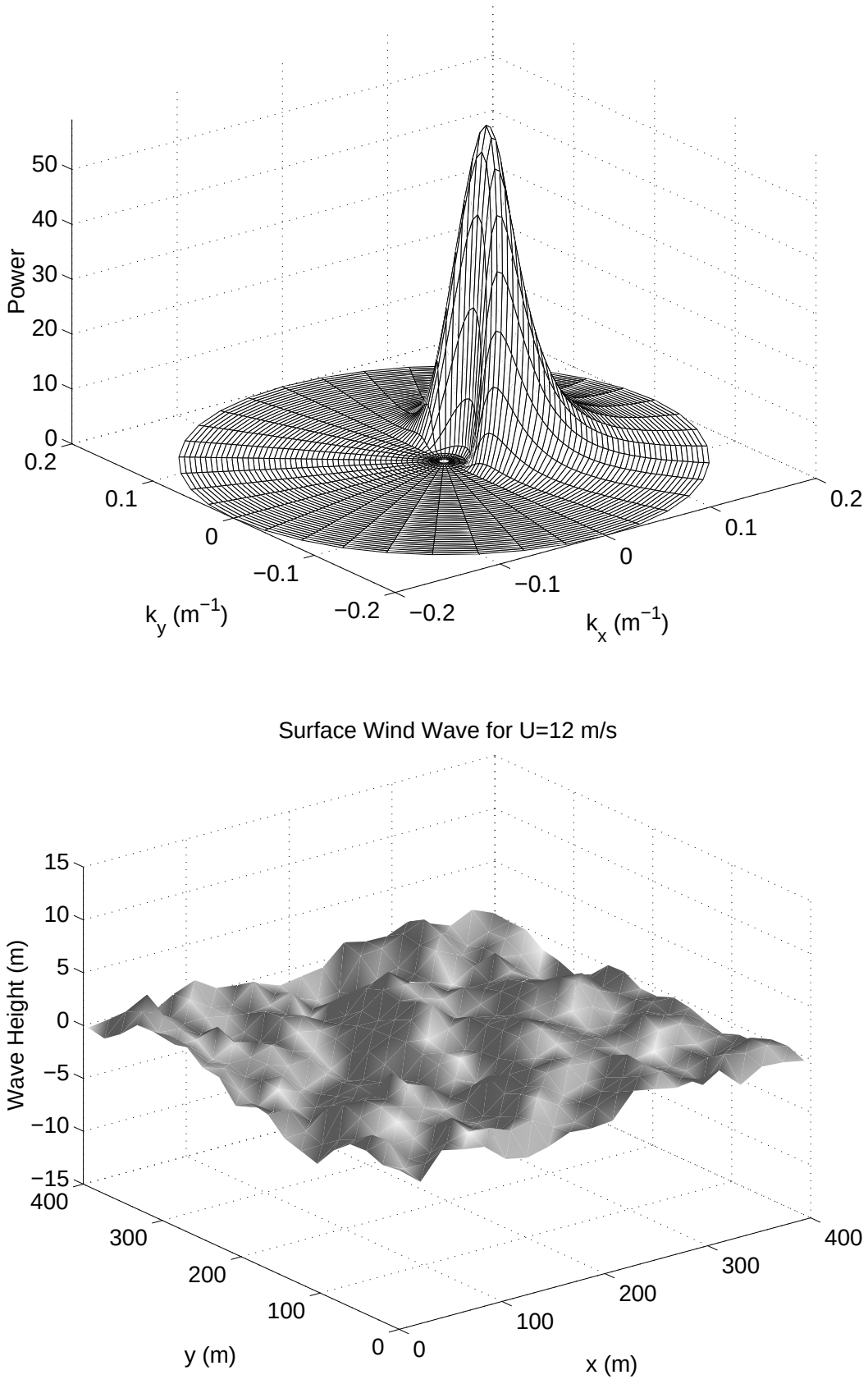

Figure 2.16: Pierson-Moskowitz wavenumber spectrum with $U = 12$ m/s.

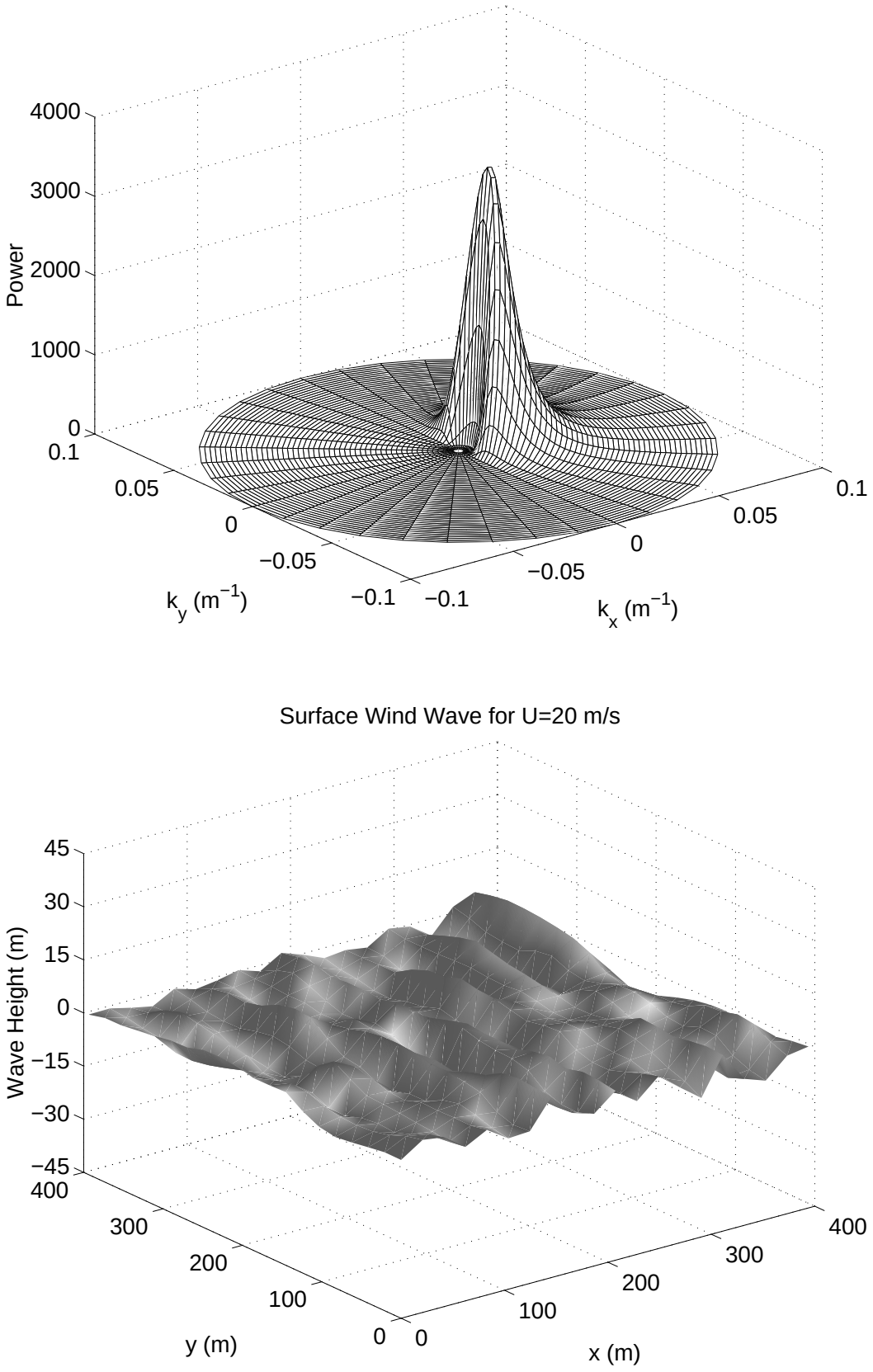

Figure 2.17: Pierson-Moskowitz wavenumber spectrum with $U = 20$ m/s.

Chapter 3

Scattering From Perfectly Reflecting Surfaces

The main theme of the present analysis to study the acoustic wave scattering from random rough surfaces. The objective is to analyze the pressure scattering field due to various kinds of rough surfaces. Our major interests are to simulate the acoustic scattering in time domain and examine the basic scattering mechanisms. In order not to obscure our purpose, the geometry of the problem is chosen to be simple. Here we shall consider a plane wave incident upon a perfectly reflecting surfaces which are either flat or rough.

We begin our discussion with a simple problem as a prelude: the Rayleigh reflection problem of a plane wave incident upon a flat interface separating two homogeneous media. Even though, this problem may not seem to belong to the chapter entitled, it is still within the framework of the present study, and illuminates many basic features of a plane wave interacting with a discontinuity of a medium. We shall present the solution of this problem in a dynamic manner using MATLAB, with a hope that it might bring up some new perspectives which are not generally appreciable on a line graph. We then continue to study the scattering from a periodic surface composed of a finite number of Fourier components. The problem of scattering from a periodic surface may serve as a benchmark for the further investigation to be followed. Finally, we consider the scattering from random rough surfaces with the power spectra which closely resemble the sea surface or seabed.

3.1 Prelude: Rayleigh Reflection Problem

Consider the reflection of a monotonic plane wave with frequency ω incident upon an interface separating two homogeneous fluid media with density ρ_1 and ρ_2 and sound speed c_1 and c_2, respectively, as shown in Figure 3.1. The pertinent grazing angles with the horizontal in the xz-plane are denoted by θ. Assuming the incident plane wave to have unit amplitude and denoting

the amplitudes of the reflected and transmitted waves by R and T which are the reflection coefficient and transmission coefficient, respectively, we can write the acoustic pressures as

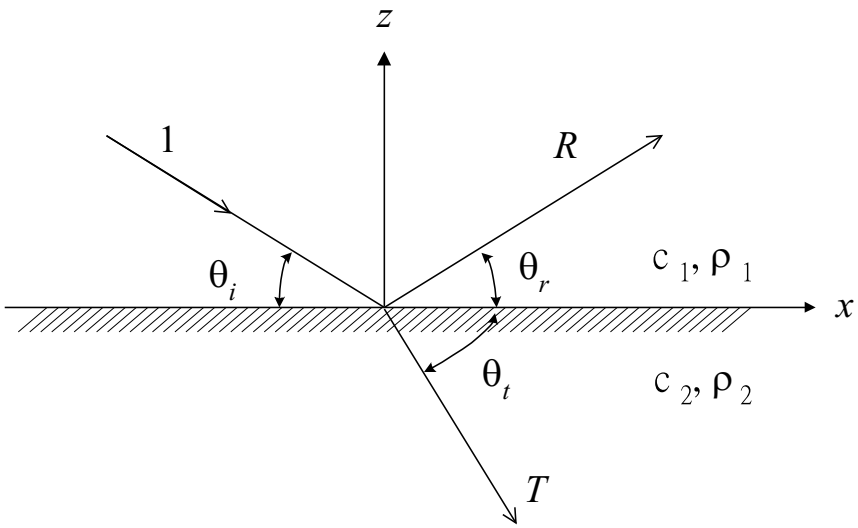

Figure 3.1: Plane wave reflection from and transmission across a plane interface between two fluid media.

$$\begin{aligned} p_i &= e^{i(\mathbf{k}_{x,1}\hat{\mathbf{i}}-\mathbf{k}_{z,1}\hat{\mathbf{k}})\cdot\mathbf{r}} &&= e^{ik_1(x\cos\theta_i - z\sin\theta_i)} \\ p_r &= R\, e^{i(\mathbf{k}_{x,1}\hat{\mathbf{i}}+\mathbf{k}_{z,1}\hat{\mathbf{k}})\cdot\mathbf{r}} &&= R\, e^{ik_1(x\cos\theta_r + z\sin\theta_r)} \\ p_t &= T\, e^{i(\mathbf{k}_{x,2}\hat{\mathbf{i}}-\mathbf{k}_{z,2}\hat{\mathbf{k}})\cdot\mathbf{r}} &&= T\, e^{ik_2(x\cos\theta_t - z\sin\theta_t)} \end{aligned} \tag{3.1}$$

where $k_{x,i}$ and $k_{z,i}$ are respectively the horizontal and vertical wavenumber of the ith medium, and $k_i = \sqrt{k_{x,i}^2 + k_{z,i}^2} = \omega/c_i$ is the wavenumbers of the medium i. It is understood that in the above expressions the time-dependent term $\exp(-i\omega t)$ is neglected.

The unknown quantities R, T, θ_r and θ_t are determined from the boundary conditions requiring continuities of pressure and vertical particle velocity across the interface at $z = 0$. These boundary conditions can be mathematically stated as

$$p_i + p_r\big|_{z=0} = p_t\big|_{z=0} \tag{3.2}$$

$$\frac{1}{i\omega\rho_1}\frac{\partial(p_i+p_r)}{\partial z}\bigg|_{z=0} = \frac{1}{i\omega\rho_2}\frac{\partial p_t}{\partial z}\bigg|_{z=0} \tag{3.3}$$

The boundary condition Equation (3.3) are derived from the momentum equation for the acoustic wave. Substituting Equation (3.1) into Equations (3.2) and (3.3) results in

$$\exp(ik_1 x\cos\theta) + R\exp(ik_1 x\cos\theta_r) = T\exp(ik_2 x\cos\theta_t) \tag{3.4}$$

$$\frac{\sin\theta}{\rho_1 c_i}\left[\exp(ik_1 x\cos\theta) + R\exp(ik_1 x\cos\theta_r)\right] = T\frac{\sin\theta_t}{\rho_2 c_2}\exp(ik_2 x\cos\theta_t) \tag{3.5}$$

From the requirement of continuity of pressure at $z = 0$, we find that the horizontal phase along and across the interface are invariable. So the reflection angle is

$$\theta_r = \theta_i \tag{3.6}$$

which expresses the specular law of reflection. Also the transmission angle is determined by the horizontal phase matching, and is given by

$$\frac{\cos\theta_t}{c_2} = \frac{\cos\theta_i}{c_1} \tag{3.7}$$

which expresses the law of the refraction, known as *Snell's Law*. That is, both θ_r and θ_t are determined via the condition that boundary moves with a phase dependence dictated by the incident wave, which in turn dictates the horizontal phase of the reflected and transmitted waves.

With Equations (3.6) and (3.7), we can rewrite Equation (3.2) and Equation (3.3) in the form

$$1 + R = T \tag{3.8}$$

$$\frac{\sin\theta}{\rho_1 c_1}(1 - R) = \frac{\sin\theta_t}{\rho_2 c_2} T \tag{3.9}$$

The above two equations may be solved for the reflection coefficient R and the transmission coefficient T, which are respectively given by

$$R = \frac{m\sin\theta - \sqrt{n^2 - \cos^2\theta}}{m\sin\theta + \sqrt{n^2 - \cos^2\theta}} \tag{3.10}$$

$$T = \frac{2m\sin\theta}{m\sin\theta + \sqrt{n^2 - \cos^2\theta}} \tag{3.11}$$

where $m = \rho_2/\rho_1$ and $n = c_1/c_2$, being the mass ratio and index of refraction of the interface, respectively. It is seen that both reflection and transmission coefficients are function of mass ratio, index of refraction, and incident angle.

In general, both R and T can be a complex number, which means that both reflection and transmission waves have relative amplitude and phase change with respect to the incident wave. In terms of magnitude and phase, R and T may be represented by

$$R = |R|e^{i\phi_R} \tag{3.12}$$

$$T = |T|e^{i\phi_T} \tag{3.13}$$

where $|R|$ and ϕ_R are, respectively, the modulus and phase of the reflection coefficient, and $|T|$ and ϕ_T are those of transmission coefficient. If n is less than unity, then there exists an incident angle θ_c such that $\cos\theta_c = n$. This angle is referred to as *critical angle* of reflection. For all the incident angles less than θ_c, the magnitude of R is equal to unity, i.e., $|R| = 1$. Thus the incoming wave is totally reflected. There also may have cases in which an incident wave incoming at a particular angle completely transmits through the interface even if the media stand strong contrast to each other.

A few examples may help to fix the idea. Figure 3.2 and Figure 3.3 show the magnitude and phase of the reflection and transmission coefficients for the following parameters: $c_1 = 1500$ m/s, $\rho_1 = 1000$ kg/m^3 in the water, and $c_2 = 1800$ m/s, $\rho_2 = 1800$ kg/m^3 in the bottom. Both

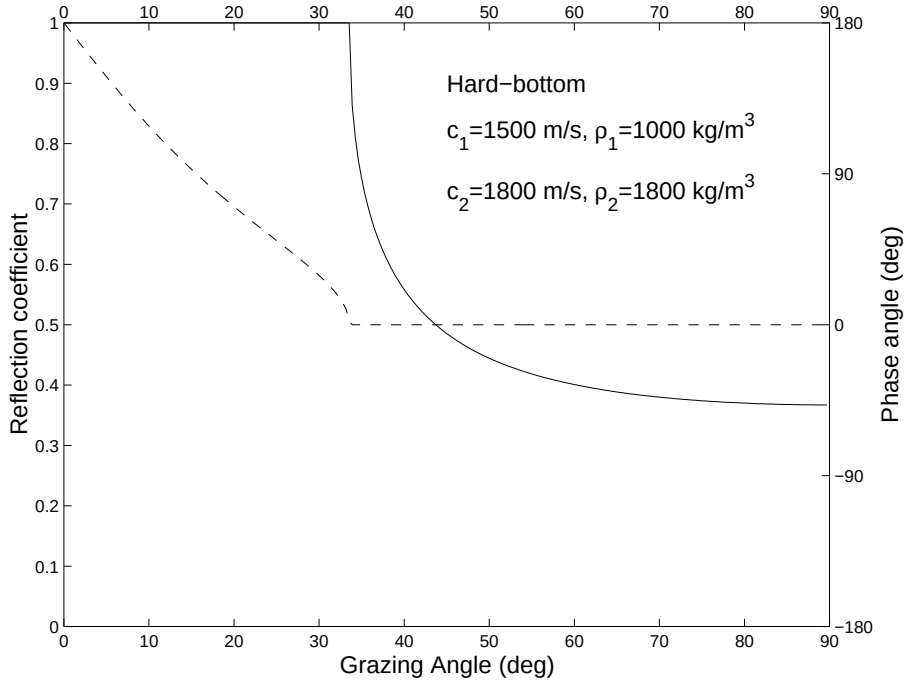

Figure 3.2: Reflection coefficient as a function of grazing angle for a hard-bottom half-space. Solid curve is for the modulus and the dashed curve is for phase.

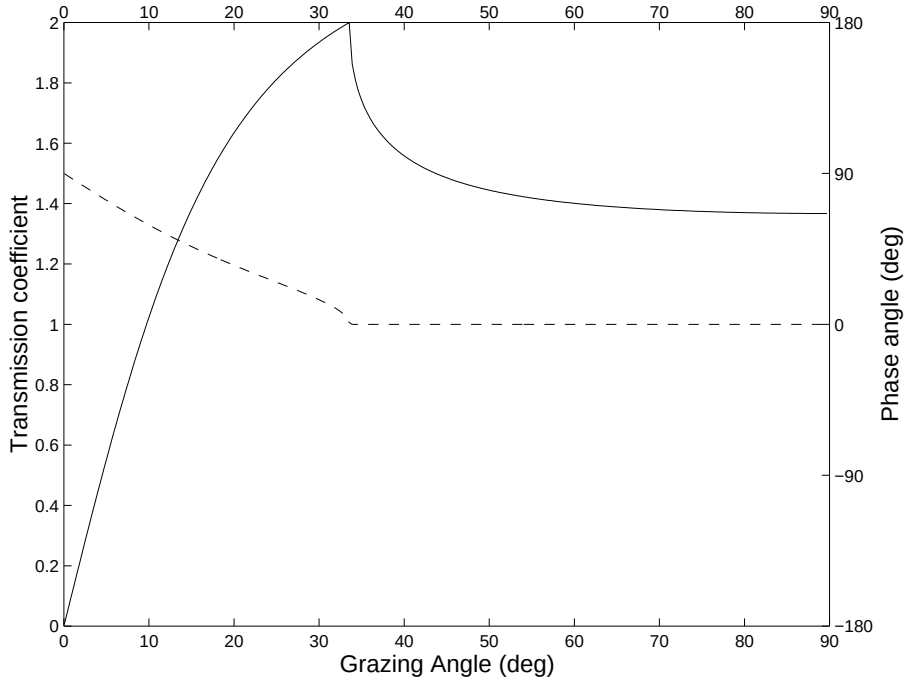

Figure 3.3: Transmission coefficient as a function of grazing angle for a hard-bottom half-space. Solid curve is for the magnitude and the dashed curve is phase.

the sound speed and density of the bottom medium is larger than those of upper medium. This is referred to as *hard bottom* in view of the fact that a larger sound-speed medium is generally harder. In this case, there exists a critical angle $\theta_c = \cos^{-1}(k_2/k_1) = 33.5°$, so that the reflection coefficient is unity for the grazing angle less than θ_c. For the incident angle greater than the critical angle, both the reflection and transmission coefficients decrease as the grazing angle increases. This means that the amplitudes of the pressure of both reflection and transmission waves become smaller as the incident angle turns steeper. This is in consistent with our common experience in that the glare of sun light reflected from flat roadway makes one hard view as one faces the sun during the sunset. It is also interesting to note that the transmission coefficient reaches a maximum value of 2, and then quickly decays to zero as the grazing angle decreases. As for the phase is concerned, it is seen that there is no phase shift when the incoming wave is steeper than the critical angle, and then increases to π and $\pi/2$ for reflection wave and transmission wave, respectively, when the incident angle decreases from the critical down to zero.

Another example represents a *soft bottom* case, in which the sound speed in the lower medium is smaller than that in the upper medium. Figure 3.4 and Figure 3.5, respectively, shows the magnitude and phase of the reflection coefficient and transmission coefficient for the following parameters: $c_1 = 1500$ m/s, $\rho_1 = 1000$ kg/m^3, and $c_2 = 1300$ m/s, $\rho_2 = 1800$ kg/m^3. It is seen that for incident angle greater than zero the reflection coefficient is less than unity. This is in contrast to Figure 3.2 in that Figure 3.4 shows no total reflection for incident angle lying within the physically realizable space. Thus, for soft bottom case, the interface is always penetrable, allowing energy to be transmitted into the bottom through refraction without having change of phase as shown in Figure 3.5. It is also interesting to note that at the incident angle equal to $\sin^{-1}\left(\sqrt{\frac{n^2-1}{m^2-1}}\right)$, which is amounted to 22.6° in this case, the reflection coefficient vanishes with transmission coefficient being unity. That is to say that the incoming wave does not feel the existence of the interface. This angle is referred to as Brewster angle, which is occurred when $m > n > 1$. There are other interesting cases derivable from Equations (3.10) and (3.11); those who are interested may consult with Reference [26].

A remark regarding the conservation of energy might be worth mentioning. Since the incoming wave is the only energy supplier, it is obvious that the energy carried by the reflection wave *and* the transmission wave should be equal to that of incident wave. This may easily lead to conclude that $p_i = p_r + p_t$, however, this is clearly mistaken. Rather, the correct statement should be $\mathbf{I}_i \cdot \hat{n} = \mathbf{I}_r \cdot \hat{n} + \mathbf{I}_r \cdot \hat{n}$, where $\mathbf{I}$ is the intensity and $\hat{n}$ is the outward normal of the interface. In terms of pressure, the statement of energy conservation is

$$\frac{p_i^2}{\rho_1 c_1} \sin\theta = \frac{p_r^2}{\rho_1 c_1} \sin\theta + \frac{p_t^2}{\rho_2 c_2} \sin\theta_t \tag{3.14}$$

The equation is easily verified by substituting relevant parameters derived above.

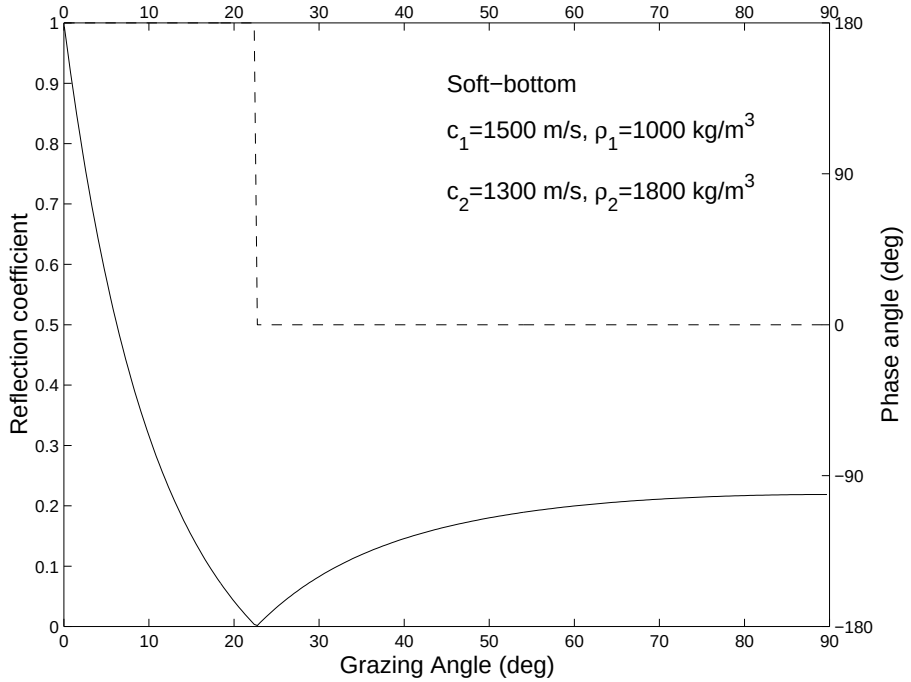

Figure 3.4: Reflection coefficient as a function of grazing angle for a soft-bottom half-space. Solid curve for magnitude and dashed curve for phase.

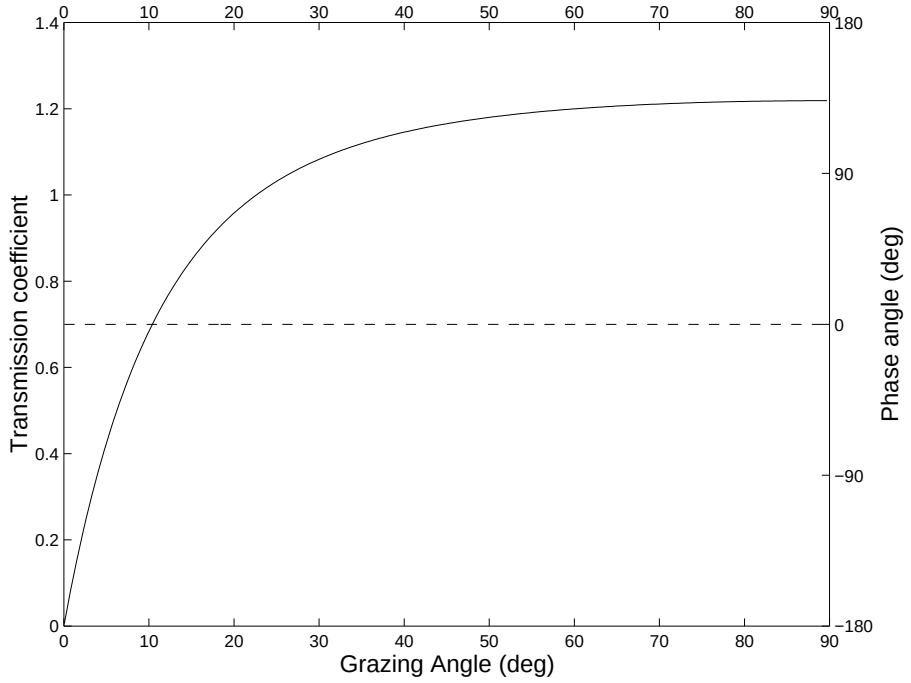

Figure 3.5: Transmission coefficient as a function of grazing angle for a soft-bottom half-space. Solid curve for magnitude and dashed curve for phase.

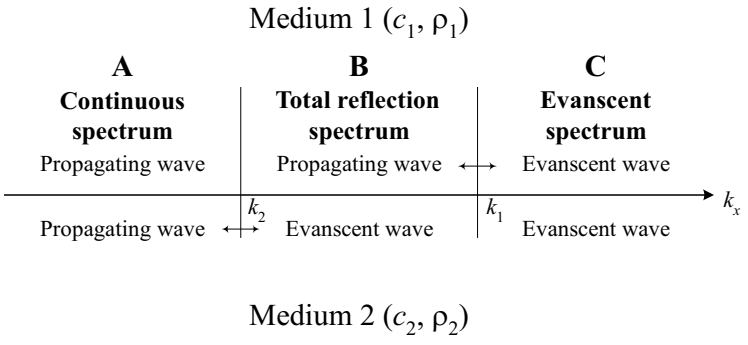

Figure 3.6: Spectral domains for a hard bottom, $k_2 < k_1$.

3.2 Spectral Regions

A broader perspective for the wave field in each medium may be provided by the wavenumber spectrum, which expresses the energy contents of the wave field in terms of wavenumber. The wavenumber spectrum is discussed in details in many textbooks. Here, we simply note that with the expressions for the pressure fields given by Equation (3.1), the vertical wavenumber is

$$k_{z,i} = \pm\sqrt{k_i^2 - k_{x,i}^2} \tag{3.15}$$

Therefore, if the horizontal wavenumber is smaller than the medium wavenumber, i.e., $k_{x,i}^2 < k_i^2$, then $k_{z,i}$ is real in the medium i, which means that the wave in that medium is in propagating wave. On the other hand, if the horizontal wavenumber is larger than the medium wavenumber, i.e., $k_{x,i}^2 > k_i^2$, then the vertical wavenumber becomes complex number so that the vertical component of the wave varies exponentially. Moreover, to satisfy physical constraints, the $\pm$ sign should be properly chosen in Equation (3.15), such that it renders wave exponential decay in the medium. For this case, the wave in the medium becomes exponential decay away from the interface; it is referred to evanescent wave.

According to the above discussion, the complete wave field may be divided into three regions, in which the waves in different region possess different characteristics. To illustrate, let consider the following two cases of the Rayleigh reflection problem:

Hard Bottom Case

For the hard bottom, the medium wavenumber in the bottom is smaller than the wavenumber in the water, $k_2 < k_1$. There are three different spectral regions as shown in Figure 3.6:

Region A : For those waves with horizontal wavenumber less than the bottom medium wavenumber, i.e., $k_x < k_2$, the waves are *propagating* in both media, representing that the incoming wave is reflected partially from and transmitted partially through the interface. This re-

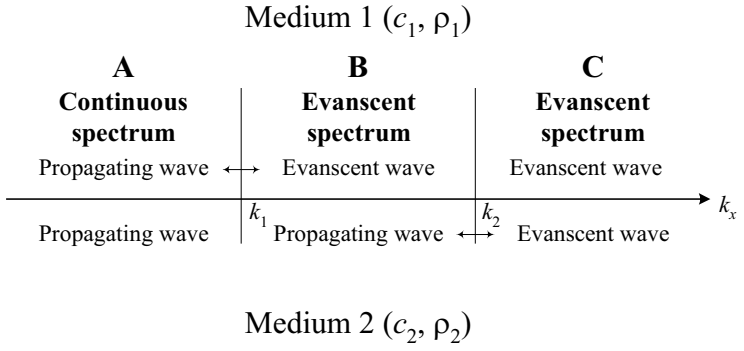

Figure 3.7: Spectral regions for a soft bottom, $k_1 < k_2$.

gion is called *continuous spectral region* for both media. It is noted that in this region, $|R| < 1$.

Region B : For $k_2 < k_x < k_1$, waves are *propagating* in the upper medium, but are *evanescent* in the lower medium. Physically, this means that the lower medium can not support real wave, and therefore no energy is allowed to propagate away from the interface. This region corresponds to total reflection, i.e., $|R| = 1$, so that it is referred to as *total reflection region* for the upper medium.

Region C : For waves with $k_x > k_1$, waves are *evanescent* in both media, and therefore, all the waves are decayed away from the interface. For an incoming wave with horizontal wavenumber greater than the medium wavenumber, the "incident grazing angle" is larger than $\pi/2$, which is not a real entity in space, but is only a mathematical object which is required to make up the complete spectrum of the wave field. This region is referred to as *evanescent spectral region.*

Soft Bottom Case

A soft bottom is referred to the case that the sound speed of the upper medium greater than that of lower medium, i.e., $c_1 > c_2$ or equivalently $k_1 < k_2$. Again, the wavenumber spectrum may be divided into three different regions, as shown in Figure 3.7.

Region A : For $k_x < k_1$, waves are *propagating* in both media, signifying that the incoming wave is partially reflected into the upper medium and partially transmitted into the lower medium so that $|R| < 1$. This is *continuous spectral region.*

Region B : For $k_1 < k_x < k_2$, waves are *evanescent* in the upper medium but are *propagating* in the lower medium. In this case, $|R| = 1$ (why?).

Region C : For $k_2 < k_x$, waves are *evanescent* in both media, and $|R| < 1$ (why?).

It is noted that for soft bottom case, there is no region in which the upper medium is propagating and lower medium is evanescent; therefore, there is no total reflection.

3.3 Dynamic Simulation for Rayleigh Reflection Problem

In this section, we shall demonstrate the plane wave reflection in a dynamic manner. In this way, the reflection phenomenon may be vividly displayed so that the reflection characteristic is self evident. The program is written with MATLAB computer language with the simulated propagation driven by the functions moviein, getframe, and movie. The details can be found from the MATLAB user guides [30].

The presentation will follow the sequence discussed in the previous section so that a comparison with the line graphs can be made. Many results will be shown dynamically on computer; those sections will be signified by the symbol [DEMO].

Hard Bottom Case

[DEMO]

Plate 3.1 shows a plane wave with a grazing angle 65° incident upon an interface at $z = 0$. The medium properties are the same as those employed in Figure 3.2. The upper left sector in Plate 3.1 shows the incoming wave, and the upper right sector shows reflected wave. The lower part is for transmitted wave. This plate indicates that the transmitted wave is slightly refracted, and the reflection pressure is much weaker than that of the transmission. It also shows that there is no relative phase shift with the incident wave, consistent with those shown in Figures 3.2 and 3.3. When these waves are set in motion, the speed of propagation depends upon the sampling time in the simulation.

Plate 3.2 is the same as the Plate 3.1, except that the upper part shows the total field of summing incident and reflection waves. The interfering pattern is indicated by the highs and lows in the upper part of the figure. In this case, the interference is not so severe that the total field is dominated by the incident wave.

Plate 3.3 is the results for a plane wave incident at critical angle 33.5°. In this case, the reflected pressure is almost as strong as the incident wave, and the transmitted wave is refracted significantly so that wave fronts are perpendicular to the interface. It is noted that the pressure of the transmitted waves only slightly decay away from the interface. Again, there is no phase shift in this case.

When the incident waves and the reflected waves in Plate 3.3 are superimposed, the result is shown in Plate 3.4. In this case, the interfering is so severe that the total field becomes a standing wave in vertical direction, and propagating wave in horizontal direction. The nodal lines at about z=18, 50, 82 m are clearly shown in the figure.

Plate 3.5 shows the results for a plane wave with incident grazing angle 25°, which is smaller than the critical angle. In this case, the reflected wave has the same magnitude as the incident wave, but there is a slight phase shift. The transmitted wave is totally different from the previous results, with the evanescent nature clearly demonstrated in the figure. The pressure field in the lower medium nearly vanishes except in a region closed to the interface. The total field in the upper medium is shown in Plate 3.6, in which it shows a similar interfering pattern as in Plate 3.4, except that the nodal lines are now slightly distorted due to phase interference.

Soft Bottom Case

[DEMO]

In this case, we choose the parameters the same as in Figure 3.4. Plate 3.7 and Plate 3.8 show the results for incident angle 60°. From Figure 3.5, it is seen that the reflection coefficient is about 0.2 and phase angle 0, thus the total field of the upper medium is dominated by the incident wave. For the transmitted wave, the figure shows a very slight refraction as expected for an interface with small ratio of index of refraction.

Plate 3.9 and Plate 3.10 are for the wave incident at the Brewster angle, which is 22.6° in this case. From Figures 3.4 and 3.5, we find that the reflection coefficient is zero and tradition coefficient is unity. These characteristics are clearly shown in these plates, in which the total field of the upper medium is unaffected by the interface. The incident wave simply changes course when it travels across the interface.

Plate 3.11 and Plate 3.12 consider a low incident angle at 10°. The major difference from Plate 3.7 is that the reflected waves are in 180° phase shift with respect to incident wave. The total field in the upper medium is twisted by the phase shift.

Finally, we demonstrate a pathological case, in which the incoming wave incident upon the interface horizontally. Plate 3.13 shows that the reflected wave is parallel with the incident wave, but is completely out of phase. Moreover, the transmission field is empty. As a result, the whole sound field is completely silent as shown in Plate 3.14. This may form the basis for the application on counter balancing the unwanted noise as usually desired in many occasions.

3.4 Scattering From Perfectly Reflecting Rough Surfaces

In the remainder of this chapter, we shall consider plane wave scattering from perfectly reflecting rough surfaces. These surfaces are characterized by vanishes of either the total pressure or vertical displacement at the interface. The former is referred to as pressure-release surface, and the latter rigid or hard surface. Although not absolutely correct, these cases fairly approximate the sea surface and sea floor.

In this section, we shall derive the formulation which is capable of describing the scattering

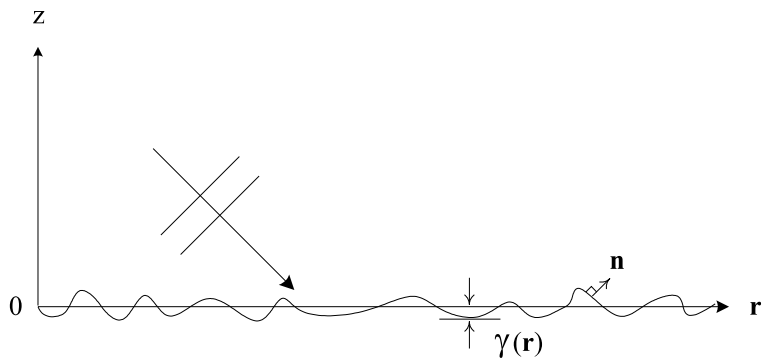

Figure 3.8: Coordinate system of a rough surface.

from single rough surface. Figure 3.8 shows the geometry of the surface. The roughness of the surface is usually specified by the *Rayleigh parameter* P, which is defined as

$$P = 2k\sqrt{\langle\gamma\rangle^2}\cos\theta \tag{3.16}$$

The Rayleigh parameter is to gauge the vertical scale of the roughness with respect to the vertical wavelength of the incident wave. If $P \ll 1$, the roughness of the surface is small so that the major part of energy of incident wave propagates in the specular direction as a coherent wave. If $P \gg 1$, corresponding to large scale roughness, the wave will scatter into a relative wide angle, causing the energy to diffuse all over the space. The schematic diagram was shown in Figure 1.1.

There are essentially two approaches to deal with scattering problem from rough surfaces: the *perturbation method* and the *tangent plane method* (also referred to as Kirchhoff approximation). The former is suitable for the roughness scale which is small, and the latter for roughness which is large and smooth such as undulation of extensive terrain. Here we shall be emphasized on the rough surfaces which have roughness scale smaller than or comparable with the wavelength so that the perturbation method will be employed. The validity of the perturbation method will be discussed following the derivation of the formulation.

3.4.1 Formulation of the Scattered Field

The wave propagation in a homogeneous medium is governed by the wave equation:

$$\frac{\partial^2 p}{\partial t^2} = c^2\nabla^2 p \tag{3.17}$$

The solution of the above equation must be accompanied with the initial and boundary conditions. The initial condition is specified by the phase $e^{-i\omega t}$, which stipulates the time dependence of the sound field. Here, ω is the angular frequency of the plane wave. The boundary conditions

for the problem we are concerned with can be expressed mathematically as

$$\begin{aligned} p|_{z=\gamma(\mathbf{r})} &= 0, \quad \text{pressure-release surface} \\ (\nabla p \cdot \mathbf{n})|_{z=\gamma(\mathbf{r})} &= 0, \quad \text{rigid surface} \end{aligned} \tag{3.18}$$

where $\mathbf{n} = (\mathbf{n}_h, n_z)$ is the unit vector of the inner normal to the rough surface, and $\nabla = \left(\nabla_h, \frac{\partial}{\partial z}\right)$, where the subscript h represents the horizontal components. It is noted that the boundary conditions, Equation (3.18), are specified at an elevated surface deviated from the mean surface. Since we are dealing with a random surface, the application of these boundary conditions at each individual point is horrendously difficult, if not impossible, and therefore other approaches have to be sought.

To proceed, we perturb the boundary conditions at $z = \gamma$ with respect to the roughness to $z = 0$, which is the mean surface. The perturbation is accomplished by Taylor series expansion with respect to γ, and then retaining the first-order term to yield the boundary conditions for pressure-release and rigid surface respectively as given below:

$$\begin{aligned} p + \gamma \frac{\partial p}{\partial z}\bigg|_{z=0} &= 0 \\ \frac{\partial p}{\partial z} + \gamma \frac{\partial^2 p}{\partial z^2} - \nabla_h p \cdot \nabla_h \gamma\bigg|_{z=0} &= 0 \end{aligned} \tag{3.19}$$

The accuracy of the above expansion is correct up to $\mathcal{O}(\gamma)$.

Following the standard practice of the perturbation method, the total field may be expressed as

$$p(\mathbf{r}, z, t) = p_0(\mathbf{r}, z, t) + p_1(\mathbf{r}, z, t) + \text{higher-order terms} \tag{3.20}$$

In the above equation, p_0 is the zeroth-order term, which is the solution for unperturbed surface, and p_1 is the first-order term, which is the same order as γ. Since we have assumed that the roughness is small so that $|p_1| \ll |p_0|$. The rest is referred to as higher-order terms which are to be discarded in this approximation. Substituting Equation (3.20) into Equation (3.17) and Equation (3.19) and equating separately the terms of the order of γ^0 and γ, we obtain the wave equations and boundary conditions (BC's) at the plane $z = 0$ for the zero-order and first-order problem as follows.

Wave Equations:

$$\frac{\partial^2 p_0}{\partial t^2} = c^2 \nabla^2 p_0 \tag{3.21}$$

$$\frac{\partial^2 p_1}{\partial t^2} = c^2 \nabla^2 p_1 \tag{3.22}$$

Pressure-Release BC's:

$$p_0 = 0 \tag{3.23}$$

$$p_1 = -\gamma \frac{\partial p_0}{\partial z} \tag{3.24}$$

Rigid Surface BC's:

$$\frac{\partial p_0}{\partial z} = 0 \tag{3.25}$$

$$\frac{\partial p_1}{\partial z} = -\gamma \frac{\partial^2 p_0}{\partial z^2} + \nabla_h p_0 \cdot \nabla_h \gamma \tag{3.26}$$

It is seen that the first-order problem involves the zeroth-order solution so that the zero-order problem must be solved first.

To solve for the problem for monotonic wave, we first separate the time dependence by letting

$$p(\mathbf{r}, z, t) = p_\omega(\mathbf{r}, z) e^{-i\omega t} \tag{3.27}$$

Substituting Equation (3.27) into Equation(3.21), we can obtain the *Helmholtz equation*

$$\left(\nabla^2 + k^2\right) p_{0,\omega} = 0 \tag{3.28}$$

For simplicity, the subscript ω will be dropped in the following presentations. Equation (3.28) is subject to the undisturbed boundary conditions, Equations (3.23) and (3.25), respectively, for pressure-release and rigid surface.

The zero-order solution for a plane wave incident upon a perfectly reflecting interface is readily shown to be

$$p_0 = \exp(i\,\mathbf{k_r} \cdot \mathbf{r}) \left[\exp(-i\,k_z z) \pm \exp(i\,k_z z)\right] \tag{3.29}$$

where the $-$ sign is for the solution for pressure-release surface, and the $+$ sign for the rigid surface. Also, $\mathbf{k_r}$ and k_z are the horizontal and vertical components of the wave vector $\mathbf{k}$ of the incident wave satisfying the condition

$$|\mathbf{k_r}|^2 + k_z^2 = k^2 \qquad (k = |\mathbf{k}|)$$

Substituting Equation (3.29) into Equations (3.24) and (3.26), we obtain the boundary conditions for which the first-order problem must satisfied at $z = 0$:

Pressure-Release BC's:

$$p_1(\mathbf{r}, 0) = 2\,i\,k_z \gamma(\mathbf{r}) \exp(i\,\mathbf{k_r} \cdot \mathbf{r}) \tag{3.30}$$

Rigid Surface BC's:

$$\frac{\partial p_1(\mathbf{r}, 0)}{\partial z} = 2\left[k_z^2 \gamma(\mathbf{r}) + i\,\mathbf{k_r} \cdot \nabla_h \gamma(\mathbf{r})\right] \exp(i\,\mathbf{k_r} \cdot \mathbf{r}) \tag{3.31}$$

It is the common practice that the roughness $\gamma(\mathbf{r})$ be represented by its Fourier components, which is defined as

$$\gamma(\mathbf{r}) = \int A(\mathbf{p}) \exp(i\,\mathbf{p} \cdot \mathbf{r})\, d\mathbf{p} \tag{3.32}$$

where $A(\mathbf{p})$ is the amplitude spectrum of the roughness, and $\mathbf{p}$ is the wave vector components.

Substituting Equation (3.32) into Equations (3.30) and (3.31), and introducing the factor $\exp(i\,q_z z)$ to account for wave propagating away from the interface, we may obtain the scattered field solution for pressure-release rough surface as

$$p_1(\mathbf{r}, z) = 2i\,k_z \int A(\mathbf{p}) \exp[i(\mathbf{k_r} + \mathbf{p}) \cdot \mathbf{r} + iq_z z] d\mathbf{p} \tag{3.33}$$

It is noted that $q_z = \sqrt{k^2 - |\mathbf{k_r} + \mathbf{p}|^2}$ is the vertical component of the scattered wave, and the square-root must be chosen so that $\mathrm{Im}(q_z) > 0$ to satisfy physical constraint. By defining $\mathbf{q} = \mathbf{k_r} + \mathbf{p}$ as the horizontal wavenumber of the scattered wave, Equation (3.33) may be written as

$$p_1(\mathbf{r}, z) = 2ik_z \int A(\mathbf{q} - \mathbf{k_r}) \exp[i(\mathbf{q} \cdot \mathbf{r} + q_z z)] d\mathbf{q} \tag{3.34}$$

Equation (3.34) is a convolution integral which clearly indicates that the scattered pressure at a particular observation point $(\mathbf{r}, z)$ is the overall contribution of all scattered plane waves propagating with amplitude components $A(\mathbf{q} - \mathbf{k_r})$. The amplitude of each plane wave component is dictated by the magnitude of the roughness spectrum at component $\mathbf{p}$, which is the part of wave vector to be made up for $\mathbf{k_r}$ so that the incident wave is able to scatter into direction $\mathbf{q}$. This is the Bragg's law of scattering.

Similar derivation will yield the scattered field solution for rigid rough surfaces as

$$p_1(\mathbf{r}, z) = 2ik_z \int \left[-\frac{k_z^2 - \mathbf{k_r} \cdot (\mathbf{q} - \mathbf{k_r})}{k_z q_z} \right] A(\mathbf{q} - \mathbf{k_r}) \exp[i(\mathbf{q} \cdot \mathbf{r} + q_z z)] d\mathbf{q} \tag{3.35}$$

This equation is similar to the pressure-release surface, except now a factor (the bracket term in the integrand) is weighted for the amplitude to account for the change of boundary condition.

3.4.2 Validity of the Perturbation Approximation

The accuracy of the perturbation approximation for scattering from one-dimensional randomly rough pressure release surfaces with a Gaussian roughness spectrum was studied by Thorsos and Jackson [48]. In general, the conditions given for the validity of perturbation theory are that (1) the RMS surface height should be small compared with the wavelength, and (2) the RMS surface slope is small compared to 1, although condition (2) is not necessary to be explicitly used in deriving the scattering field. It was found by Thorsos and Jackson that, comparing with the solutions obtained by the method of integral equation and high-order perturbation prediction, the condition (1) is insufficient to ensure the accurate of first-order perturbation theory for Gaussian roughness spectrum. Another parameter, the roughness correlation length, plays an important role in defining the region of validity.

The study has shown that reducing the surface slope by increasing the correlation length for a fixed RMS height actually causes the first-order perturbation predictions to fail. A numerical calculation of the region of validity was provided in terms of $k\sqrt{\langle \gamma^2 \rangle}$ and kl (l being correlation length), and the results demonstrated that increasing kl will reduce the resonance wavenumber

for the forth-order terms (the scattering cross section), leading to a contribution larger than the second-order terms. However, it should be noted that since their analysis is based upon the Gaussian roughness spectrum, the results may not necessarily apply to roughness spectra that exhibit power laws.

An explicit criterion for the region of validity for the first-order perturbation method applying on the Gaussian spectrum was established, which stipulates that $k\sqrt{\langle\gamma^2\rangle} \ll 1$ and $kl \leq 6$. In this study we shall use this criterion as an important guideline whenever the Gaussian roughness spectrum is employed.

3.5 Scattering From One-Dimensional Periodic Surface

[DEMO]

In this section, we consider a plane wave impinging upon a one-dimensional periodic rough surface. The surface is assumed to consist of a finite number of Fourier components, each with a phase angle which is randomly chosen over 0 and 2π. The surface may be represented by

$$\gamma(x) = \sum_{i=1}^{N} a_i \sin(\kappa_i x + \varphi_i) \tag{3.36}$$

where a_i, κ_i and φ_i are, respectively, the component amplitude, the component wavenumber and the phase angle, and N is the number of Fourier components. The Fourier transforms[1] of Equation (3.36) yields

$$A(\kappa) = \frac{1}{4\,\pi\,i} \sum_{i=1}^{N} a_i[\delta(\kappa - \kappa_i) - \delta(\kappa + \kappa_i)] \tag{3.37}$$

where δ is the Dirac delta function.

To obtain the scattered field due to the periodic surface, we substitute Equation (3.37) into Equation (3.34) to get

$$p_1 = \frac{k_z}{2\pi} \sum_{i=1}^{N} a_i \left\{\exp[i(k_x + \kappa_i)x + iq_z z] - \exp[i(k_x - \kappa_i)x + iq'_z z]\right\} \tag{3.38}$$

where $q_z = \sqrt{k^2 - (k_x + \kappa_i)^2}$ and $q'_z = \sqrt{k^2 - (k_x - \kappa_i)^2}$

Similarly, for rigid surface with the same rough surface, the scattered field solution is

$$p_1 = -\frac{1}{2\pi} \sum_{i=1}^{N} a_i \left\{\left(\frac{k_z^2 - \kappa_i k_x}{q_z}\right) \exp[i(k_x + \kappa_i)x + iq_z z] - \left(\frac{k_z^2 + \kappa_i k_x}{q'_z}\right) \exp[i(k_x - \kappa_i)x + iq'_z z]\right\} \tag{3.39}$$

A plane wave of 20 Hz incident upon a periodic surface with 45° grazing angle is considered. Plate 3.15 and Plate 3.16 with their propagation pattern shown dynamically are the

[1] $A(\kappa) = \frac{1}{2\pi} \int \gamma(x) \exp(-i\,\kappa\,x)\,dx$

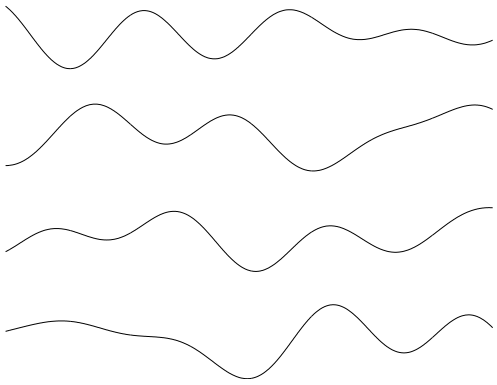

Figure 3.9: Sample periodic rough surfaces.

scattered field solutions for pressure-release and rigid periodic surface, respectively. The amplitude components and wavenumber components are generated by the random function rand in MATLAB, which are given by the following sequences:

a_i	14.89	26.99	24.65	19.35	24.54	19.81	10.26	8.69	10.24	16.02
κ_i	0.0254	0.0108	0.0293	0.0199	0.0130	0.0246	0.0191	0.0156	0.0243	0.0217

The sample surfaces are shown in Figure 3.9. Both plates show that there is a dominant scattering angle and a few minor scattering angles. It is also shown that the scattered field is less coherent for rigid case than pressure-release case. This may be attributable to the weighting factor in Equation (3.35), with which it acts as shading function and renders a stronger interference.

3.6 Scattering From Random Rough Surfaces

In this section, we shall present the scattering fields for random rough surfaces with power spectra discussed in Chapter 2. The results were presented in spatial domain for the pressure field. Although random in nature, these results give a good sense of the sound field distribution in space, allowing comparison with the realization of the spectra generated with the procedure given in Section 2.5.

3.6.1 Random Surface With Gaussian Spectrum

We first consider a random rough surface with Gaussian power spectrum. As mentioned before, the simplicity of the spectrum may well serve as a benchmark problem under consideration. For the purpose of comparison with the previous results, we first consider a one-dimensional Gaussian spectrum, which is given as follows:

$$P(\kappa) = \frac{l\,h^2}{2\sqrt{\pi}} \exp(-\frac{\kappa^2 l^2}{4}) \tag{3.40}$$

In this equation, h and l are, respectively the RMS height and correlation length.

Plate 3.17 is the solution for a plane wave of 20 Hz incident at 45° upon a rough surface with $h = 100$ m and $l = 50$ m. It is seen that the wave front is randomly severed due to interference of scattered waves in various directions. The dynamic demonstration will show that increasing h or decreasing l will make the scattered field even more random, as expected. All the level of observation in this section is chosen to be 50 m away from the rough surface, i.e., $z = 50$ m. [DEMO]

Plate 3.18 and Plate 3.19 are for the rough surface with power spectrum shown in Figure 2.12. It is a non-isotropic Gaussian with correlation length 60 m and 10 m in major and minor axis of the spectrum respectively. Plate 3.18 shows the result for a plane wave incident at 45° grazing angle and along the direction with shorter correlation, and Plate 3.19 is for the same condition except along the direction with longer correlation. These two results indicate that the pressure amplitude is larger for wave coming in along the direction with shorter correlation. This is reasonable because the surface appears to be rougher in that direction. Moreover, the results also show that the "patches" on Plate 3.18 appear to be parallel to the strikes of the rough surface, indicating that the plane wave is scattered sequentially as the wave front impinges the strikes. For Plate 19, the high pressure patches are scattered more randomly, showing that there seems no preference scattered direction, as one can imagine in view of the realization shown in Figure 2.12.

Plate 3.20 shows a result for a plane wave incoming horizontally along the direction with shorter correlation. The zero grazing angle makes the roughness appear to be flat so that the pressure field is nearly zero, however, the scattering pattern seems to reserve.

3.6.2 Random Surfaces With Goff-Jordan Spectrum

Here, we consider the scattering from a rigid rough surface with Goff-Jordan spectrum as shown in Figure 2.14. It is intended to simulate scattering from a rough seabed. Plate 3.21 is for a plane wave incident normally. It is seen that the scattering pattern resembles the topography of the rough surface shown in Figure 2.14. This is easily rationed because the wave is incident symmetrically, and therefore the sound field must have the similar distribution as the roughness.

Plate 3.22 and 3.23 are for a plane wave incident upon the rough surface with 45° normal angle, but the azimuthal direction being facing and along the strikes, respectively. The spatial characteristics of these two plates are similar to Plates 3.18 and 3.19. That is, the scattering is stronger and the pressure distribution is more similar to the rough surface, when the incoming plane is incident in the direction facing the strikes.

3.6.3 Random Surfaces With Pierson-Moskowitz Spectrum

Here we consider a plane wave impinges upon a pressure-release surface having a Pierson-Moskowitz power spectrum. It is a good model for studying sea surface scattering. Plate 3.24 and Plate 3.25 are, respectively, for a plane wave interacts with ocean surface shown in Figure 2.16 for wind speed of 12 m/s and Figure 2.17 for wind speed of 20 m/s. The incident angle is 45° and is in the direction of the wind. These results show that the difference of pressure amplitude is about one order, with that corresponding to wind speed of 20 m/s being larger. Furthermore, these two plates maps relatively in consistent in distribution with the roughness of the ocean surface, with Plate 3.25 showing scattering from ocean surface populated with larger waves.

Finally, Plate 3.26 is for the same condition as in Plate 3.25, except the incident azimuthal angle is different, where Plate 3.25 is for plane wave coming in along the direction of the wind, and Plate 3.26 is for plane wave coming in the direction perpendicular to the wind. It is seen that the orientation of the sound field changes accordingly as the incident angle changes. Also, the distributions of the pressure highs are different.

3.7 Summary

The main theme of this chapter is to study the pressure sound field for a plane wave impinging upon a rough interface. The Rayleigh reflection problem was studied first. Through the use of modern computing and data processing language such as MATLAB, it is very helpful to illustrate the reflection and transmission characteristics of the problem.

We then continue to investigate the plane wave scattering from rough surfaces. Under the framework of small perturbation method, the formulation for the scattered pressure field from perfectly reflecting rough surface was derived. The formulation was then employed to obtain the scattered field in conjunction with various power spectra, including the Gaussian spectrum, Goff-Jordan spectrum, and Pierson-Moskowitz spectrum. Many results for the random pressure field were presented and analyzed.

It is interesting to note that the sound field distributions bear close resemblance with the roughness distribution. So, in principle the scattered sound may be used to invert the sea surface roughness as many ongoing research attempted.

Chapter 4

Intensity and Correlation of the Scattered Field

In the previous chapter 3, we devoted ourselves in obtaining the scattered pressure field. Since the surface is random, so the scattered field is also random. Therefore, each solution of the pressure field merely represents one of the infinitely many samples. Although the random field itself is helpful in understanding the distribution of the pressure field, it does not provide firm information in terms of deterministic quantity as we usually wish to have.

There are two quantities which characterize the random scattered field: the intensity distribution and the spatial correlation. The former provides the expected value of the pressure level at each point in space, and the latter presents the coherence of the random pressure. Both quantities are important in understanding of the scattered field as well as in applications. In this chapter, we shall concentrate on these two subjects and obtain the results which are relevant to marine environment.

4.1 Average Intensity

The intensity of the scattered field is one of the most important parameters describing the scattered field. Due to the assumption of zero mean for the random surfaces, the mean value of the scattered field is also zero; however, the intensity which is proportional to the mean square of the acoustic pressure is not zero.

The intensity of the scattered field is related to the mean square pressure as follows:

$$I_1 = \frac{\langle p_1 \, p_1^\star \rangle}{\rho c^2} \tag{4.1}$$

where the asterisk denotes the complex conjugate quantity. For simplicity, we use $I_s = \rho c^2 I_1$ to denote a quantity representing the intensity of the scattered field. Here the subscript s denotes scattered field.

First we consider the pressure-release surface. Substituting Equation (3.33) into Equation (4.1), we obtain

$$I_s = 4k_z^2 \int\int \langle A(\mathbf{p}) A^\star(\mathbf{p}') \rangle \exp\left[i(\mathbf{q} - \mathbf{q}') \cdot \mathbf{r} + i(q_z - q_z')z \right] d\mathbf{q}\, d\mathbf{q}' \tag{4.2}$$

where $q_z = \sqrt{k^2 - |\mathbf{k_r} + \mathbf{p}|^2}$ and $q_z' = \sqrt{k^2 - |\mathbf{k_r} + \mathbf{p}'|^2}$. This formulation expresses the intensity of the scattered field as ensemble average of the amplitude spectrum, which is related with the power spectrum as follows:

$$\langle A(\mathbf{p}) A^\star(\mathbf{p}') \rangle = P(\mathbf{p}) \delta(\mathbf{p} - \mathbf{p}') \tag{4.3}$$

Equation (4.3) is derived in Appendix A. It is noted that the power spectrum is defined as

$$P(\mathbf{p}) = \frac{1}{(2\pi)^2} \int_{-\infty}^{\infty} d\bar{\mathbf{r}}\, C(\bar{\mathbf{r}}) e^{-i\mathbf{p}\cdot\bar{\mathbf{r}}} \tag{4.4}$$

where $C(\bar{\mathbf{r}})$ is the correlation function for a stationary random rough surface. Substituting Equation (4.3) into Equation (4.2) and integrating over $\mathbf{p}$ yields

$$I_s = 4k_z^2 \int P(\mathbf{p}) d\mathbf{p} = 4k_z^2 \langle \gamma^2 \rangle \tag{4.5}$$

This equation shows that the intensity is merely linearly proportional to mean-square roughness, and quadratically to vertical wavenumber.

Figure 4.1 shows the intensity as function of incident grazing angles for a plane wave impinging upon the sea surface, i.e., pressure-release surface with Pierson-Moskowitz power spectrum. The wind speed is shown inside the graphs. It is seen that the intensity increases as the grazing angle increases. Also, as the wind speed increases, the intensity increases as well.

4.2 Scattering Coefficients

The *scattering coefficient*, $m_s(\theta, \phi)$, for a scatterer with differential surface area dS is defined as

$$dI_s = I_i \frac{m(\theta, \phi)}{R^2}\, dS \tag{4.6}$$

where I_i is the incident intensity, R is the distance from the observation point to the scatterer, θ is the angle between the scattered wave and the vertical axis, and ϕ is the azimuth angle. The coordinate system is chosen so that the incident plane wave lies on the xz-plane as shown in Figure 4.2. Moreover, we shall assume that the observation point is far enough so that only the propagating, non-attenuating, waves make contributions. This is called the far zone, or Fraunhofer zone, of the scattered field, which satisfies the following conditions:

$$L \ll R, \quad lL/\lambda \ll R \tag{4.7}$$

where L is linear dimension of the area.

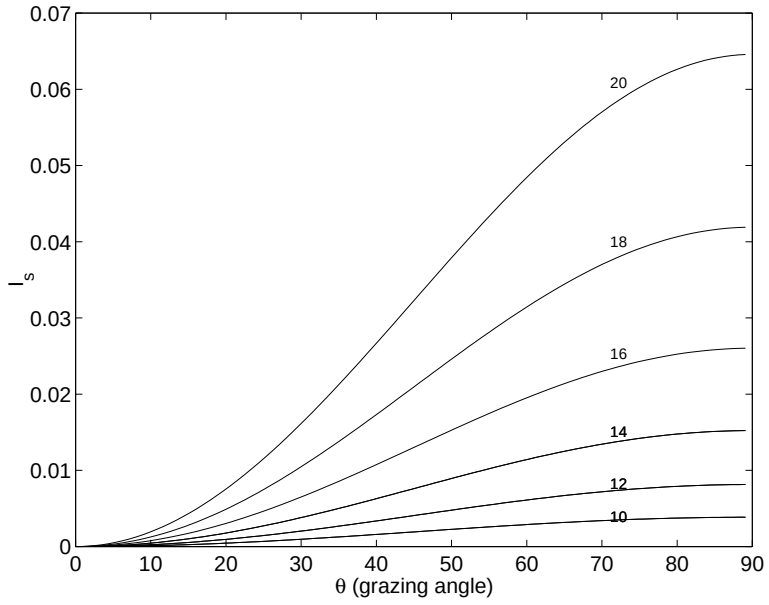

Figure 4.1: Intensity as function of grazing angles and wind speeds.

It is clear from the definition that the scattering coefficient is only function of angles, not the distance. It represents the angular distribution of the scattered energy per unit scattering surface, thus it is the a quantity which characterizes the roughness. If we take the incident intensity as unity, and consider the surface as infinite extent, then the intensity due to an infinite plane is

$$I_s = \int \frac{m_s(\theta,\phi)}{R^2}\, dS = \int_0^{2\pi} \int_0^{\pi/2} m_s(\theta,\phi) \tan\theta \, d\phi \, d\theta \tag{4.8}$$

where the differential area $dS = R^2 \tan\theta \, d\theta \, d\phi$ is employed. Equation (4.8) must be the same as Equation (4.5). For pressure-release surface, Equation (4.5) can be written as

$$I_s = 4\cos^2\theta_0 \, k^4 \int_0^{2\pi} \int_0^{\pi/2} P(\mathbf{p}) \sin\theta \cos\theta \, d\phi \, d\theta \tag{4.9}$$

in which the relationships $d\mathbf{p} = \xi d\xi d\phi$ and $\xi = k\sin\theta$ are applied. Equating Equation (4.8) and Equation (4.9) yields the scattering coefficient for pressure-release surface as

$$m_s(\theta,\phi) = 4k^4 \cos^2\theta_0 \cos^2\theta \; P(\mathbf{p}) \tag{4.10}$$

where $\mathbf{p} = (k\sin\theta\cos\phi - k\sin\theta_0, k\sin\theta\sin\phi)$.

For rigid surface, the derivation of the scattering coefficient is more complicated due to the fact that the boundary condition involves the surface height function and its gradients, which is also assumed to be zero mean. The derivation may be found in Reference [34] so that it will not to be reiterated here. The result is given as

$$m_s(\theta,\phi) = 4k^4(1 - \sin\theta_0 \sin\theta\cos\phi)^2 \; P(\mathbf{p}) \tag{4.11}$$

where again it is noted that $\mathbf{p} = \mathbf{q} - \mathbf{k}$.

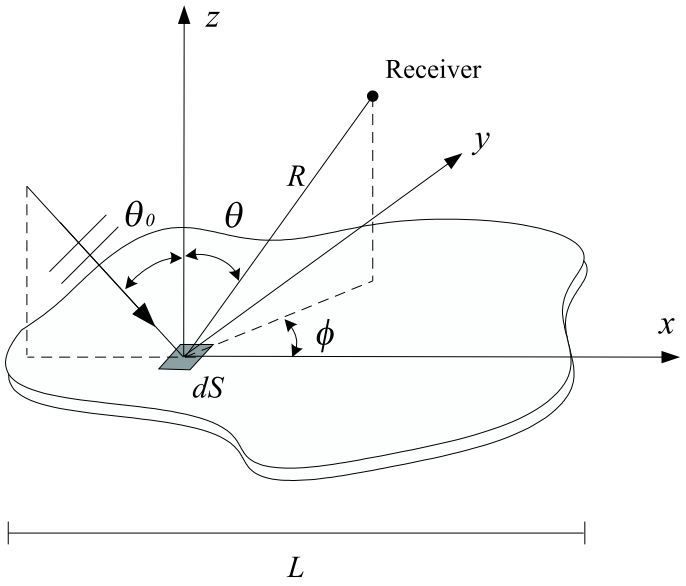

Figure 4.2: Coordinate system for the scattered field.

Examples

Here we show a few examples of the scattering coefficients for various kinds of roughness. Figure 4.3 shows the scattering coefficients for a plane incident at 45° onto a rigid rough surface with isotropic Gaussian spectrum whose RMS height is 5 m and four different correlation lengths are respectively 5, 15, 25, and 50 m. The frequency is 20 Hz. The results show that, for small correlation length ($\lambda = 5$ m), the energy is scattered mainly into the backward ($\phi = 180°$) and horizontal direction ($\theta = 90°$). This is because of the fact that for small correlation, the surface is rougher so that the incoming wave is more likely to be scattered backwards. When the correlation length increases to 15 m, the energy is gradually turned to the forward and vertical sector, and eventually, as the correlation increases to 50 m, the scattered energy is concentrated in the forward (0°) and specular direction (45°), which is seen in the subplot corresponding to $\lambda = 50$ m in the figure. It is noted that for large correlation length the surface is smooth so that the wave mainly scatters into specular and forward direction as expected.

Figure 4.4 shows the scattering coefficients for the same conditions as in Figire 4.3 except the surface is being changed to pressure-release. The results indicate that in the large correlation limit the two results are almost identical, but the difference occurs at small correlation length, in which the scattering coefficient is smaller for pressure-release surface than that for rigid surface. Also, the major scattering angle is in the normal direction. Similar interpretation for the results prevails.

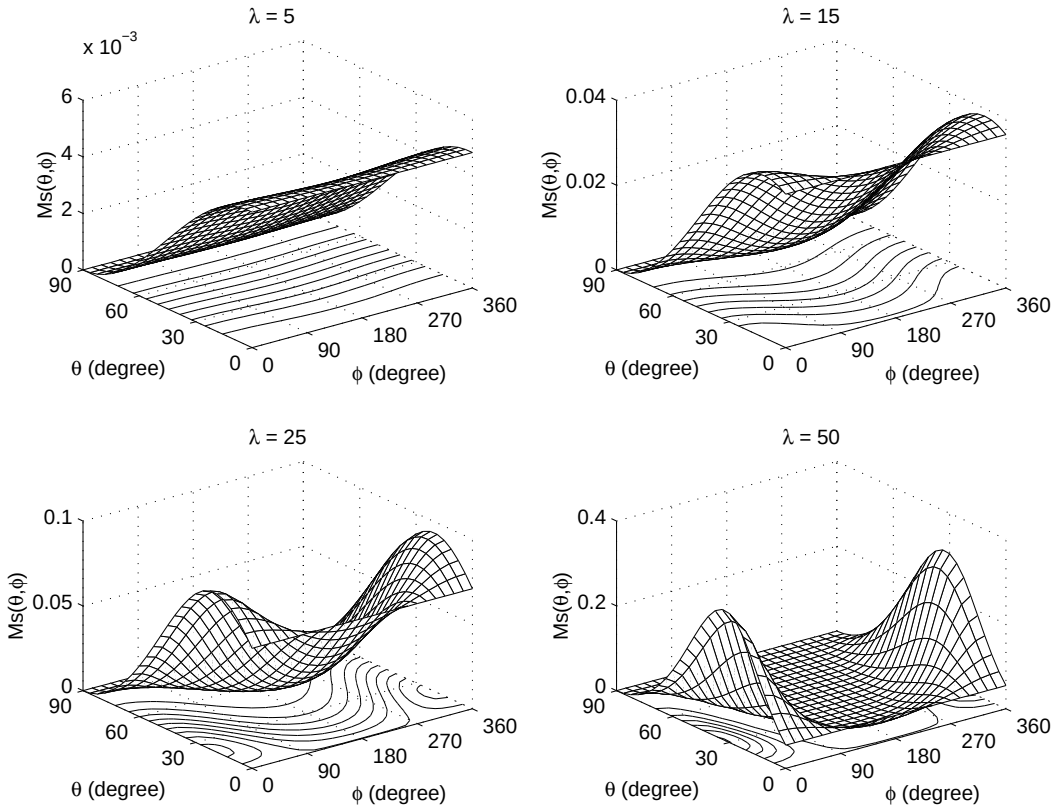

Figure 4.3: Scattering coefficients for rigid isotropic Gaussian spectrum with RMS height of 5 m, and four correlation lengths: 5, 15, 25, and 50 m.

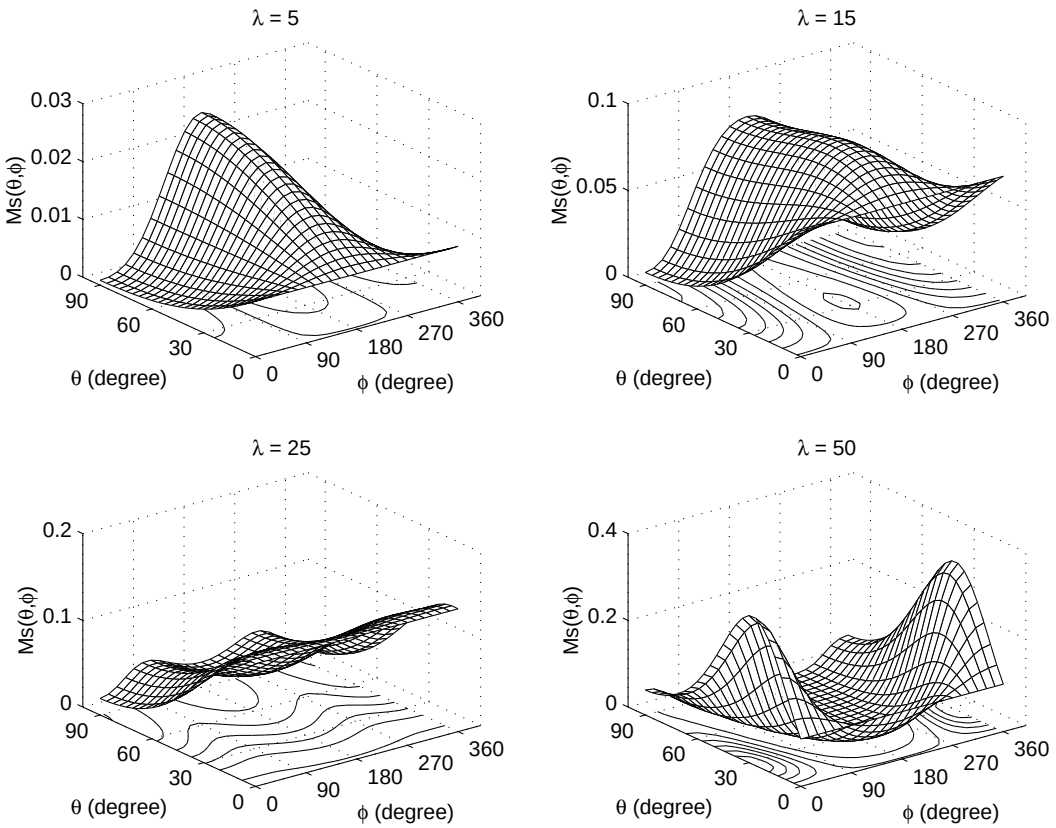

Figure 4.4: Scattering coefficients for pressure-release isotropic Gaussian spectrum with RMS height of 5 m, and four correlation lengths: 5, 15, 25, and 50 m.

4.3 Correlation Function of the Scattered Field

An important characteristic of a scattered field is the spatial correlation function. In some cases this function allows us to obtain the solution of an inverse problem, i.e., to find the correlation function of the roughness. It is also the correlation function which characterizes the spatial structure of the scattered field.

The spatial correlation function is defined as

$$B_s(\bar{\mathbf{r}}, \eta) = \langle p_s(\mathbf{r}_1, z_1) p_s^\star(\mathbf{r}_2, z_2) \rangle \tag{4.12}$$

Here, again we assume that the rough surface is infinite, and the incident wave is a plane wave. We are mainly concerned with the correlation property for observation point far away from the rough surface, i.e., far zone. Similar to the derivation of the scattered intensity in Section 4.1, we may derive the correlation functions for pressure-release as follows:

$$B_s(\bar{\mathbf{r}}, \eta) \quad = \quad 4k_z^2 \int_\Gamma P(\mathbf{p}) \exp[-i(\mathbf{q} \cdot \bar{\mathbf{r}} + q_z \eta)] d\mathbf{q} \tag{4.13}$$

where $\bar{\mathbf{r}} = \mathbf{r}_2 - \mathbf{r}_1$, $\eta = z_2 - z_1$, $q_z = \sqrt{k^2 - q^2}$, and Γ is a domain of q corresponding to real values of q_z. It should be noted that the horizontal correlation may be obtained by setting $\eta = 0$, and compute the value of B_s as function of $\bar{\mathbf{r}}$. Likewise, the vertical correlation is obtained by setting $\bar{\mathbf{r}} = 0$, and compute B_s as function of η. Furthermore, the intensity is the value of correlation function at zero separation of the receiver, i.e., $B_s(\mathbf{0}, 0)$.

Examples

In this section, we demonstrate a few cases for correlation function for pressure-release rough surface. Plate 4.1–Plate 4.4 is the two-dimensional correlation function for a plane wave incident at 45° upon a one-dimensional Gaussian rough surface with four different correlation length. The RMS height is taken to be 10 m, and the correlation lengths of the rough surface are, respectively, 1000, 100, 45, and 10 m. It is clear that the scattered field is very coherent for very large correlation length (Plate 4.1), and as the correlation length decreases to 100 m, the coherent part of the scattered field becomes narrow, with high correlation mainly in the specular direction (Plate 4.2). As the correlation length continues to decrease to 45 m, the coherent part begins to turn blur, and eventually when correlation length reduces to 10 m, the scattered becomes completely diffuse. This is a very good example to show how the correlation length of the rough surface affects the coherency of the sound field.

Figure 4.5 and Plate 4.5 show the horizontal correlation of the sound field for a plane wave incident normally upon the sea surface with Pierson-Moskowitz spectrum for wind speed of 12 m/s. The result indicates that the sound field is more correlated in y direction than in x-direction, and is characterized by two low negative correlation regions.

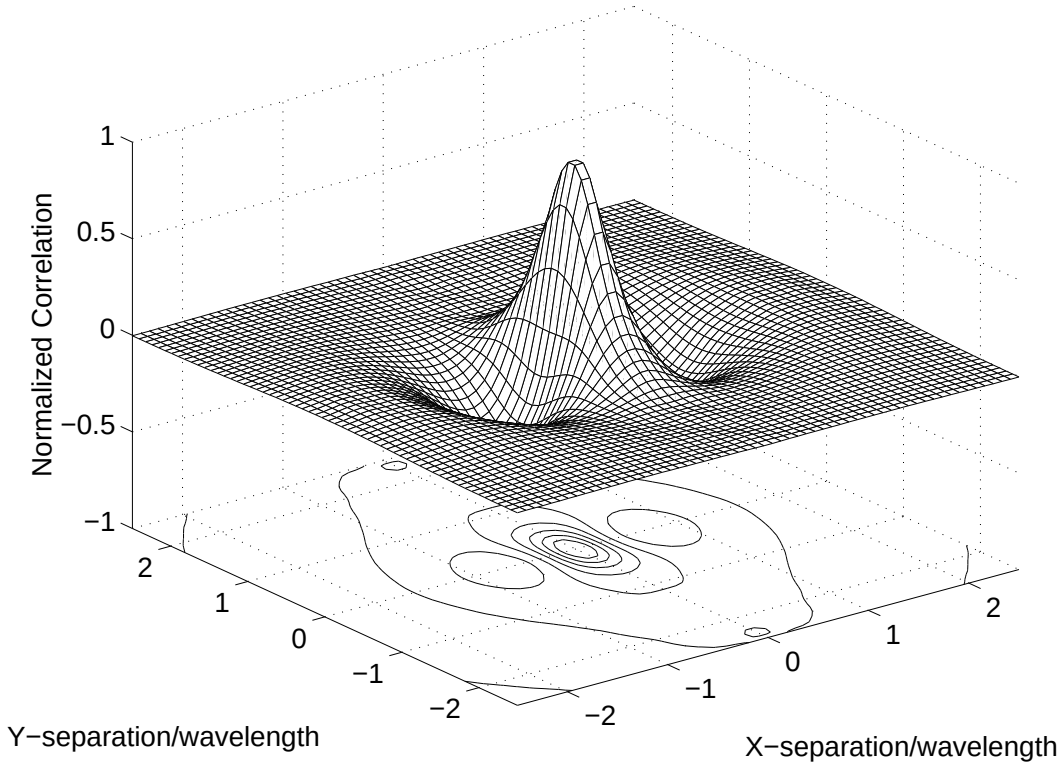

Figure 4.5: Horizontal correlation function for Pierson-Moskowitz power spectrum with wind speed 12 m/s. The plane incident upon the surface normally.

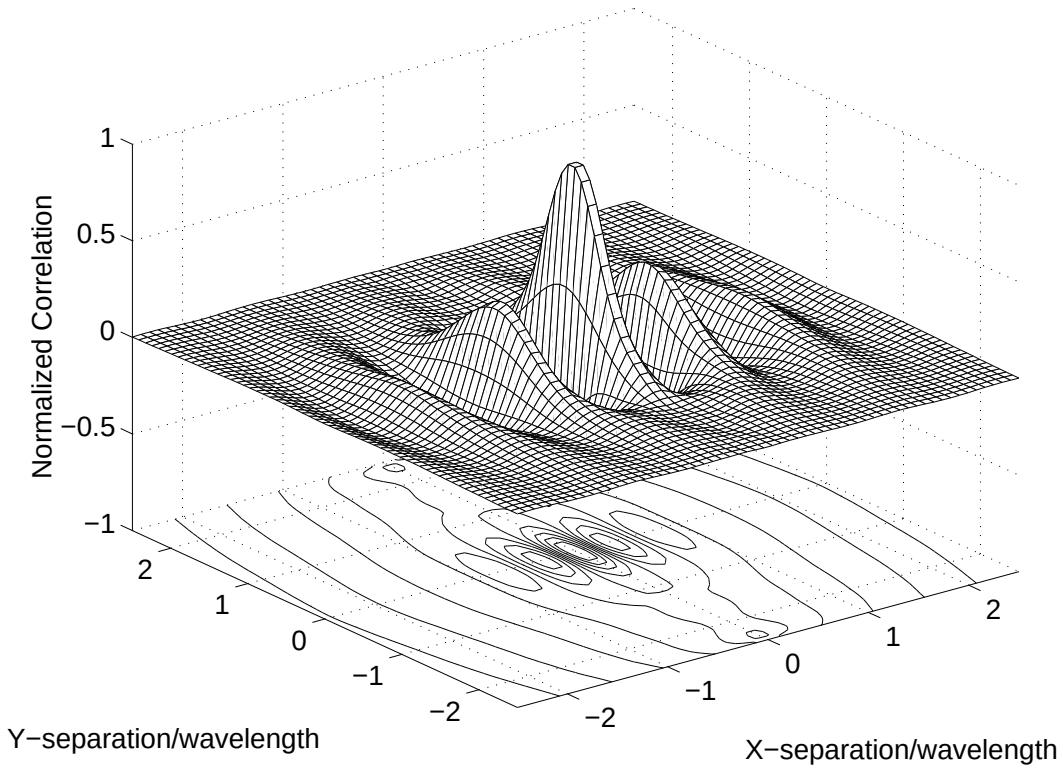

Figure 4.6: Horizontal correlation function for Pierson-Moskowitz power spectrum with wind speed 12 m/s. The plane incident upon the surface with 45° incident grazing angle and along the direction of the wind field.

Figure 4.6 and Plate 4.6 demonstrate the horizontal correlation function of the scattered field for the same roughness spectrum as that in Figure 4.5, except that the incident plane wave is coming onto the surface with 45° degree grazing angle and along the direction of the wind. In this case, the correlation function shows two high coherent zone neighboring the major high coherent zone.

The correlation function of the scattered field such as those shown in the above two figures has many implications, and thus deserves further discussion. To understand the structure of the function, it is noted from its definition that the correlation function has significance both in scattering strength and phase interference. A low value of correlation between two points in space may signify that the two received pressure fields have either low pressure picked up by both or one of the receivers, or the phases between the two pressure fields are not related to each other. With this mind, the correlation pattern shown in Figure 4.6 implies that the incoming plane wave is scattered mostly into the forward sector of the space, so that the correlation function has several high-value zones in the forward direction. The decaying structure of the correlation function shows that although the scattered field is more coherent in the direction normal to the wind, the energy scattered into that direction is less significant, while in the direction along the wind field, there is more energy but less coherent. This is consistent with our perception of the

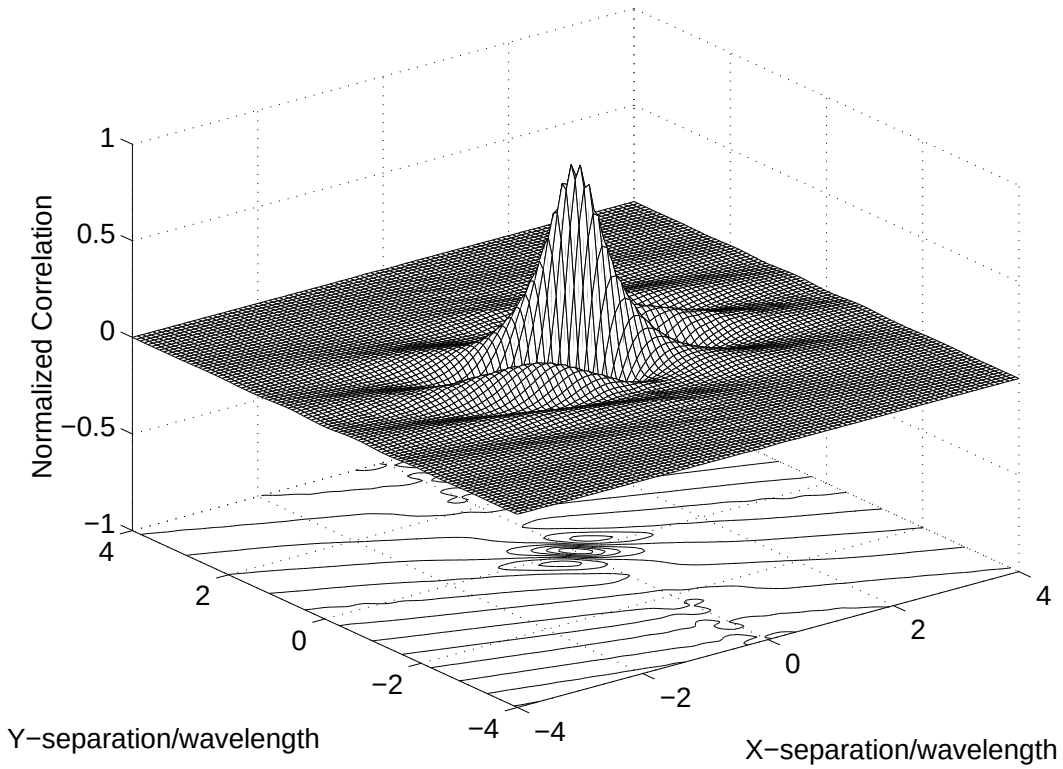

Figure 4.7: Horizontal correlation function for Pierson-Moskowitz power spectrum with wind speed 12 m/s. The plane incident upon the surface with 45° incident grazing angle and normal to the direction of the wind field.

scattered field in view of the wave field distribution shown in Figure 2.16.

Figure 4.7 and Plate 4.7 presents the horizontal correlation for the same conditions as in Figure 4.6, except that the incident azimuthal direction is normal to wind field. This figure shows a skew symmetric distribution, indicating that most energy are scattered into direction which makes an angle of 45° with the direction of incident azimuthal angle. The fast decaying structure of in the direction of high energy indicates that the scattered field is even less ordered than previous cases.

Finally, the correlation for a plane wave incident normally to a sea surface when the driving wind speed is 20 m/s is shown in Figure 4.8 and Plate 4.8. This is similar to Figure 4.5, except now the scattered field looks more coherent. This is conceivable in that the wave fields are dominated by trains of large waves which appear to be less random, as a result, the scattered field has longer correlation lengths when compared with Figure 4.8.

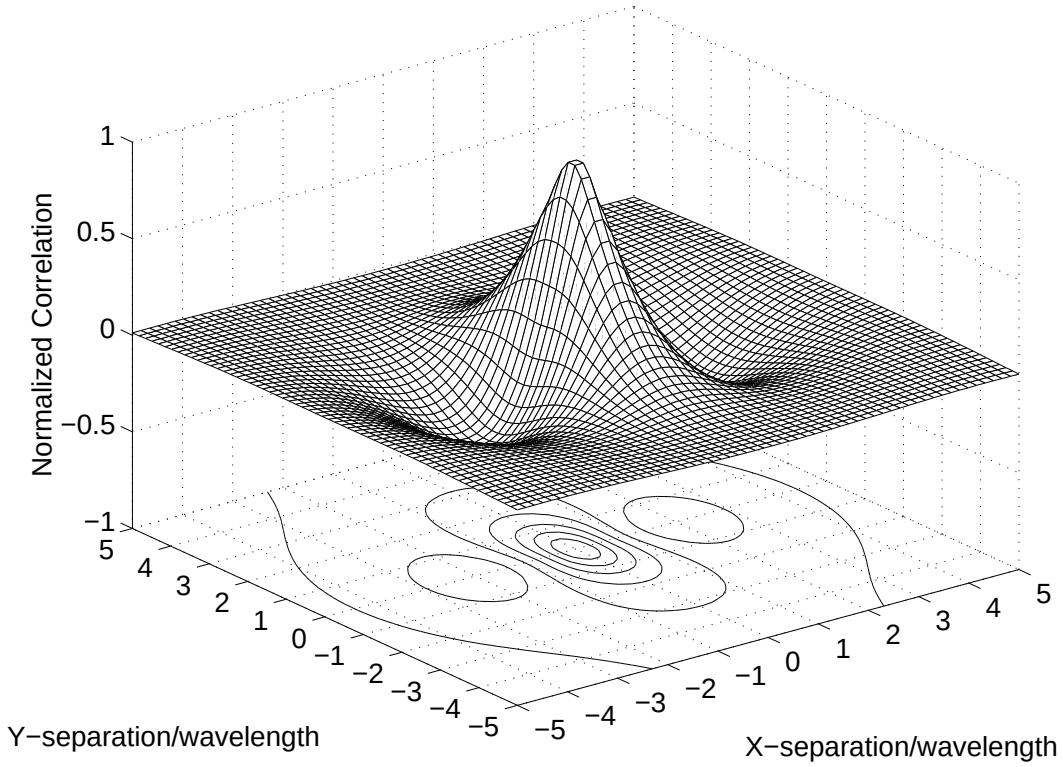

Figure 4.8: Correlation function for Pierson-Moskowitz power spectrum with wind speed 20 m/s. The plane incident upon the surface normally.

4.4 Summary

In this chapter, we have studied some of the most important properties of the scattered field, including average intensity, scattering coefficients, and spatial correlation. These results provide many useful information embedded in the scattered field.

Comparing with previous chapter, the quantities presented in this chapter are all deterministic. Although less prominent in terms of direct visualization, these quantities characterize the scattered fields, and serve as the basis for the applications of inversion of the rough surfaces.

Chapter 5

Scattering From an Interface over a Penetrable Layered Medium

The previous chapter deals with a simple environmental model in that only a single perfectly reflecting surface is considered. This problem has illustrated the basic scattering characteristics and mechanisms, which shed light on the general properties of scattering from a rough surface in a more complex environment.

The sea surface is an interface between sea water and air, and because of the strong impedance contrast between these two media, the sea interface may well be approximated as a perfectly reflecting pressure-release surface. However, the sea floor is an interface between water and elastic medium. Their impedance ratio is much smaller than that of sea surface, and therefore, treating the sea floor as a perfectly reflecting surface is less justifiable.

In this chapter, we shall consider a more realistic case, in which the rough surface is being treated as an interface overlying a penetrable layered medium. With the assumption of perfectly reflecting being released, it opens a new realm of scattering problem. The general theory of wave scattering from a layered medium or waveguide must be developed. It is expected that due to the increase of complexity, analytical solution such as we obtain in the previous chapter will no loner to exist, and numerical method must then be employed.

It is to be stressed here that we do not intend to embark on a full investigation of the problem entitled to this chapter. Rather, we shall review the theoretical model and apply current available software OASES to the problems of our interest. While OASES is an extensive program which is capable of solving for many acoustic propagation problem in an oceanic environment, it is remained to be developed for scattering from a rough interface overlying a medium with continuously varying acoustic properties. Therefore, we shall propose a model for this problem and attach to Appendix B. It is the intent of this author to continue investigation of this problem following the completion of this thesis work.

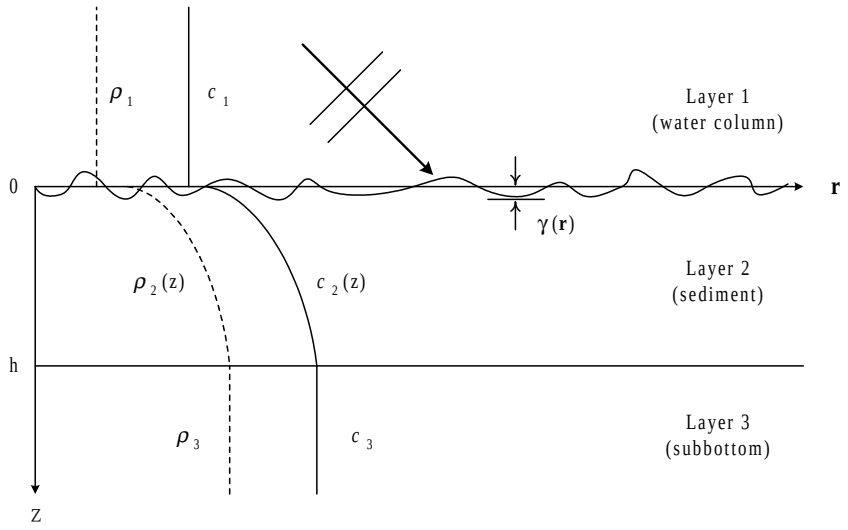

Figure 5.1: A realistic model.

5.1 A Realistic Model

Consider a plane wave impinges a rough interface overlying a nonhomogeneous medium as shown in Figure 5.1. The medium is assumed to be horizontally stratified, which means the acoustical properties of the medium depend upon the depth and not in range. From many geological surveys, it has been shown that both sound speed and density vary gradually to a certain depth and then remain constant afterwards. To solve the problem, the standard practice is to discretize the medium into several layers in which the acoustic properties may be assumed to be constant. This is shown in Figure 5.2

In this chapter, we shall approximate the problem shown in Figure 5.1 by a model shown in Figure 5.2. This is reasonable if the gradients of sound speed and density is small. When the gradients of the properties are large, it may seem probable to obtain solution by increasing the number of layers and decrease the depth of each layer. However, the very assumption for the perturbation method to work is that the layer depth must be much larger than the RMS roughness of the surface, which might be violated in some cases. As a result, for roughness greater than the length scale of the variation, only coarse subdivision may be taken in order to satisfy the assumption. Therefore the quality of solutions may be degraded to such a degree that other solution method may require to be employed.

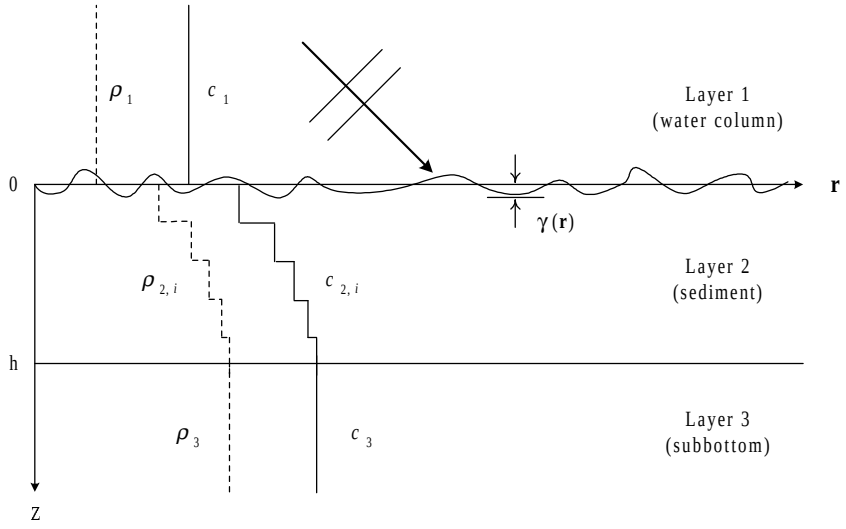

Figure 5.2: A model for discretized horizontally-stratified medium.

5.2 General Perturbation Theory for Wave Scattering From Rough Surfaces Over a Stratified Medium

In this section, we briefly review the perturbation theory for wave scattering from rough surfaces over a horizontally stratified medium. Since many relevant papers may be found from literature, such as Liu & Henrik [26], Kuperman & Henrik [23], so only the essential formulations are summarized here.

5.2.1 Wave Equation for Nonhomogeneous Media

The wave equation in an ideal fluid can be derived from hydrodynamics and the adiabatic relation between pressure and density. The governing equations include the equation of continuity, the Euler's equation, and the equation of state, which are, respectively, given by

$$\frac{\partial \rho}{\partial t} = -\nabla \cdot \rho \mathbf{v} \tag{5.1}$$

$$\rho \frac{\partial \mathbf{v}}{\partial t} + \rho \mathbf{v} \cdot \nabla \mathbf{v} = -\nabla p(\rho) \tag{5.2}$$

$$\frac{Dp}{Dt} = \frac{\kappa}{\rho} \frac{D\rho}{Dt} \tag{5.3}$$

In the above equations, ρ is the density, $\mathbf{v}$ the particle velocity, p the pressure, κ for the bulk modulus.

A standard procedure to extract acoustic wave is by assuming that $p = p_0 + p'$, $\rho = \rho_0 + \rho'$, and $\mathbf{v}$ is also a small quantity. The mean flow is assumed to be zero. The linear approximations, which lead to the acoustic wave equation, involve retaining only first-order terms in the hydrodynamic equations. These are

$$\frac{\partial \rho'}{\partial t} = -\nabla \cdot (\rho_0 \mathbf{v}) \tag{5.4}$$

$$\rho_0 \frac{\partial \mathbf{v}}{\partial t} = -\nabla p' \tag{5.5}$$

$$\frac{\partial p'}{\partial t} + \mathbf{v} \cdot \nabla p_0 = \frac{\kappa_0}{\rho_0} \left(\frac{\partial \rho'}{\partial t} + \mathbf{v} \cdot \nabla \rho_0 \right) \tag{5.6}$$

Equation (5.5) can be somewhat simplified. Its right-hand side can be transformed, with the help of Equation (5.4), to yield the equation

$$\frac{\partial p'}{\partial t} + \mathbf{v} \cdot \nabla p_0 + \kappa_0 \nabla \cdot \mathbf{v} = 0 \tag{5.7}$$

In the following sections, p_0 shall be considered constant throughout the fluid, i.e. term depending on ∇p_0 shall be disregarded. Equation (5.7) then takes the form

$$\frac{\partial p'}{\partial t} + \kappa_0 \nabla \cdot \mathbf{v} = 0 \tag{5.8}$$

To derive the wave equation, it is necessary to eliminate $\mathbf{v}$, which may be achieved by taking divergence on Equation (5.4) and differentiation on Equation (5.8), with appropriate manipulation of some parameters. The results of a subsequent subtraction will yield

$$\frac{1}{\kappa_0} \frac{\partial^2 p'}{\partial t^2} = \nabla \cdot \left(\frac{1}{\rho_0} \nabla p' \right) \tag{5.9}$$

where we consider that the medium is of varying density. For brevity, we drop the superscript $'$ and the subscript 0 and Equation (5.9) can be rewritten as [4]

$$\nabla^2 p - \frac{1}{c^2} \frac{\partial^2 p}{\partial t^2} = \frac{1}{\rho} \nabla \rho \cdot \nabla p \tag{5.10}$$

with $c^2 = \frac{\kappa_0}{\rho_0}$. Equation (5.10) is the wave equation with density and sound speed stratification. It is seen that the term on right-hand-side is due to the density stratification. If the density is constant in space, Equation (5.10) is reduced to the standard form of wave equation.

$$\nabla^2 p - \frac{1}{c^2} \frac{\partial^2 p}{\partial t^2} = 0 \tag{5.11}$$

5.2.2 Solutions of Wave Equation for Homogeneous Media

For an isotropic medium, the acoustic wave field in terms of pressure can be expressed by Equation (5.11). Define Fourier transform in time as follows:

$$p_\omega(\mathbf{r}, z) = \frac{1}{\sqrt{2\pi}} \int dt \; p(\mathbf{r}, z, t) e^{-i\omega t} \tag{5.12}$$

$$p(\mathbf{r}, z, t) = \frac{1}{\sqrt{2\pi}} \int d\omega \; p_\omega(\mathbf{r}, z) e^{i\omega t} \tag{5.13}$$

Then, application of the above transform on wave equation will yield Helmholtz equation as

$$(\nabla^2 + k^2) p_\omega = 0 \tag{5.14}$$

where $k = \omega/c$ is the wavenumber. Since the medium properties do not depend upon the range, the range dependence may again be removed by using two-dimensional spatial Fourier transform defined as

$$\tilde{p}_\omega(\mathbf{k_r}, z) = \frac{1}{2\pi} \int d^2\mathbf{r} \; p_\omega(\mathbf{r}, z) e^{i\mathbf{k_r}\cdot\mathbf{r}} \tag{5.15}$$

$$p_\omega(\mathbf{r}, z) = \frac{1}{2\pi} \int d^2\mathbf{k_r} \; \tilde{p}_\omega(\mathbf{k_r}, z) e^{-i\mathbf{k_r}\cdot\mathbf{r}} \tag{5.16}$$

where $k_r = |\mathbf{k_r}|$ is the horizontal wavenumber. Application of the transform will lead to the an equation which only depends on depth, thus referring to depth-separated wave equation as follows:

$$\left(\frac{d^2}{dz^2} + [k^2(z) - k_r^2] \right) \tilde{p}_\omega(\mathbf{k_r}, z) = 0 \tag{5.17}$$

where $k_r^2 = |\mathbf{k_r}|^\mathbf{2}$ is the horizontal wavenumber. The subscript ω signifies the quantities being monotonic with frequency ω. Since it is implied throughout the following presentation, the subscript ω is dropped for brevity.

The depth-dependence wave equation, Equation (5.17), is a linear ordinary differential equation in z, with the horizontal wavenumber k_r being a parameter. Therefore, the general solution for the depth dependence of the field, the so-called depth-dependent Green's function, takes the form

$$\tilde{p}(\mathbf{k_r}, z) = \mathcal{A}^-(\mathbf{k_r}) \tilde{p}^-(\mathbf{k_r}, z) + \mathcal{A}^+(\mathbf{k_r}) \tilde{p}^+(\mathbf{k_r}, z) + \hat{\tilde{p}}(\mathbf{k_r}, z) \tag{5.18}$$

where $\mathcal{A}^-(\mathbf{k_r})$ and $\mathcal{A}^+(\mathbf{k_r})$ are arbitrary coefficients to be determined, and $\hat{\tilde{p}}(\mathbf{k_r}, z)$ is a particular solution to account for the source field if a source is present in the medium.

For a stratification of isovelocity layers with the propagation in each layer governed by Equation (5.17) with $k(z) = k_i$, the solutions of Equation (5.17) are of exponential form. Thus the homogeneous solution for the layer i has the integral representation:

$$p_i(\mathbf{r}, z) = \frac{1}{2\pi} \int d^2\mathbf{k_r} \, e^{-j\mathbf{k_r}\cdot\mathbf{r}} \left[p_i^-(\mathbf{k_r}) e^{-\alpha_i z} + p_i^+(\mathbf{k_r}) e^{+\alpha_i z} \right] \tag{5.19}$$

where $\alpha_i = \sqrt{k_r^2 - k_i^2}$. The subscript i stands for i^{th} layer. Equation (5.19) may be interpreted as decomposition of the acoustic field into up- and down-going plane waves with horizontal wavevector $\mathbf{k_r}$ and amplitudes $p_i^-(\mathbf{k_r})$ and $p_i^+(\mathbf{k_r})$, respectively.

Equation (5.19) is the general solution of the Helmholtz equation for isovelocity layer with the unknown amplitudes p_i^- and p_i^+ yet to be determined from the physical constraints of the problem. In the present context, these constraints are continuities of pressure and vertical

displacement at the interface. Using a differential operator notation B_i introduced in Ref. [23], these conditions can be expressed as:

$$B_i(p_{i;i+1}) = 0, i = 1, 2, \ldots, N-1 \tag{5.20}$$

where N is the total number of layers, including the upper and lower half-spaces. Again, the Fourier transform is applied to the boundary conditions, Equation (5.20), replacing the differential operators by algebraic operators

$$\tilde{B}_i(\mathbf{k_r}) \left[\tilde{p}^{\mp}_{i;i+1}(\mathbf{k_r}) + \hat{\tilde{p}}^{\mp}_{i;i+1}(\mathbf{k_r})\right] = 0, i = 1, 2, \ldots, N-1 \tag{5.21}$$

with $\tilde{p}^{\mp}_{i;i+1}(\mathbf{k_r})$ being a vector containing the unknown plane-wave amplitudes for the homogenous solution in the layers i and $i+1$, and $\hat{\tilde{p}}^{\mp}_{i;i+1}(\mathbf{k_r})$ is added to account for the amplitudes of the source field in the two layers.

It should be noted that the linear system, Equation (5.21), cannot be directly solved locally at interface i since the number of unknowns $\tilde{p}^{\mp}_{i;i+1}$ is larger than the number of equations. However, these local systems may be assembled to form a global system, which when supplemented by the radiation conditions for $z \to \pm\infty$ may be directly solved for the unknown plane-wave amplitudes, and the solution of the Helmholtz equation is then determined by carrying out the wavenumber integral, Equation (5.19). The above procedure is known as *direct global matrix* (DGM) approach and has formed the backbone of the OASES code.

5.3 Solution for Rough Boundaries

Here, we review the boundary perturbation approach developed in Reference [23] for the model geometry shown in Figure 5.1, which extends the application of the spectral field representation in Equation (5.21) to a stratification with small interface roughness.

Assume that the interface at depth z_i between two layers i and $i+1$ is randomly rough with elevation $\gamma(\mathbf{r}) = z - z_i$, with mean zero, $\langle\gamma(\mathbf{r})\rangle = 0$, as sketched in Figure 5.3. Since boundary conditions must be applied at $z = \gamma(\mathbf{r}) + z_i$, the boundary conditions can be expressed in a rotated system defined by the local tangent plane of the rough interface.

Let the capital letters W, U, N, and T represent the displacements and stresses in the rotated coordinate system, corresponding to the unperturbed parameters w, $\mathbf{u} = (u_x, u_y)$, $n = \sigma_{zz}$, and $\mathbf{t} = (\sigma_{xz}, \sigma_{yz})$, respectively. Further assuming the slope of the surface is small, i.e. $|\gamma'| \ll 1$, where γ' is the gradient of the surface defined as

$$\gamma'(\mathbf{r}) = (\gamma_{,x}, \gamma_{,y}) = \left(\frac{\partial\,\gamma(\mathbf{r})}{\partial x}, \frac{\partial\,\gamma(\mathbf{r})}{\partial y}\right) \tag{5.22}$$

then the rotation transformation of displacements and stresses is [23]

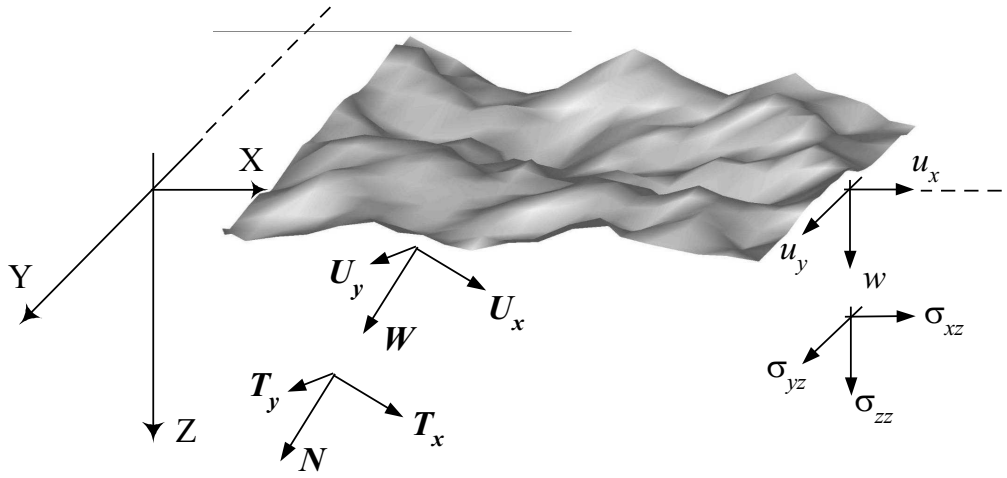

Figure 5.3: Coordinate system of a rough surface

$$\begin{aligned} W &= w - \gamma' \cdot \mathbf{u} \\ U &= \mathbf{u} + \gamma' w \\ N &= n - 2\gamma' \cdot \mathbf{t} \\ T &= \mathbf{t} + (\gamma_{,x}\left[\sigma_{zz} - \sigma_{xx}\right] - \gamma_{,y}\sigma_{xy}, \gamma_{,y}\left[\sigma_{zz} - \sigma_{yy}\right] - \gamma_{,x}\sigma_{xy}) \end{aligned} \tag{5.23}$$

where only terms to the first order in the roughness have been retained. The rotated boundary conditions can now be expressed as a perturbation of the original boundary conditions, Equation (5.20) , in the operator form

$$B_i^*(p_{i;i+1}) = B_i(p_{i;i+1}) + \gamma' \circ b_i(p_{i;i+1}) \tag{5.24}$$

where the operator symbol $\circ$ represents the various vector operations in Equation (5.23).

Now, the total field in layer number i is decomposed into a coherent or mean field $\langle p_i \rangle$ and an incoherent, scattered field, s_i

$$p_i = \langle p_i \rangle + s_i \tag{5.25}$$

where the scattered field is assumed to be of order γ. Following the development in Reference [23], one then arrives at a set of equations which must be satisfied by the solutions of mean and scattered fields at the average interface depth z_i, respectively. Thus, we obtain boundary condition for the mean field as follows:

$$\left\{ \tilde{B}_i(\mathbf{k_r}) + \frac{\langle \gamma^2 \rangle}{2} \frac{\partial^2}{\partial z^2} \tilde{B}_i(\mathbf{k_r}) + I_1(\mathbf{k_r}) + I_2(\mathbf{k_r}) \right\} \langle \tilde{p}_{i;i+1}^{\mp}(\mathbf{k_r}) \rangle = 0 \tag{5.26}$$

where

$$\begin{aligned} I_1(\mathbf{k_r}) &= -\frac{\langle \gamma^2 \rangle}{2\pi} \int d^2\mathbf{q} P(\mathbf{q} - \mathbf{k_r}) \frac{\partial \tilde{B}_i(\mathbf{q})}{\partial z} \\ &\quad \times \tilde{B}_i^{-1}(\mathbf{q}) \left[\frac{\partial \tilde{B}_i(\mathbf{k_r})}{\partial z} - j(\mathbf{q} - \mathbf{k_r}) \circ \tilde{b}_i(\mathbf{k_r}) \right] \end{aligned} \tag{5.27}$$

$$I_2(\mathbf{k_r}) = -\frac{\langle\gamma^2\rangle}{2\pi}\int d^2\mathbf{q}P(\mathbf{q}-\mathbf{k_r})j(\mathbf{q}-\mathbf{k_r})\circ\tilde{b}_i(\mathbf{q}) \times\tilde{B}_i^{-1}(\mathbf{q})\left[\frac{\partial\tilde{B}_i(\mathbf{k_r})}{\partial z}-j(\mathbf{q}-\mathbf{k_r})\circ\tilde{b}_i(\mathbf{k_r})\right] \quad (5.28)$$

The equation for the scattered field is

$$\tilde{B}_i(\mathbf{q})\tilde{s}_{i;i+1}(\mathbf{q}) = -\frac{1}{2\pi}\int d^2\mathbf{k_r}\tilde{\gamma}(\mathbf{q}-\mathbf{k_r}) \times\left[\frac{\partial\tilde{B}_i(\mathbf{k_r})}{\partial z}-j(\mathbf{q}-\mathbf{k_r})\circ\tilde{b}_i(\mathbf{k_r})\right]\langle\tilde{p}^{\mp}_{i;i+1}(\mathbf{k_r})\rangle \quad (5.29)$$

In the above expressions, $\langle\tilde{p}^{\mp}_{i;i+1}(\mathbf{k_r})\rangle$ and $\tilde{s}_{i;i+1}$ are vectors containing the unknown plane-wave amplitudes in layers i and $i+1$ for coherent and incoherent components, respectively. The power spectrum, $P(\mathbf{q})$, is defined by Equation (2.15). It is also noted that the above equations are based upon the expansion of the rotated boundary condition, Equation (5.26), in a Taylor series to second order in the roughness parameter γ. Thus, the results are correct to $\mathcal{O}\left[\kappa\gamma^2_{\rm rms}\right]$

5.4 Numerical Examples

Based upon the formulation described in the previous section, a numerical code SAFARI – Seismo-Acoustic Fast Field Algorithm for Range-Independent Environment was developed by Henrik Schmidt [44], and later is upgraded to improve stability and subsequently renamed to as OASES. The OASES includes many moduli which allow to carry out many applications of wave propagation in an oceanic environment. For example, Module **oasr** allows computation for reflection coefficient for stratified medium up to 200 layers (default), Module **oast** for transmission loss, Module **oass** for scattering, and many other more.

In this section, we shall apply the scattering module to a problem shown in Figure 5.2, and analyze the scattering spectrum. It is the limitation of OASES that only one-dimensional Gaussian and Goff-Jordan power spectra are built in the software.

Here we consider the problem shown in Figure 5.2. The environment consists of upper layer which is water (sound-speed 1500 m/s, density 1000 kg/m^3), an intermediate layer which has sound-speed 1725 m/s, and density 1400 kg/m^3, and a lower layer with sound speed 2000 m/s, and density 1800 kg/m^3. The thickness of the intermediate layer is 100 m, and the frequency is taken to be 100 Hz. The one-dimensional Gaussian spectrum is employed to describe the roughness. A sequence of commands built in OASES, including **oasr** and **oass** are invoked to initiate computation.

Figure 5.4 – Figure 5.6 are the scattering spectra corresponding to correlation lengths 1, 5, 10 m, respectively.

It is clear from these results that the major scattering is in the backward direction when the correlation is small (1 m), and as the correlation increases, the major scattering gradually

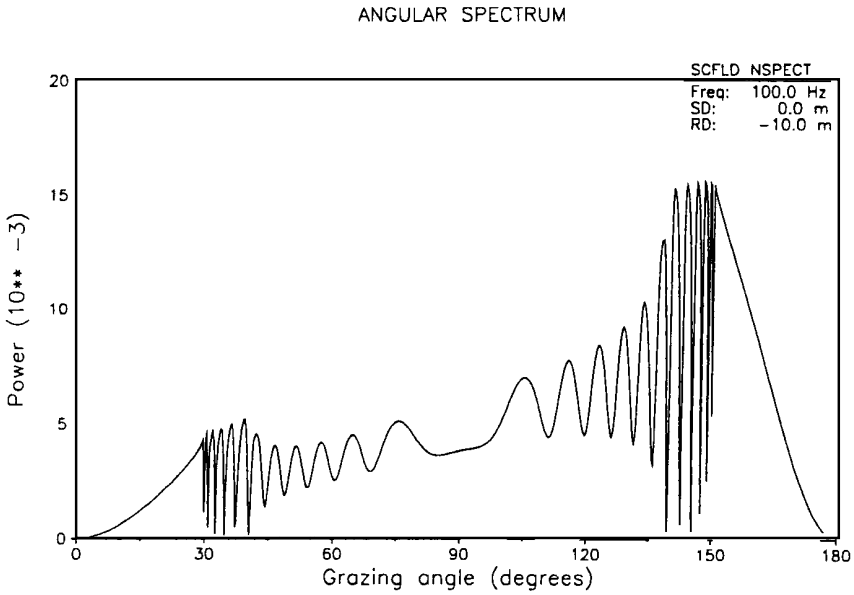

Figure 5.4: Scattering spectrum for correlation length 1 m.

shifts towards forward direction. The energy level is larger for larger correlation length. This is in complete consistence with the results obtained in the examples shown in Section 4.2.

Remark

There are much more features which can be found in OASES. We make no attempt and also definitely assume no needs to list all of them, except feel obligated to directing the readers who are interested in this software to a public domain where a complete package may be obtained without any charge. The ftp address is ftp@keel.mit.edu. Just login with your username as password, and get the file oases-export.tar.Z in the pub directory. The rest is yours.

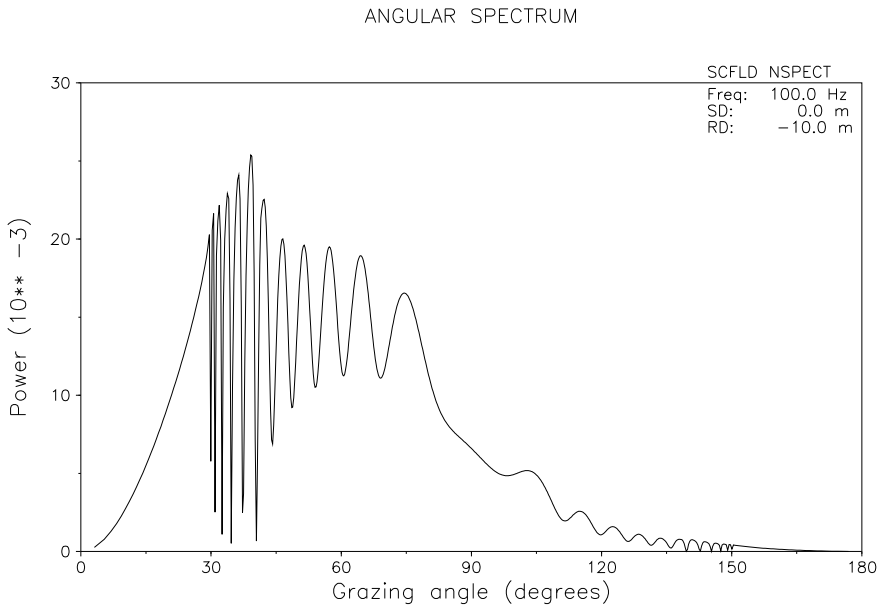

Figure 5.5: Scattering spectrum for correlation length 5 m.

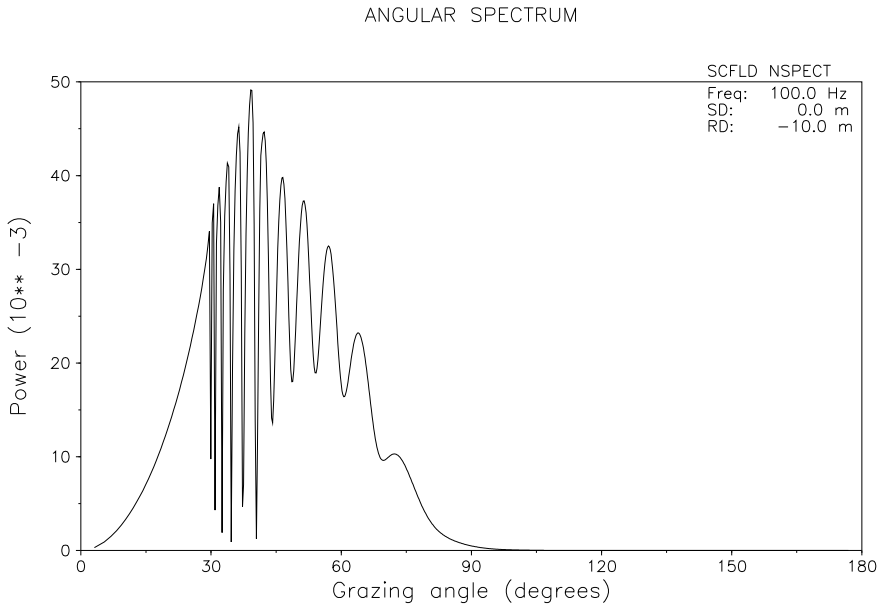

Figure 5.6: Scattering spectrum for correlation length 10 m.

Chapter 6

Conclusions

This thesis project has accomplished the following:

1. Various rough surfaces relevant to oceanic environment are studied in terms of their statistics, including height probability function, correlation function, power spectrum and its realization. Many graphs were generated to facilitate analysis and discussion.

2. The Rayleigh reflection were examined using dynamic simulation with MATLAB. This exercise allows us to generate virtual reflection and refraction waves, and thus provides a much better means than traditional line graphs.

3. Scattering from perfectly reflected surfaces were studied. This problem closely resembles acoustical wave scattering from sea surface and seabed. The distributions of the random pressure field corresponding to various power spectra for pressure-release and rigid surfaces were generated. The results provide a good sense on how the pressure field distributes.

4. The statistics of the scattered field in terms of average intensity and correlation function were obtained and analyzed.

5. A model for further pursuit of scattering from a penetrable surface was proposed and formulated. A few examples using sc oases were given, which demonstrates the capacity of the current state-of-the-art software in this realm.

Of course, there still have many issues remained to be cultivated. This project attempts to develop a MATLAB-based toolbox which solves for acoustic wave propagation problems in an oceanic environment, and the present analysis serves as an initiation of the project along this line. It is expected that, with time, the versatility of the MATLAB language will offer a very convenient, if not dominant, means for problems-solving in many communities, academic or industry, including ocean acoustic community. For this matter, the author look forward to the day when all such practices are produced.

Appendix A

Derivation of Correlation For Amplitude Spectrum

The purpose of this appendix is to prove the relation

$$\langle A(\mathbf{p})A^{\star}(\mathbf{p}')\rangle = P_s(\mathbf{p})\delta(\mathbf{p}-\mathbf{p}') \tag{A.1}$$

where

$$P_s(\mathbf{p}) = \frac{1}{(2\pi)^2}\int C(\bar{\mathbf{r}})e^{-i\mathbf{p}\cdot\bar{\mathbf{r}}}d\bar{\mathbf{r}} \tag{A.2}$$

From Equation (3.32), the amplitude spectrum of the roughness is

$$A(\mathbf{p}) = \frac{1}{(2\pi)^2}\int \gamma(\mathbf{r}_1)e^{-i\mathbf{p}\cdot\mathbf{r}_1}d\mathbf{r}_1 \tag{A.3}$$

Likewise,

$$A^{\star}(\mathbf{p}') = \frac{1}{(2\pi)^2}\int \gamma^{\star}(\mathbf{r}_2)e^{i\mathbf{p}'\cdot\mathbf{r}_2}d\mathbf{r}_2 \tag{A.4}$$

The correlation of the amplitude spectrum is given by

$$\langle A(\mathbf{p})A^{\star}(\mathbf{p}')\rangle = \frac{1}{(2\pi)^4}\iint \langle\gamma(\mathbf{r}_1)\gamma^{\star}(\mathbf{r}_2)\rangle \exp[-i(\mathbf{p}\cdot\mathbf{r}_1 - \mathbf{p}'\cdot\mathbf{r}_2)]d\mathbf{r}_1 d\mathbf{r}_2 \tag{A.5}$$

Now, let $\bar{\mathbf{r}} = \mathbf{r}_2 - \mathbf{r}_1$, so $\mathbf{r}_2 = \bar{\mathbf{r}} + \mathbf{r}_1$, and with the definition of the correlation function, Equation (2.13), Equation (A.5) becomes

$$\langle A(\mathbf{p})A^{\star}(\mathbf{p}')\rangle = \frac{1}{(2\pi)^4}\iint C(\bar{\mathbf{r}})\exp[-i(\mathbf{p}-\mathbf{p}')\cdot\mathbf{r}_1]\exp(i\mathbf{p}'\cdot\bar{\mathbf{r}})d\mathbf{r}_1 d(\bar{\mathbf{r}}+\mathbf{r}_1) \tag{A.6}$$

Applying the identity

$$\delta(\mathbf{p}-\mathbf{p}') = \frac{1}{(2\pi)^2}\int \exp[-i(\mathbf{p}-\mathbf{p}')\cdot\mathbf{r_1}]d\mathbf{r}_1$$

and note that

$$\frac{1}{(2\pi)^2}\int C(\bar{\mathbf{r}})e^{i\mathbf{p}'\cdot\bar{\mathbf{r}}}d\bar{\mathbf{r}} = P_s(-\mathbf{p}')$$

where $d(\bar{\mathbf{r}} + \mathbf{r}_1) = d\bar{\mathbf{r}}$, the integration results in

$$\langle A(\mathbf{p}) A^\star(\mathbf{p}') \rangle = \delta(-\mathbf{p}' + \mathbf{p}) P_s(-\mathbf{p}') \tag{A.7}$$

Because $\gamma(\mathbf{r})$ is a real function, we have

$$\mathcal{F}\{\gamma(\mathbf{r})\} = A(\mathbf{p}) = A^\star(-\mathbf{p}) \tag{A.8}$$

Therefore,

$$\begin{aligned} \langle A(\mathbf{p}) A^\star(\mathbf{p}') \rangle &= \langle A^\star(-\mathbf{p}) A(-\mathbf{p}') \rangle \\ &= \delta(\mathbf{p} - \mathbf{p}') P_s(\mathbf{p}) \end{aligned} \tag{A.9}$$

The above result says that the Fourier components themselves of any function are no correlation, i.e., they are totally incoherent to each other.

Appendix B

Scattering From an Interface Over a Medium With Continuous Varying Sound Speed and Density

B.1 Introduction

In this appendix, we shall derive the formulation which is appropriate for solving scattering from a rough surface overlying a medium with continuous varying sound speed under the framework of perturbation. The environment is shown in Figure 5.1.

The reasons for this exercise are two folds. First, as we mentioned in the beginning of Section 5.1, if the gradients of the medium acoustic properties is large, then subdividing the medium into thin layers may violate the basic assumptions of perturbation method, and as a result, OASES or any other similar methods may not be able to obtain good solutions. Therefore, fitting the layers with non-constant function so that analytical solutions for depth-dependent equation may be obtained should be an alternative. Secondly, the boundary operators such as B and b employed in Section 5.2 may seem esoteric without appropriate demonstration. Therefore, the later part of this appendix uses the problem shown in Figure 5.1 as an example and then derives all the relevant operators. This serves as an example for demonstrating the derivation of the boundary operators.

B.2 Solutions for Unperturbed Problem

In a medium of varying sound speed and density, the frequency-domain wave equation or *modified Helmholtz equation* is

$$\left[\nabla^2 + k^2(z)\right] p_\omega = \frac{1}{\rho(\mathbf{r}, z)} \nabla \rho(\mathbf{r}, z) \cdot \nabla p \tag{B.1}$$

Assuming that the density depends only on the vertical coordinate z, Equation (B.1) becomes

$$\left[\nabla^2 + k^2(z)\right] p_\omega = \frac{1}{\rho(z)} \frac{d\rho(z)}{dz} \frac{\partial p}{\partial z} \tag{B.2}$$

By applying the forward Fourier transform with respect to range on Equation (B.2), the depth-dependent wave equation for $\tilde{p}_\omega(\mathbf{k_r}, z)$ is obtained

$$\left\{ \frac{d^2}{dz^2} - \frac{1}{\rho(z)} \frac{d\rho(z)}{dz} \frac{d}{dz} + \left[k^2(z) - k_r^2\right] \right\} \tilde{p}_\omega(\mathbf{k_r}, z) = 0 \tag{B.3}$$

The depth-dependent equation may be simplified by introducing the variable transformation

$$q(z) = \frac{1}{\sqrt{\rho_s(z)}} \tilde{p}_\omega(\mathbf{k_r}, z) \tag{B.4}$$

Equation (B.3) is transformed to

$$\frac{d^2 q}{dz^2} + \left\{ k^2(z) - k_r^2 + \left[\frac{1}{2\rho_s(z)} \frac{d^2\rho_s(z)}{dz^2} - \frac{3}{4} \left(\frac{1}{\rho_s(z)} \frac{d\rho_s(z)}{dz} \right)^2 \right] \right\} q = 0 \tag{B.5}$$

B.2.1 Density Stratification

If the density distribution is of the form

$$\rho_s(z) = \frac{A\ e^{b_2 z}}{(e^{b_2 z} + a_2)^2} \tag{B.6}$$

then it can be shown that the density distribution satisfies the following equation

$$\frac{1}{2\rho_s(z)} \frac{d^2\rho_s(z)}{dz^2} - \frac{3}{4} \left(\frac{1}{\rho_s(z)} \frac{d\rho_s(z)}{dz} \right)^2 = -\frac{b_2^2}{4} \tag{B.7}$$

Substituting the above equation into Equation (B.5) will yield

$$\frac{d^2 q}{dz^2} + \left[k^2(z) - k_r^2 - \frac{b_2^2}{4} \right] q = 0 \tag{B.8}$$

It is worth noting that Equation (B.7) is valid for any value of the parameter "a_2" in Equation (B.6), and Equation (B.8) does not contain "a_2." Thus the same solution for q will be obtained for a family of density profiles, defined by Equation (B.6), in which b_2 is held constant while a_2 varies. In such case the effect of the density profile, on acoustic pressure in the transition layer, is manifested only via Equation (B.4). In general, however, the value of b_2, as well as a_2, must be altered to model a variety of density profiles of practical interest, so the solution for q will usually be directly affected. Next, we will present the solutions of the depth-dependence wave equation for the three sound speed profiles.

B.2.2 Sound Speed Stratification

The depth-dependence wave equation, Equation (B.3), is a second-order linear ordinary differential equation with variable coefficients, in which the horizontal wavenumber k_r is a parameter. In the most general case, even though the solution may be obtained by the standard method such as power series expansion or numerical method, it must be noted that in order to carry out the inverse transform, the depth-dependence wave equation must be solved for each value of k_r, and therefore, the key to the success heavily relies upon the efficiency of the solution method employed. As a result, the search for the distributions of the sound speed and the density which render analytical solutions to the equation becomes an important issue. In this aspect, Robins [38, 39, 40] attempted to investigate various types of profiles which permits the existence of exact solutions, and the results were documented in [40]. These functions were used to fit the existing geo-acoustical data and were found reasonable agreement in a wide range of depth.

The sound-speed variation in the sediment may take any of three forms. These are:

- constant value, c_1.
- "linear k^2" profile in which the square of the wavenumber varies linearly with depth:

$$\frac{1}{c_s^2(z)} = \frac{1+mz}{c_1^2} \tag{B.9}$$

- inverse-square profile described by the equation:

$$\frac{1}{c_s^2(z)} = \frac{b_1^2}{c_0^2} + \left(\frac{1}{c_1^2} - \frac{b_1^2}{c_0^2}\right)\frac{1}{(1-\gamma z)^2} \tag{B.10}$$

By suitable choice of the constants A, a_2, b_1, b_2, c_0, c_1, and γ it is possible to achieve a close fit to typical measured density and sound-speed profiles in marine sediments.

B.2.3 Solutions of the Wave Equation

In the following, we derive the solutions for wave equation corresponding to the sound-speed and density distributions discussed in the previous section. The density profile is given by Equation (B.6), and the sound-speed will be presented below.

A. Constant Sound Speed

The simplest case is that of a constant sound speed c_1 in the transition layer. Equation (B.8) becomes

$$\frac{d^2q}{dz^2} - \alpha^2 q = 0 \tag{B.11}$$

where

$$\alpha = \sqrt{k_r^2 - k^2 + \frac{b_2^2}{4}} \tag{B.12}$$

The solution of depth-dependence wave equation for this case is

$$\tilde{p}_\omega(\mathbf{k_r}, z) = \tilde{p}_\omega^-(\mathbf{k_r})\sqrt{\rho_s(z)}e^{-\alpha z} + \tilde{p}_\omega^+(\mathbf{k_r})\sqrt{\rho_s(z)}e^{\alpha z} \tag{B.13}$$

B. Linear k^2 Sound-Speed Profile

With sound-speed profile given by Equation (B.9), the equation for q becomes

$$\frac{d^2q}{dz^2} + \left[(1+mz)k_1^2 - k_r^2 - \frac{b_2^2}{4}\right] q = 0 \tag{B.14}$$

Defining the variable η by

$$\eta = -(mk_1^2)^{-2/3}\left[(1+mz)k_1^2 - k_r^2 - \frac{b_2^2}{4}\right] \tag{B.15}$$

it is easily shown that Equation (B.14) becomes

$$\frac{d^2q}{d\eta^2} = \eta q \tag{B.16}$$

The solution of depth-dependence wave equation for this case is

$$\tilde{p}_\omega(\mathbf{k_r}, z) = \tilde{p}_\omega^-(\mathbf{k_r})\sqrt{\rho_s(z)}Ai(\eta) + \tilde{p}_\omega^+(\mathbf{k_r})\sqrt{\rho_s(z)}Bi(\eta) \tag{B.17}$$

C. Inverse-Square Sound-Speed Profile

For the sound-speed profile of Equation (B.10), the solution may be written in terms of Hankel function. By introducing a new variable ζ as

$$\zeta = 1 - \gamma z \tag{B.18}$$

Equation (B.8) then takes the form

$$\gamma^2\frac{d^2q}{d\zeta^2} + \frac{\omega^2}{\zeta^2}\left(\frac{1}{c_1^2} - \frac{b_1^2}{c_0^2}\right) q + \left(\frac{\omega^2}{c_0^2}b_1^2 - k_r^2 - \frac{b_2^2}{4}\right) q = 0 \tag{B.19}$$

It is shown that the solution to Equation (B.19) is given by

$$q = \sqrt{\zeta}\left[E'\,H_\nu^{(1)}(\beta\zeta) + F'\,H_\nu^{(2)}(\beta\zeta)\right] \tag{B.20}$$

where E', F' are arbitrary constants and the parameters β, ν are defined by

$$\beta^2 = \frac{1}{\gamma^2}\left(b_1^2\frac{\omega^2}{c_0^2} - k_r^2 - \frac{b_2^2}{4}\right) \tag{B.21}$$

$$\nu^2 = \frac{1}{4} - \frac{\omega^2}{\gamma^2}\left(\frac{1}{c_1^2} - \frac{b_1^2}{c_0^2}\right) \tag{B.22}$$

The solution of depth-dependence wave equation for this case is

$$\tilde{p}_\omega(\mathbf{k_r}, z) = \tilde{p}_\omega^-(\mathbf{k_r})\sqrt{\rho_s(z)\zeta(z)}H_\nu^{(1)}(\beta\zeta) + \tilde{p}_\omega^+(\mathbf{k_r})\sqrt{\rho_s(z)\zeta(z)}H_\nu^{(2)}(\beta\zeta) \tag{B.23}$$

With the above solutions, the pressure has the following integral representation

$$p_\omega(\mathbf{r}, z) = \frac{1}{2\pi}\int d\,\mathbf{k_r}\, e^{-j\mathbf{k_r}\cdot\mathbf{r}}\left[\tilde{p}_\omega^-(\mathbf{k_r})\mathcal{G}(\mathbf{k_r}, z) + \tilde{p}_\omega^+(\mathbf{k_r})\mathcal{H}(\mathbf{k_r}, z)\right] \tag{B.24}$$

where $\mathcal{G}$ and $\mathcal{H}$ are to represent the solutions for depth-dependent equation, and $\tilde{p}_\omega^-(\mathbf{k_r})$, $\tilde{p}_\omega^+(\mathbf{k_r})$ could be determined from the matching conditions discussed in next section.

B.3 Linear Systems

The linear systems governing the mean and scattered field, Equations (5.26) and (5.29) are expressed in terms of the boundary operator $\tilde{B}(\mathbf{k_r})$ and the rotational operator $\tilde{b}(\mathbf{k_r})$. In this section we gives a detailed derivation for these operators for the case of an isovelocity water column overlying an transition layer.

B.3.1 Wavenumber Integrals

The present analysis considers the scattering from a *one-dimensional* rough surface, and the resultant scattered fields generated by an incoming wave with horizontal wavenumber k_x is *two-dimensional*. For the homogeneous media, layer i, the solution of pressure has the following integral representation

$$p_i(x, z) = \int d\,k_x\, e^{-jk_x x}\left[\tilde{p}_i^-(k_x)e^{-\alpha_i z} + \tilde{p}_i^+(k_x)e^{+\alpha_i z}\right] \tag{B.25}$$

In the transition sediment layer, layer $i+1$, the solution of the pressure for varying density and sound-speed has the following integral representation

$$p_{i+1}(x, z) = \int d\,k_x\, e^{-jk_x x}\left[\tilde{p}_{i+1}^-(k_x)\mathcal{G}(k_x, z) + \tilde{p}_{i+1}^+(k_x)\mathcal{H}(k_x, z)\right] \tag{B.26}$$

where $\alpha_i = \sqrt{k_x^2 - k_i^2}$ with k_i being the wavenumber in the layer i. The amplitudes $\tilde{p}_i^\mp$ are arbitrary functions of the horizontal wavenumber k_x. The solutions of depth-dependence wave equation for varying density and sound-speed, respectively, are

$$\tilde{p}_\omega(k_x, z) = \begin{cases} \tilde{p}_\omega^-(k_x)\sqrt{\rho_s(z)}e^{-\alpha z} + \tilde{p}_\omega^+(k_x)\sqrt{\rho_s(z)}e^{\alpha z} & \text{Case A} \\ \tilde{p}_\omega^-(k_x)\sqrt{\rho_s(z)}Ai(\eta(z)) + \tilde{p}_\omega^+(k_x)\sqrt{\rho_s(z)}Bi(\eta(z)) & \text{Case B} \\ \tilde{p}_\omega^-(k_x)\sqrt{\rho_s(z)\zeta(z)}H_\nu^{(1)}(\beta\zeta(z)) + \tilde{p}_\omega^+(k_x)\sqrt{\rho_s(z)\zeta(z)}H_\nu^{(2)}(\beta\zeta(z)) & \text{Case C} \end{cases} \tag{B.27}$$

The displacement components are obtained from the pressure by

$$u_i = \frac{1}{\rho\omega^2}\frac{\partial p}{\partial x_i} \tag{B.28}$$

Carrying out the tensor operation yields

$$u = \frac{1}{\rho\omega^2}\frac{\partial p}{\partial x} \tag{B.29}$$

$$w = \frac{1}{\rho\omega^2}\frac{\partial p}{\partial z} \tag{B.30}$$

For the present environment, the integral representation of the existing wavefield pressures are

$$p_1(x,z) = \int d\,k_x\, e^{-jk_x x}\tilde{p}_1^+(k_x)e^{+\alpha_1 z} \tag{B.31}$$

$$p_2(x,z) = \int d\,k_x\, e^{-jk_x x}\left[\tilde{p}_2^-(k_x)\mathcal{G}(k_x,z) + \tilde{p}_2^+(k_x)\mathcal{H}(k_x,z)\right] \tag{B.32}$$

$$p_3(x,z) = \int d\,k_x\, e^{-jk_x x}\tilde{p}_3^-(k_x)e^{-\alpha_3 z} \tag{B.33}$$

where the radiation conditions are applied to eliminate the downgoing waves in the layer 1 and upgoing components in the layer 3.

It should be noted that if a source is present in a particular layer, the wavefield should be supplemented by a particular solution. Here we assume the source is in the water column, 1ayer 1, at depth z_s, thus the source field is

$$\hat{p}_1(x,z;z_s) = \int d\,k_x\, e^{-jk_x x}\hat{\tilde{p}}_1(k_x,z) \tag{B.34}$$

where

$$\hat{\tilde{p}}_1(k_x,z) = \frac{S_w}{4\pi\alpha_1}e^{-\alpha_1|z-z_s|} \tag{B.35}$$

B.3.2 Unperturbed Problem

The unknown wavefield amplitudes are determined from the boundary conditions. For an interface separating two layers, the normal displacement w and pressure p must be continuous. Thus for the three-layer problem the conditions are:

$$(w_i - w_{i+1})_{i;i+1} = 0 \tag{B.36}$$

$$(p_i - p_{i+1})_{i;i+1} = 0 \tag{B.37}$$

When the above displacements are written in terms of pressure, and related kernels are inserted, these conditions result in a linear system of equations in the wavefield amplitudes

$$\tilde{B}_g(k_x)\tilde{p}_g^{\mp}(k_x) = \tilde{C}(k_x) \tag{B.38}$$

where $\tilde{p}_g^{\mp}(k_x)$ is a column vector containing the unknown amplitudes

$$\{\tilde{p}_g^{\mp}(k_x)\}^T = \{\tilde{p}_1^{+}(k_x), \tilde{p}_2^{-}(k_x), \tilde{p}_2^{+}(k_x), \tilde{p}_3^{-}(k_x)\} \tag{B.39}$$

and

$$\tilde{B}_g(k_x) = \begin{bmatrix} \frac{\alpha_1}{\rho_1\omega^2} & -\frac{1}{\rho_2(0)\omega^2}\frac{\partial \mathcal{G}(0)}{\partial z} & -\frac{1}{\rho_2(0)\omega^2}\frac{\partial \mathcal{H}(0)}{\partial z} & 0 \\ 1 & -\mathcal{G}(0) & -\mathcal{H}(0) & 0 \\ 0 & \frac{1}{\rho_2(h)\omega^2}\frac{\partial \mathcal{G}(h)}{\partial z} & \frac{1}{\rho_2(h)\omega^2}\frac{\partial \mathcal{H}(h)}{\partial z} & \frac{\alpha_3}{\rho_3\omega^2} \\ 0 & \mathcal{G}(h) & \mathcal{H}(h) & -1 \end{bmatrix}$$

The column vector $\tilde{C}(k_x)$ representing the integration kernel for the source field for a source in the wave at depth z_s, is

$$\tilde{C}(k_x) = \begin{Bmatrix} \frac{S_w}{4\pi\rho_1\omega^2} e^{-\alpha_1|z_s|} \\ -\frac{S_w}{4\pi\alpha_1} e^{-\alpha_1|z_s|} \\ 0 \\ 0 \end{Bmatrix}$$

B.3.3 Perturbed Problem

For two-dimensional wave propagation in the presence of a one-dimensionally rough surface, the rotated boundary conditions simplify significantly, since all rotation operations become scalar and $\sigma_{xx},\ \sigma_{xz},\ \sigma_{xy} = 0$:

$$\begin{aligned} W &= w - \gamma_{,x} u \\ N &= p \end{aligned} \tag{B.40}$$

The total field in the layer number i is decomposed into a coherent or mean field $\langle p_i \rangle$ and an incoherent, scattered components, s_i. So for the problem at hand, we have:

$$p_i^{\mp} = \begin{Bmatrix} \langle p_i^{-} \rangle + s_i^{-} \\ \langle p_i^{+} \rangle + s_i^{+} \end{Bmatrix}$$

The global vectors containing plane-wave amplitudes are

$$\langle \tilde{p}_g^{\mp} \rangle^T = \{\tilde{p}_1^{+}, \tilde{p}_2^{-}, \tilde{p}_2^{+}, \tilde{p}_3^{-}\} \tag{B.41}$$

$$\tilde{s}_g^{\mp\ T} = \{\tilde{s}_1^{+}, \tilde{s}_2^{-}, \tilde{s}_2^{+}, \tilde{s}_3^{-}\} \tag{B.42}$$

where the radiation condition has eliminated the downgoing waves in the layer 1 and upgoing components in the bottom halfspace.

Next, the expression for the local operators $\tilde{B}_i(k_x)$ for the smooth boundary, and rotation boundary operator $\tilde{b}_i(k_x)$ will be presented. In the previous section, we have derived the global system, $\tilde{B}_g(k_x)$, for all three layers.

The rotation boundary operator $\tilde{b}_1(k_x)$ is derived in a similar way, representing the discontinuous of the following field parameters according to Equation (B.40):

$$\tilde{b}_1(k_x)\tilde{p}_{1;2}^{\mp}(k_x) = \begin{Bmatrix} -\tilde{u}_1 + \tilde{u}_2 \\ 0 \end{Bmatrix} \tag{B.43}$$

By inserting the wavenumber kernel for the horizontal displacements, we get

$$\tilde{b}_2(k_x) = \begin{bmatrix} \frac{ik_x}{\rho_1\omega^2} & -\frac{ik_x\mathcal{G}(0)}{\rho_2(0)\omega^2} & -\frac{ik_x\mathcal{H}(0)}{\rho_2(0)\omega^2} & 0 \\ 0 & 0 & 0 & 0 \end{bmatrix} \tag{B.44}$$

B.4 Summary

This appendix formulates a problem which describes a realistic model. Solutions may be pursued following the DGM method. Although not completed in this thesis, the research group to which this author belongs will soon undertake this project.

Bibliography

[1] Bass, F.G. and I.M. Fuks, *Wave Scattering From Statistically Rough Surfaces* (Pergamon, 1979).

[2] Bell, T.H., "Statistical features of sea floor topography," *Deep Sea Res.*, **22**, 883–892, (1975b).

[3] Beckmann, P. and A. Spizzichino, *The Scattering of Electromagnetic Waves From Rough Surfaces*, (Pergamon, 1963).

[4] Bergmann, P.G., "The wave equation in a medium with a variable index of refraction," *J. Acoust. Soc. Am.*, **17**, 329–333 (1946).

[5] Berman, D.H., "Simulation of rough interface scattering," *J. Acoust. Soc. Am.*, **89**, 623–636 (1991).

[6] Chen, C.-S.,, *Effects of elastic seabed and waveguide environment on the ambient noise generated by surface random processes*, *Master Thesis*, Department of Marine Environment, National Sun Yat-sen University (1996).

[7] Caruthers, J.W. and J.C. Novarini, "Numerical modeling of randomly rough surfaces with application to sea surfaces," *Technical Report* 71-13-T, Department of Oceanography, Texas A & M University (1971).

[8] Dashen, R., F.S. Henyey, and D. Wurmser, "Calculations of acoustic scattering from the ocean surface," *J. Acoust. Soc. Am.*, **88**, 310–323 (1990).

[9] Eckart, C., "The scattering of sound from the sea", *J. Acoust. Soc. Am.*, **25**, 566–570 (1953).

[10] Fortuin, L., "Survey of literature on reflection and scattering of sound waves at the sea surface" *J. Acoust. Soc. Am.*, **47**, 1209–1228 (1969).

[11] Fortuin, L. and J.G. Boer, "Spatial and temporal correlation of the sea surface," *J. Acoust. Soc. Am.*, **49**, 1677–1678 (1971).

[12] Fox, C. G. and D. E. Hayes, "Quantitative methods for analyzing the roughness of the seafloor," *Rev. Geophys.*, **23**, 1–48 (1985).

[13] Galybin, N.N., "Backscattering of a sound by a disturbed sea surface," *Sov. Phys. Acoust.*, **22**, 193–197 (1976).

[14] Goalwin, P.W., "A stationary phase approach to the calculation of the correlation of the acoustic field scattered from a two-dimensional random sea surface," *J. Acoust. Soc. Am.*, **93**, 214–223 (1993).

[15] Goff, J.A. and T.H. Jordan, "Stochastic modeling of seafloor morphology: Inversion of Sea Beam data for second-order statistics," *J. Geophys. Res.*, **93**, No. B11, 13589–13608 (1988).

[16] Gupta, R.N., "Reflection of plane acoustic waves from transition layers with arbitrary variation of velocity and density," *Bull. Seismol. Soc. Am.*, **56**, 633–642 (1966).

[17] Hamilton, E.L., "Geoacoustic modeling of the sea floor," *J. Acoust. Soc. Am.,* **68**, 1313–1340 (1980).

[18] Hasselmann, A., "A statistical analysis of the generation of microseism," *Rev. Geophy. Space Phys.*, **1**, 177–210 (1963).

[19] Kibblewhite A. C. and K. C. Ewans, "Wave-wave interactions, microseism, an infrasonic ambient noise in the ocean," *J. Acoust. Soc. Am.*, **78**, 981– 994 (1986).

[20] Kitaigorodskii, S.A., "Application of the theory of similarity to the analysis of wind generated wave motion as a stochastic process," *Izv. Akad. Nauk. SSSR, Ser. Geofiz.*, **1**, 105–117 (1961) [Engl. Transl. 1, 73–80 (1961)].

[21] Kuperman, W.A., "Coherent component of specular reflection and transmission at a randomly rough two-fluid interface," *J. Acoust. Soc. Am.*, **58**, 365–370 (1975).

[22] Kuperman, W.A. and H. Schmidt, "Rough surface elastic wave scattering in a horizontally stratified ocean," *J. Acoust. Soc. Am.*, **79**, 1767–1777 (1986).

[23] Kuperman, W.A. and H. Schmidt, "Self-consistent perturbation approach to rough surface scattering in stratified elastic media," it J. Acoust. Soc. Am., **86**, 1511–1522 (1989).

[24] Kuperman, W.A. and F. Inginito, "Spatial correlation of surface generated noise in a stratified ocean," *J. Acoust. Soc. Am.*, **67**, 1988–1996 (1980).

[25] Liu, J.-Y., *Seismo-Acoustic Rough Interface Scattering of Surface-Generated Ambient Noise in a Stratified Ocean, Ph.D. Dissertation* at M.I.T (MIT Press, 1993).

[26] Liu, J.-Y., H. Schmidt, and W. A. Kuperman, "Effect of a rough seabed on the spectral composition of deep ocean infrasonic ambient noise," *J. Acoust. Soc. Am.*, **93**, 753–769 (1993).

[27] Liu, J.-Y. and J.L. Krolik, "The spatial correlation of rough seabed scattering of surface-generated ambient noise," *J. Acoust. Soc. Am.*, **96**, 2876–2886 (1994).

[28] Lynch, P.J., "Curvature corrections to rough-surface scattering at high frequencies," *J. Acoust. Soc. Am.*, **47**, 804–815 (1970).

[29] Mandelbrot, B.B., *The Fractal Geometry of Nature* (W. H. Freeman, NY, 1985).

[30] *Matlab User's Guide* (MathWorks, Inc).

[31] Moskowitz, L., "Estimates of the power spectrum for fully developed seas for wind speeds of 20 to 40 knots," *J. Geophy. Res.*, **69**, 5161–5179 (1964).

[32] Newman, J.N., *Marine Hydrodynamics* (MIT Press, 1977).

[33] Novarini, J.C. and J.W. Caruthers, "Numerical modeling of acoustic wave scattering from randomly rough surfaces: An image model," *J. Acoust. Soc. Am.*, **53**, 876–884 (1973).

[34] Ogilvy, J. A., *Theory of Wave Scattering From Random Rough Surfaces* (Adam Hilger, 1991).

[35] Ogilvy, A., "Wave scattering from rough surfaces," *Rep. Prog. Phys.*, **50**, 1553–1608 (1987).

[36] Papoulis, A., *Probability, Random Variable, and Stochastic Processes* (McGraw-Hill,1991).

[37] Pierson, W. J. Jr. and L. Moskowitz, "A proposal spectral form for fully developed wind seas based on the similarity theory of S. A. Kitaigorodskii," *J. Geophys. Res.*, **69**, 5181–5190 (1964).

[38] Robins, A.J., "Reflection of plane acoustic waves from a layer of varying density," *J. Acoust. Soc. Am.*, **87**, 1546–1552 (1990).

[39] Robins, A.J., "Exact solutions of the Helmholtz equation for plane wave propagation in a medium with variable density and sound speed," *J. Acoust. Soc. Am.*, **93**(3), 1686–1696 (1993).

[40] Robins, A.J., "Generation of shear and compression waves in an inhomogeneous elastic medium," *J. Acoust. Soc. Am.*, **96**(3), 1669–1676 (1994).

[41] Roussas, G.G., *A First Course in Mathematical Statistics* (Addison-Wesley Press, 1973).

[42] Rutherford, S.R. and K.E. Hawker, "Effect of density gradients on bottom reflection loss for a class of marine sediments," *J. Acoust. Soc. Am.*, **63**, 750–757 (1978).

[43] Schreiner, A.E. and L.M. Dorman, "Coherence lengths of Seafloor noise : Effect of ocean bottom structure," *J. Acoust. Soc. Am.*, **88**, 1503–1514 (1990).

[44] Schmidt, H., *SAFARI User's Guide* (Salant Undersea Research Center Report, 1988).

[45] Shiao, Tsung-Jieh, *A numerical study on ambient noise generated by surface wind waves*, *Master Thesis*, Department of Marine Environment, National Sun Yat-sen University (1995)

[46] Tolstoy, I., "Effect of density stratification on sound waves," *J. Geophys. Res.*, **70**, 6009–6015 (1965).

[47] Thorsos, E.I., "The validity of the Kirchhoff approximation for rough surface scattering using a Gaussian roughness spectrum," *J. Acoust. Soc. Am.*, **83**, 78–92 (1988).

[48] Thorsos, E.I. and D.R. Jackson, "The validity of the perturbation approximation for rough surface scattering using a Gaussian roughness spectrum," *J. Acoust. Soc. Am.*, **86**, 261–277 (1989).

[49] Voronovich, A.G., *Wave Scattering From Rough Surface* (Springer-Verlag).

Acoustic Wave Scattering From Rough Sea Surface and Seabed

by
Chen-Fen Huang

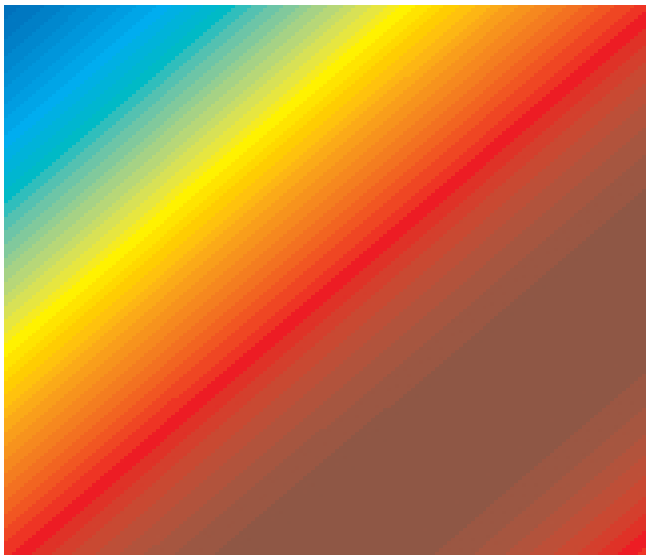

Timidly rough surface scattering

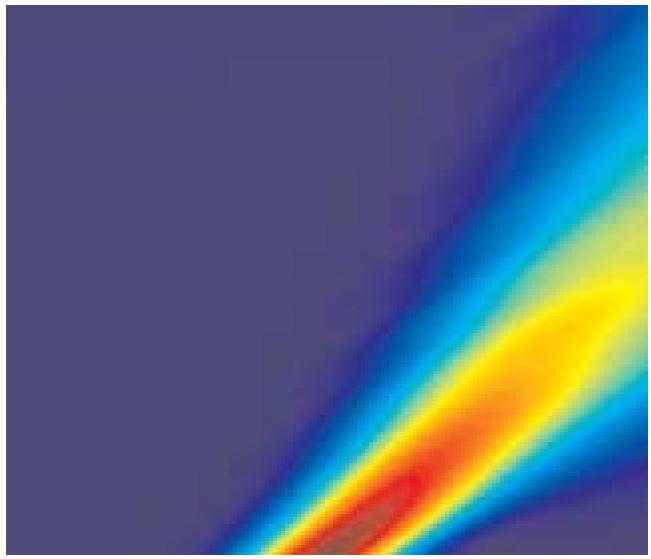

Graciously rough surface scattering

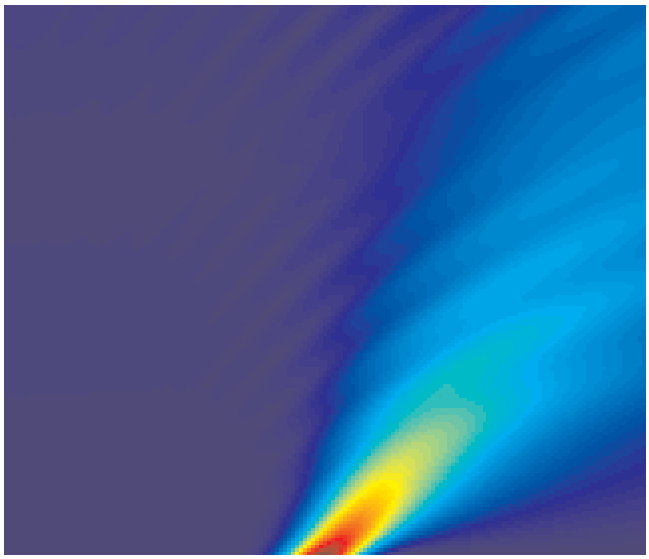

Boldly rough surface scattering

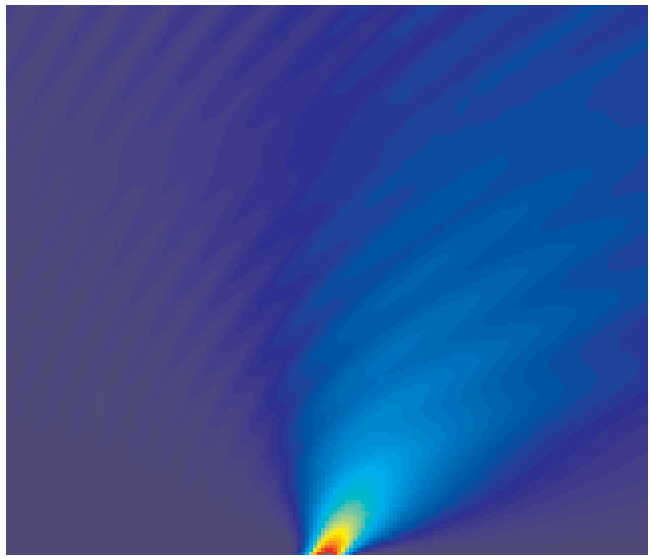

Ferociously rough surface scattering